

*Low Enrichment Fuel Evaluation  
and Analysis Program*

Summary Report for the Period  
January, 1981 - December, 1982

WILLIAM KERR, Project Director



Department of Nuclear Engineering  
and the  
Michigan-Memorial Phoenix Project

LOW ENRICHMENT  
FUEL EVALUATION  
AND  
ANALYSIS PROGRAM

Summary Report for the Period  
January, 1981 to December, 1982

William Kerr, Project Director  
Department of Nuclear Engineering  
and the  
Michigan-Memorial Phoenix Project  
The University of Michigan  
Ann Arbor, Michigan

January, 1983

PROJECT PARTICIPANTS

William Kerr

John S. King

John C. Lee

William R. Martin

Reed R. Burn

Joo Hyun Baik

Felippe Beaklini

Clifton Drumm

David Losey

Gerald Munyan

Joao Moreira

James Rathkopf

Gayle J. Stankiewicz

David Wehe

## TABLE OF CONTENTS

LIST OF FIGURES . . . . .	iv
LIST OF TABLES . . . . .	v
I. INTRODUCTION . . . . .	1
II. LEU DEMONSTATION EXPERIMENTS AT THE FNR . . . . .	3
III. SIMULATION AND ANALYSIS OF THE TEST DATA . . . . .	7
A. HEU/LEU Single Element Exchange . . . . .	8
B. LEU Critical Loading . . . . .	8
C. Thermal Flux Maps and Control Rod Worths . . . . .	8
IV. GENERIC METHODS DEVELOPMENT AND VERIFICATION . . . . .	9
A. ENDF/B-IV LEOPARD Library . . . . .	10
B. Lumped Fission Product Correlation through CINDER . . . . .	10
C. Thermal Flux Maps . . . . .	19
D. Ex-Core Spectrum Calculations . . . . .	36
E. Control Rod Worth Calculations . . . . .	39
F. Mixed LEU-HEU Control Rod Worths . . . . .	45
G. Three Dimensional Capability for 2DB-UM . . . . .	49
H. Effective Delayed Neutron Fraction . . . . .	49
V. SUMMARY AND RECOMMENDATIONS FOR FUTURE WORK . . . . .	51
REFERENCES . . . . .	54
APPENDIX A. FNR Demonstration Experiments Part I: Beam Port Leakage Currents and Spectra	
APPENDIX B. FNR Demonstration Experiments Part II: Subcadmium Neutron Flux Measurements	
APPENDIX C. Analysis of the Ford Nuclear Reactor LEU Core	

## LIST OF FIGURES

1.	Irradiated $^{233}\text{U}$ Resonance Integral . . . . .	13
2.	Irradiated $^{233}\text{U}$ Thermal Absorption Cross Section . . . . .	13
3.	Fission Product Group 1 Cross Section for the FNR Fuel . . . . .	14
4.	Fission Product Group 2 Cross Section for the FNR Fuel . . . . .	15
5.	Fission Product Group 3 Cross Section for the FNR Fuel . . . . .	16
6.	Fission Product Group 4 Cross Section for the FNR Fuel . . . . .	17
7.	$\text{D}_2\text{O}$ Fast Absorption Cross Section . . . . .	25
8.	$\text{D}_2\text{O}$ Slowing Down Cross Section . . . . .	26
9.	Thermal Flux Distribution for the December 1981 LEU Core . . . . .	27
10.	Fast Flux Distribution for the December 1981 LEU Core . . . . .	28
11.	SPND Thermal Flux Calculated by the ANISN Code	30
12.	Linear Fit of $\log(\phi(E)/E)$ vs. $E$ for HEU Fuel .	34
13.	Linear Fit of $\log(\phi(E)/E)$ vs. $E$ for LEU Fuel .	35
14.	Neutron Temperature in the Aluminum Sample Holder in HEU and LEU Fuel . . . . .	36
15.	Idealized FNR Geometry for ANDY Calculations .	40
16.	Fast and Thermal Neutron Flux Distributions Calculated by the ANDY Code . . . . .	41
17.	Neutron Flux Spectra Calculated by the ANDY Code . . . . .	42
18.	December 1981 LEU Core Map . . . . .	43
19.	Thermal Flux Distributions for the December 1981 LEU Core . . . . .	46
20.	Fast Flux Distributions for the December 1981 LEU Core . . . . .	47

## LIST OF TABLES

1. Thermal Flux Peaking in Special Element L-57 .	21
2. Thermal Flux Peaking in the Heavy Water Tank .	22
3. Rod Worths for the December 1981 LEU Core . . .	44
4. Control Rod Worths for HEU/LEU Mixed Cores . .	49
5. Effective Delayed Neutron Fraction for the FNR	52

## I. Introduction

The University of Michigan Department of Nuclear Engineering and the Michigan-Memorial Phoenix Project have been engaged in a cooperative effort with Argonne National Laboratory to test and analyze low enrichment fuel in the Ford Nuclear Reactor (FNR). The effort was begun in 1979, as part of the Reduced Enrichment Research and Test Reactor (RERTR) Program, to demonstrate, on a whole-core basis, the feasibility of enrichment reduction from 93% to below 20% in MTR-type fuel designs.

The key technical basis of the low enrichment uranium (LEU) fuel is to reduce the uranium enrichment while increasing, at the same time, the uranium loading of each fuel element in order to compensate for the reactivity loss due to the larger  $^{238}\text{U}$  content. The required uranium loading can be achieved by increasing the uranium density in the fuel meat and by increasing the fuel volume fraction. At the same time it is necessary to insure that fuel elements operate within their thermal-hydraulic limits.

The first phase in our investigation performed in preparation for the LEU fuel testing in the FNR core included (a) initiation of development of experimental and analytical techniques applicable for neutronic evaluation of the MTR-type fuel elements, (b) selection of a LEU design for the FNR, (c) preparation of a preliminary FNR license amendment, and (d) a thermal-hydraulic testing program for the MTR-type fuel elements. The 1979 Summary Report<sup>1</sup> includes a discussion of this initial phase of the FNR LEU project.

Subsequent effort during 1980 was devoted to improving and validating the experimental techniques and analytical methods to be used in characterizing the high enrichment uranium (HEU) and LEU cores for the FNR. The experimental effort focused on the measurement of in-core and ex-core spatial flux distributions and the measurement of ex-core

spectra. In the analytical area, work has continued to improve and verify the computer codes and calculational models used to predict the neutronic behavior of the FNR. This effort included comparisons of predicted results and experimental data for various FNR HEU core configurations as well as predictions of the impact of the LEU fuel on the FNR performance and operation. In addition, a series of thermal/hydraulic tests were performed for the MTR-type fuel elements and an amendment to the FNR Safety Analysis Report was submitted as part of the required License Amendment to the NRC to permit the use of the LEU fuel in the FNR. (Approval was granted in February 1981.) The 1980 Summary Report<sup>2</sup> presents the details of this phase of the LEU project.

The continuation of the project into 1981 culminated with the loading of the LEU core into the FNR and the achievement of initial criticality on December 8, 1981. The critical loading followed one-for-one replacements of HEU fuel elements with LEU fuel elements in the center and periphery of the FNR core. Following the critical loading, approximately six weeks of low power testing of the LEU core was performed including measurement of control rod worths, full core flux maps, and spectral measurements in-core and ex-core. This was then followed by two months of high power testing (2MW), during which similar measurements were taken. These measurements were performed as part of the demonstration experiments portion of the overall FNR LEU testing program. Analytical predictions of the neutronic behavior have also been made and comparisons between measured data and calculated results have been performed. This phase of the LEU project has continued through 1982 and the present report summarizes the experimental and analytical work performed during the two year period.

Section II presents the demonstration experiments and testing portion of the current project, including a detailed



discussion of the measured differences in various neutronic characteristics between the HEU and LEU cores, including spatial in-core and ex-core thermal flux distributions, ex-core (beam port) flux spectra and intensity, control rod worths, temperature coefficients, and xenon worth. Special attention is given to the subject of the measurement of the spatial thermal flux distribution, which is still a topic of current investigation. Section II makes extensive references to two papers<sup>3,4</sup> presented at the International Meeting on Research and Test Reactor Core Conversion from HEU to LEU Fuels, which was held at Argonne National Laboratory during the period November 8-10, 1982. These two papers are included as Appendices A and B to this Summary Report

Section III is devoted to the analysis of the FNR HEU and LEU core configurations and comparison with the data measured as part of the demonstration experiments portion of the LEU project. The comparisons between calculation and experiment include differential reactivity comparisons of single HEU and LEU elements, critical mass of the initial LEU core, control rod worths, various reactivity coefficients, and spatial distributions of the thermal flux, both in-core and ex-core. Similar to the discussion of the experimental program in Section II, Section III makes extensive references to a paper<sup>5</sup> presented at the aforementioned International Conference, which discusses the analysis of the LEU core and comparison with experiment and which has been included as Appendix C to this Summary Report.

The FNR LEU project has also been involved to a significant extent in the area of generic methods development for MTR-type research and test reactors. Section IV summarizes the work performed in this area over the past two years, including significant results and the status of tasks currently under investigation.

Section V summarizes the current status of the overall project, including a discussion of the tasks currently under

investigation. The principal unresolved issues are identified and recommendations are made for future effort to complete the current and planned tasks.

## II. LEU DEMONSTRATION EXPERIMENTS AT THE FNR

The Demonstration Experiments Program in this 1981-1982 report period has by and large completed the measurements on the first full LEU core required for a comparison with similar measurements made on the HEU core in the previous year. This has included mapping of subcadmium neutron fluxes in core and in H<sub>2</sub>O and D<sub>2</sub>O reflectors, thermal neutron leakage current and spectrum at beam port exits, Rhodium cadmium fractions in core and in reflectors. The comparisons of fast spectra in the LEU fuel are still in progress. Other comparison data are discussed in detail in two papers entitled FNR Demonstration Experiments, Parts I and II, presented at the Argonne National Laboratory International Meeting of November 8-10, 1982. These are reproduced as Appendices A and B in this report.

Particular effort was made to maintain the data acquisition instrumentation unchanged between the period of equilibrium HEU operation until the beginning of LEU operation in December, 1981, and throughout the LEU power operation during the first four months of 1982. Three LEU configurations were examined from January 1 through April, 1982. To verify the reproducibility of detection, a reloading back to the equilibrium HEU core was examined in May, 1982.

During the course of the LEU observations it became increasingly evident that measured subcadmium flux profiles were strongly affected by the "small core" geometry of the fresh LEU load as opposed to the "large core" equilibrium HEU core. A series of "high leakage" (HL-HEU) loadings were examined beginning in July, 1982 and extending through October, 1982. These cores retained the small core (five element) width of the LEU core in one dimension (North-South). They demonstrate that this first FNR demonstration comparison is complicated by the large change in buckling necessitated by a clean LEU critical loading.

While much of the data confirmed expected changes in

flux levels, the series of experiments of early 1982 uncovered several unexpected experimental results. Two of these are of particular importance. The foremost problem is a lack of agreement between subcadmium profiles in the  $D_2O$  reflector, relative to core center flux, when measured by our Rhodium Self Powered Neutron Detector (SPND) and when measured by both iron and rhodium wire activation. As a consequence, a number of simultaneous SPND and activation observations were initiated in late 1982 but as yet the experimental discrepancy remains unresolved. Since the SPND has been the workhorse flux map instrument, and no wire activations were thought necessary during the LEU power cycles, this discrepancy leaves the measured  $D_2O$  reflector fluxes in doubt. A second, related problem is the apparent disagreement in the ratio of LEU to HEU beam port leakage currents when measured (a) in the conversion of HEU (9-81) to LEU (1-82), as opposed to (b) the reverse conversion of LEU (4-82) to HEU (5-82). This disagreement is detailed in Table I of Appendix A. It is presumed to be due to changes in the LEU East-West loading geometries of (1-82) and (4-82). It is complicated by the fact that the leakage pattern was found to be sensitive to the source plane position and beam departure angle in the  $D_2O$  reflector tank. It would be desirable to remeasure a given LEU-HEU conversion again if only to resolve these two questions.

Despite these difficulties, the confirming results of the experimental program are substantial. We may list highlights of these results here, and refer the reader to Appendices A and B for detailed exploration:

1. Replacement of a fresh HEU element by a fresh LEU element at the center of the HEU equilibrium core reduced the midcore flux in that element by a factor of  $1.19 \pm 0.036$ . Well within experimental uncertainty, this is equal to the ratio of the LEU to HEU U-235 masses.
2. Whole core replacement of the 38 element equilibrium HEU core by a nearly unburned (<3%) 31 element LEU

core (LEU 4-82) reduced the subcadmium flux averaged over the five central core elements by a factor of  $1.17 \pm 0.02$ .

3. Simultaneous with the depression in core flux in 2), the reflector peak fluxes increased by factors of 1.53 in  $H_2O$  and 1.17 in  $D_2O$  at midcore height. These factors are dominated by the change in leakage geometry, as demonstrated by a similar response from the high leakage HEU profiles (HL-HEU 7-82). Lower factors are to be anticipated for larger equilibrium LEU cores.
4. A mild hardening of the core spectrum was demonstrated by measured cadmium fractions from rhodium wire activations. No spectral hardening was evident for the leakage currents from beam ports facing the outer edges of the  $D_2O$  reflector.

### III. SIMULATION AND ANALYSIS OF THE TEST DATA

#### A. HEU/LEU Single Element Exchange

The single element exchange experiment was performed to ascertain some of the performance differences of the LEU and HEU elements before the full LEU core was loaded into the FNR. The exercise also provided an opportunity for verification of our analytical models. The element exchange was performed by substituting a fresh LEU fuel element for a fresh HEU fuel element in an equilibrium HEU core. The swap was made twice at two different locations: at the center and periphery of the core. The exact element locations, the experimental procedure, the experimental and analytical results, together with an explanation of the analysis are presented in Appendix C.

In summary, the reactivity effects of the exchanges predicted with the perturbation code, PERTV<sup>6</sup>, agree very well with the experimental data. The LEU element was found to be less reactive than the HEU element at the center of the core but more reactive at the edge because of the "leaky" nature of the LEU fuel.

#### B. LEU Critical Loading

The first complete loading of an LEU core into the FNR took place on December 1981. The two-day loading procedure was completed at about noon on December 8 with the placement of the 23rd LEU element. At that point the reactor was slightly super-critical when all shim rods but not the regulating rod were withdrawn.

Simulation of the critical loading sequence by the 2DB-UM<sup>7</sup> code using each of the two libraries (old library and ENDF/B-IV library) for the LEOPARD code<sup>8</sup> demonstrates the superiority of the new data set. The calculations made with the old library predict the final critical core configuration to be sub-critical, whereas the ENDF/B-IV library correctly predicts the core to be slightly super-critical. A

more complete description of the results of the experiment, the sequence of fuel insertion, and the analytical calculation are given in Appendix C.

### C. Thermal Flux Maps and Control Rod Worths

Simulation of the measured thermal flux distribution and control rod worths for various LEU and HEU configurations was performed with the 2DB-UM code as described in detail in Appendix C. With a standard 6x6 mesh per assembly structure and LEOPARD-generated two-group cross sections for the unrodded fuel assemblies, the calculations generally agree well with the measured flux in the core region. Calculations reported in Appendix C, however, indicate that thermal flux peaking in the water hole in the special elements is underpredicted in the calculations. In addition, the thermal flux distribution in the core region near the heavy water reflector appears to be slightly underpredicted in the 2DB-UM calculations. For the heavy water tank itself, 2DB-UM results compare fairly well with the thermal flux distributions determined from iron wire and rhodium wire measurements. As noted in Appendix C, however, there is a considerable discrepancy between the thermal flux in the heavy water reflector determined from the SPND measurements and the corresponding wire activation measurements. Active investigation is underway to understand and resolve this discrepancy in thermal flux data in and around the heavy water reflector. Our recent activities in this area are summarized in Section IV.C.

Simulation of the shim rod worth data presented in Appendix C indicates favorable agreement for rods A and C, while rod B worth is overpredicted to a significant extent in the standard 2DB-UM calculations. This discrepancy appears to be also related to the accuracy in our overall flux distribution calculation. Results of recent investigation in this area, including the parametric studies performed, are discussed in Section IV.E.

#### IV. GENERIC METHODS DEVELOPMENT AND VERIFICATION

##### A. ENDF/B-IV LEOPARD Library

A new library for the LEOPARD code containing ENDF/B-IV data has been developed as reported in Ref. 9. The new library is necessary to remedy differences observed between data generated by the EPRI-HAMMER<sup>10</sup> and LEOPARD codes. Modifications were made to the LEOPARD code to accommodate the new library and to update some of the physical constants "hardwired" into the code. The new library and the modified version of the LEOPARD code have been verified extensively by the simulation of critical experiments, comparison with established benchmark codes, and modeling of the depletion of fissile fuel in pressurized water reactor (PWR) fuel. The verification process is described in detail in Ref. 2.

The effects of the ENDF/B-IV library have been summarized in Appendix C. On the average, the multiplication constants obtained for the fifty-five cold, clean lattices with the new library were closer to 1.0 than were the results with the old library. Better, but not perfect, agreement between the EPRI-HAMMER and LEOPARD codes has also been achieved. The comparisons between the measured concentrations of actinides in PWR fuel and those calculated with the two LEOPARD libraries indicate that their differences are slight and that both libraries model the burnup and depletion of the actinides to similar accuracy. The LEOPARD code can now be used with more confidence because of the increased reliability of the ENDF/B-IV data over the old industrial data set of the original library.

##### B. Lumped Fission Product Correlation through CINDER

As a means to account for the poisoning effect of fission products easily and efficiently, the LEOPARD code calculates lumped fission product cross sections at each burnup step. The cross sections, expressed in terms of barns per fission, represent the sum of the cross sections of all in-



dividual fission product nuclides except  $^{135}\text{Xe}$  and  $^{149}\text{Sm}$  which are handled explicitly in the code. The aggregate cross section for the thermal group is calculated by means of a third order polynomial in fuel burnup. In the fast energy range, only the epithermal (group 3) cross section is considered, again by a polynomial but of the second order in burnup. The correlations that were previously in LEOPARD were originally intended for only slightly enriched fuel (approximately 3%), and have been used to date in our neutronic analysis for the FNR core with a crude adjustment to account for greater enrichments.

In an effort to verify and improve the calculation of the lumped fission product cross sections, the EPRI-CINDER code<sup>11</sup> was modified to run on Amdahl 470V/8 computer at The University of Michigan. The EPRI-CINDER code is a point-depletion code that uses detailed fission product decay chains.

Simulation of PWR fuel with 2.6%  $^{235}\text{U}$  by both the EPRI-CINDER and LEOPARD codes indicates significant disagreement in the fission product cross sections obtained by the two codes.<sup>12</sup> The value calculated by the LEOPARD code for the epithermal absorption cross section,  $\sigma_3$ , is nearly 50% greater at beginning of life and 20% greater after fuel burnup of 20,000 MWD/tonne of uranium than the EPRI-CINDER values. The thermal absorption cross section for neutron energy of 0.025 eV,  $\sigma_0$ , shows even larger disagreement: nearly 60% over the entire depletion history.

Comparison of results from the original CINDER code<sup>13</sup> (the predecessor to EPRI-CINDER), EPRI-CINDER, and LEOPARD simulations of 3.4% enriched PWR fuel indicates that the correlation incorporated into the LEOPARD code was probably based on calculations with the original CINDER code or a program similar to it. The CINDER and LEOPARD results agree quite well with one another but not with those of EPRI-CINDER. The EPRI-CINDER results, with the ENDF/B-IV data

base for fission products, are expected to be more accurate than the old CINDER calculations. This has been verified by an EPRI-CINDER simulation of a detailed experiment performed to measure the fission product poisoning in  $^{233}\text{U}$  fuel irradiated in the Material Testing Reactor.<sup>14</sup> The EPRI-CINDER results agree fairly well with the experimental data. Figures 1 and 2 show the experimental and calculated values for the fission product resonance integral and thermal absorption cross section, respectively, as a function of irradiation time.

As in the case of the PWR-type fuel calculations, the simulation of the four primary FNR fuel types--HEU and LEU, regular and special fuel elements--by the two codes, LEOPARD and EPRI-CINDER, yield significant disagreement in the calculated fission product cross sections as seen in Figures 5 and 6. Note that the LEOPARD correlation used to date produces only one curve for each enrichment, be it for a special or regular fuel element. The LEOPARD cross sections are larger than the EPRI-CINDER results, as much as 90% in the case of the HEU regular fuel element. Because of this drastic discrepancy, new LEOPARD lumped fission product cross section correlations have been formulated based on the results of the EPRI-CINDER code.

In the new fission product correlations for the LEOPARD code, cross sections are correlated as a function of fuel burnup, where burnup is given in units of MWD/tonne of  $^{235}\text{U}$  rather than in the traditional units of MWD/tonne of U. This yields more precise correlations than possible with burnup variables chosen in other units. Figures 3 through 6 show fission product absorption cross sections for all four groups vs. fuel burnup in MWD/tonne of  $^{235}\text{U}$ .

The actual correlations in the form of polynomials were derived from the burnup-dependent absorption cross sections plotted in Figures 3 through 6. In the case of the fast-group cross sections,  $\sigma_1$ ,  $\sigma_2$ , and  $\sigma_3$ , the data for all four

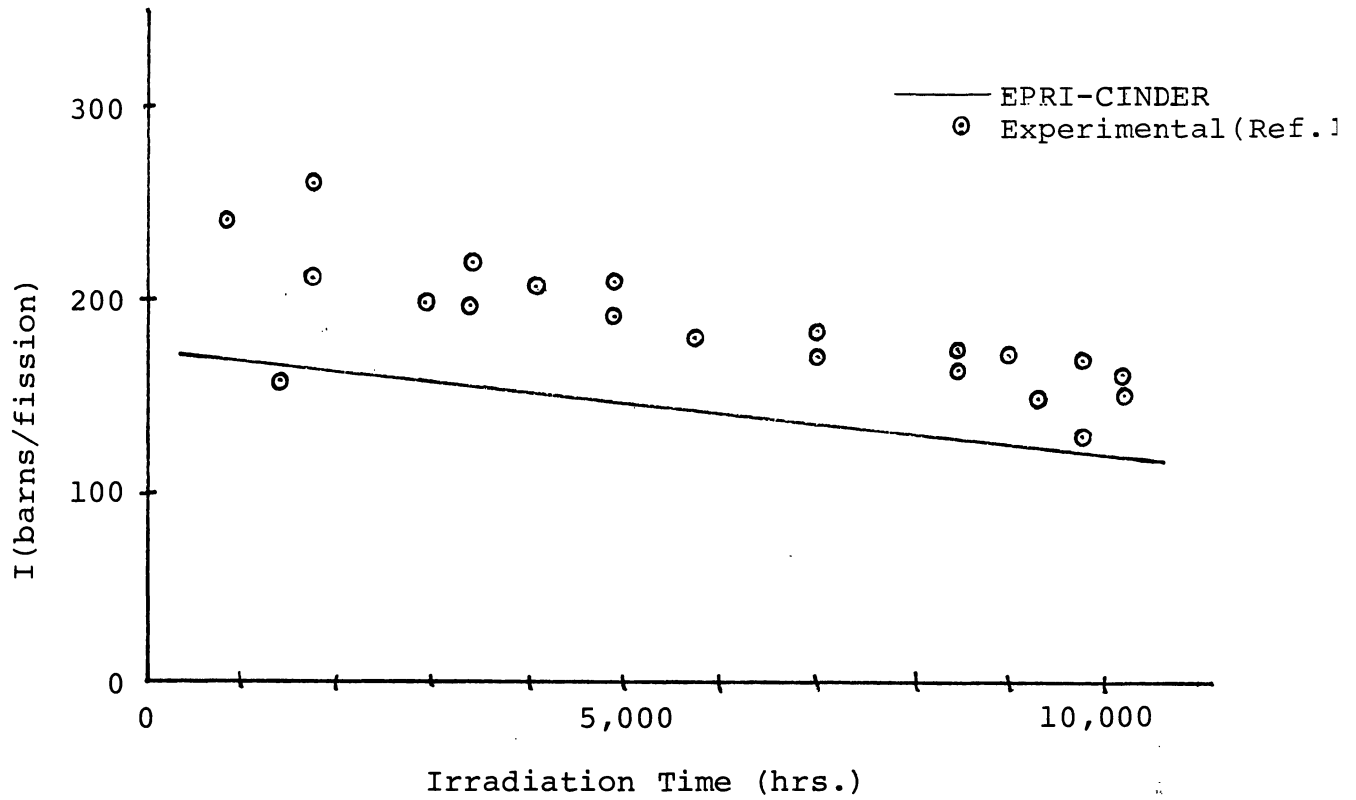


Figure 1. Irradiated  $^{233}\text{U}$  Resonance Integral

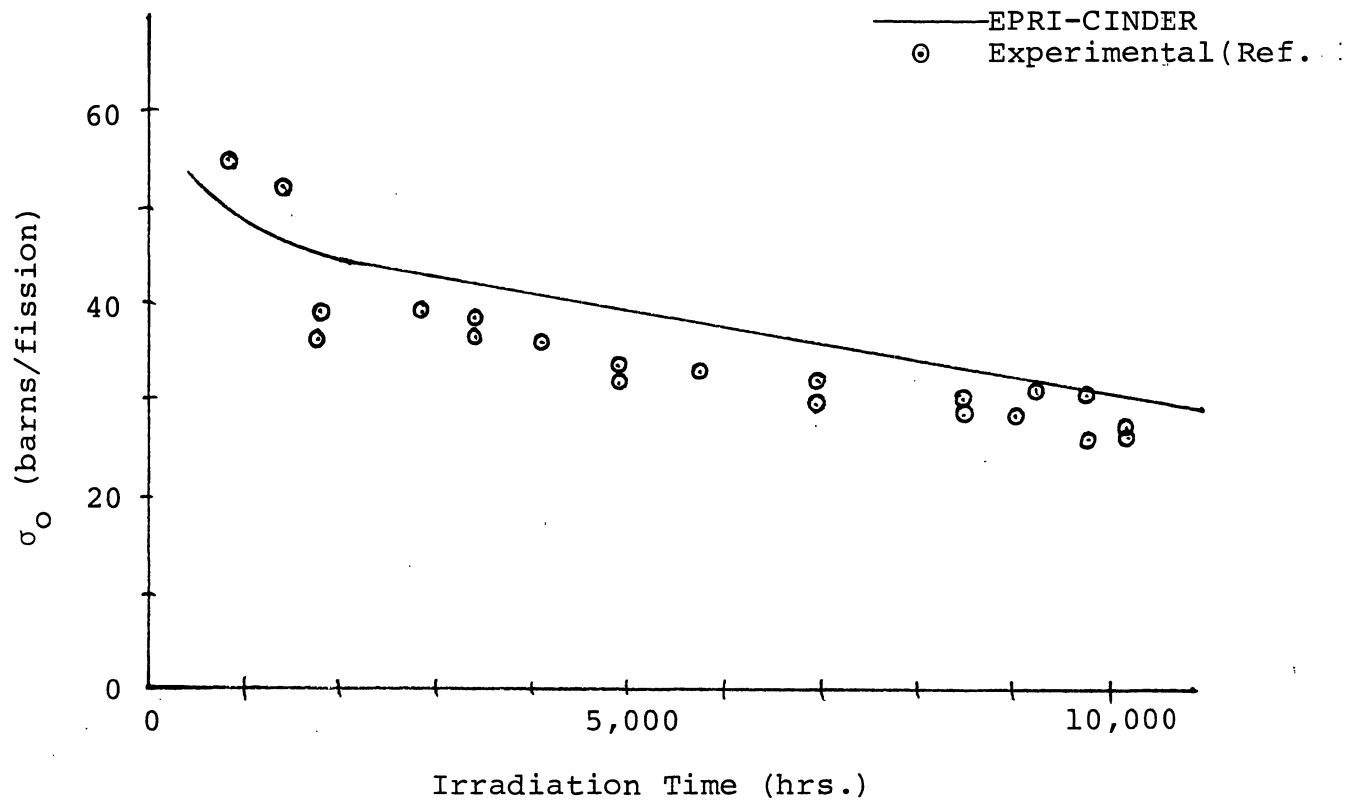


Figure 2. Irradiated  $^{233}\text{U}$  Thermal Absorption Cross Section

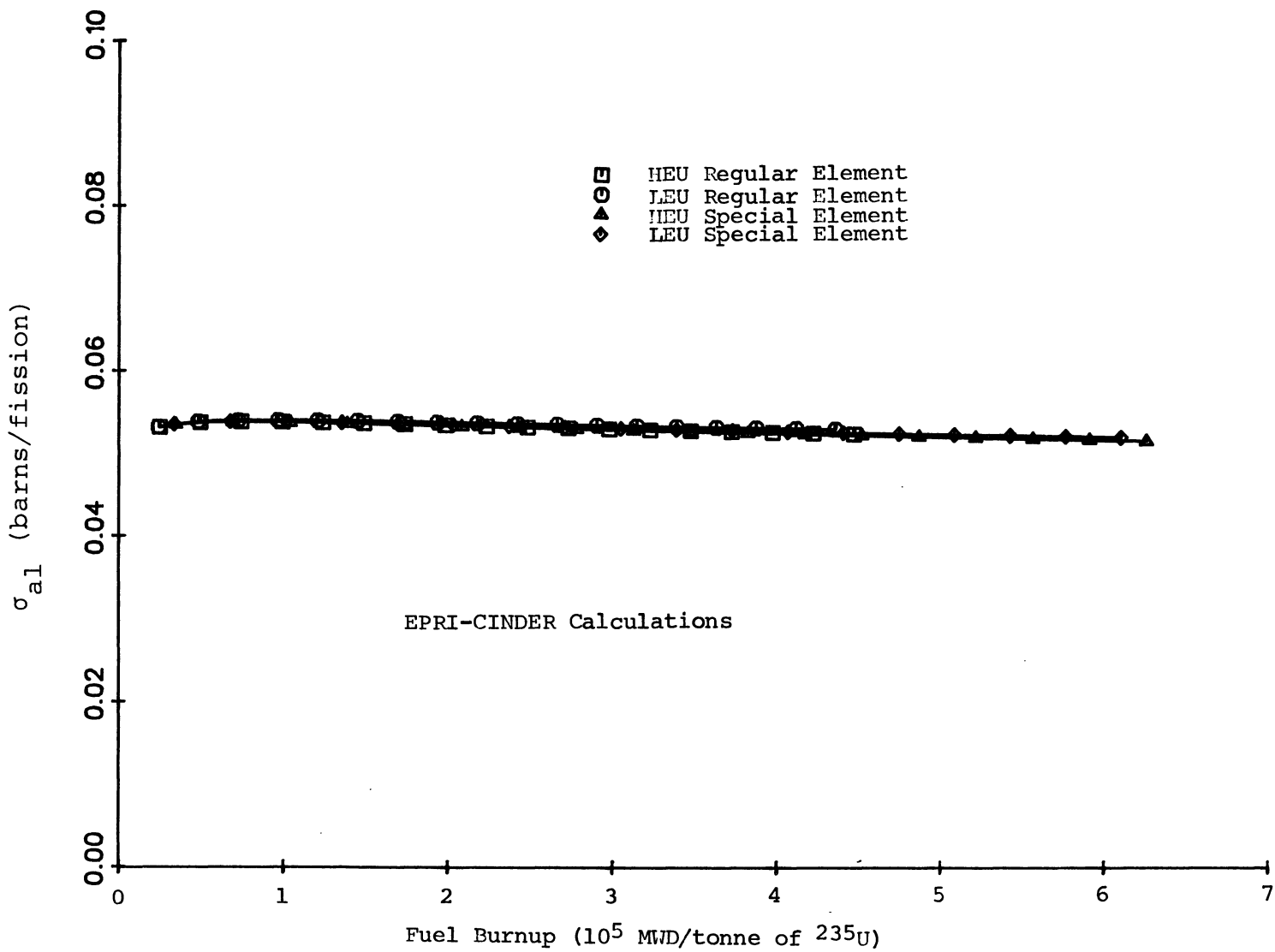


Figure 3. Fission Product Group 1 Cross Section for the FNR Fuel

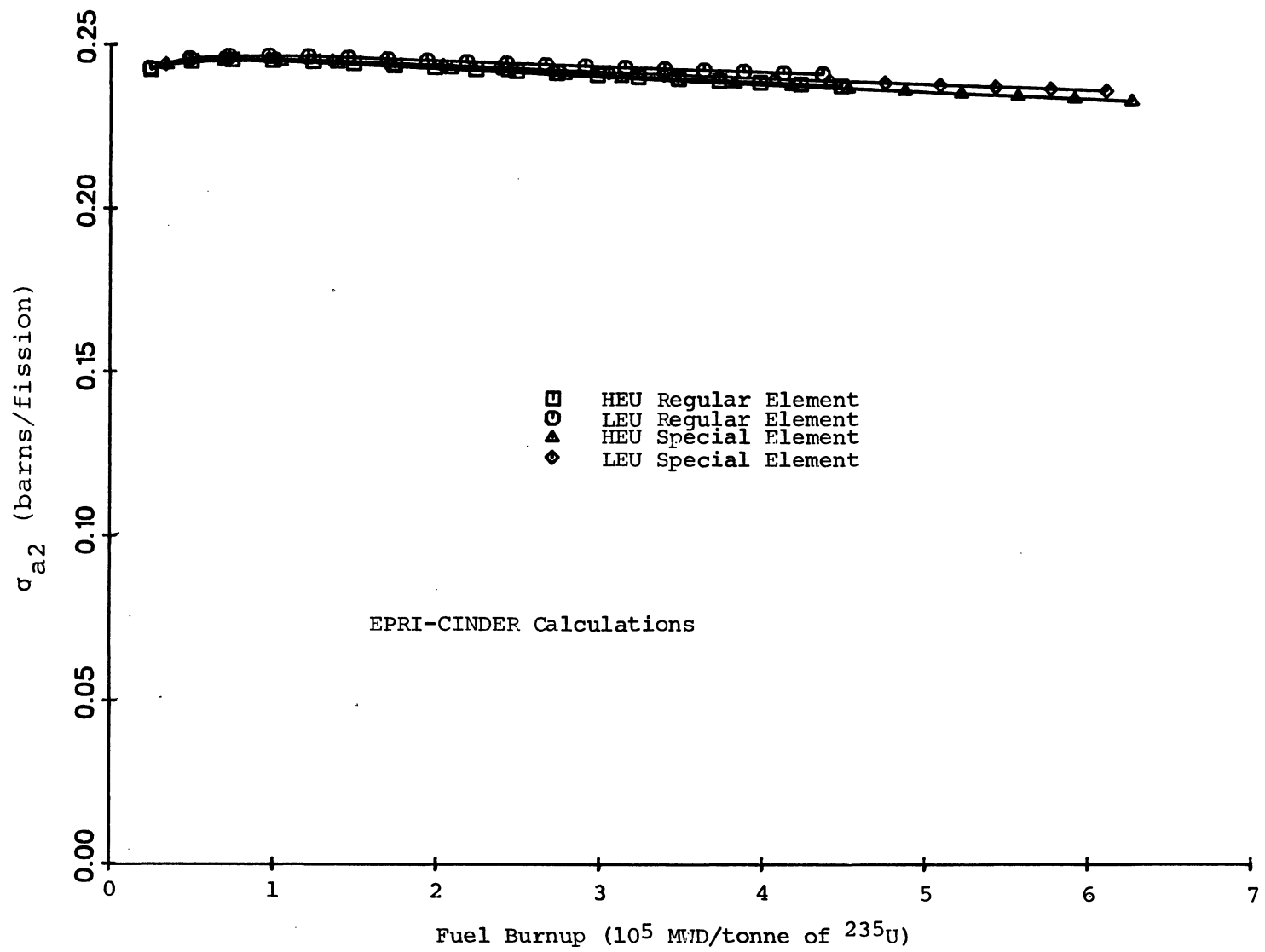


Figure 4. Fission Product Group 2 Cross Section for the FNR Fuel

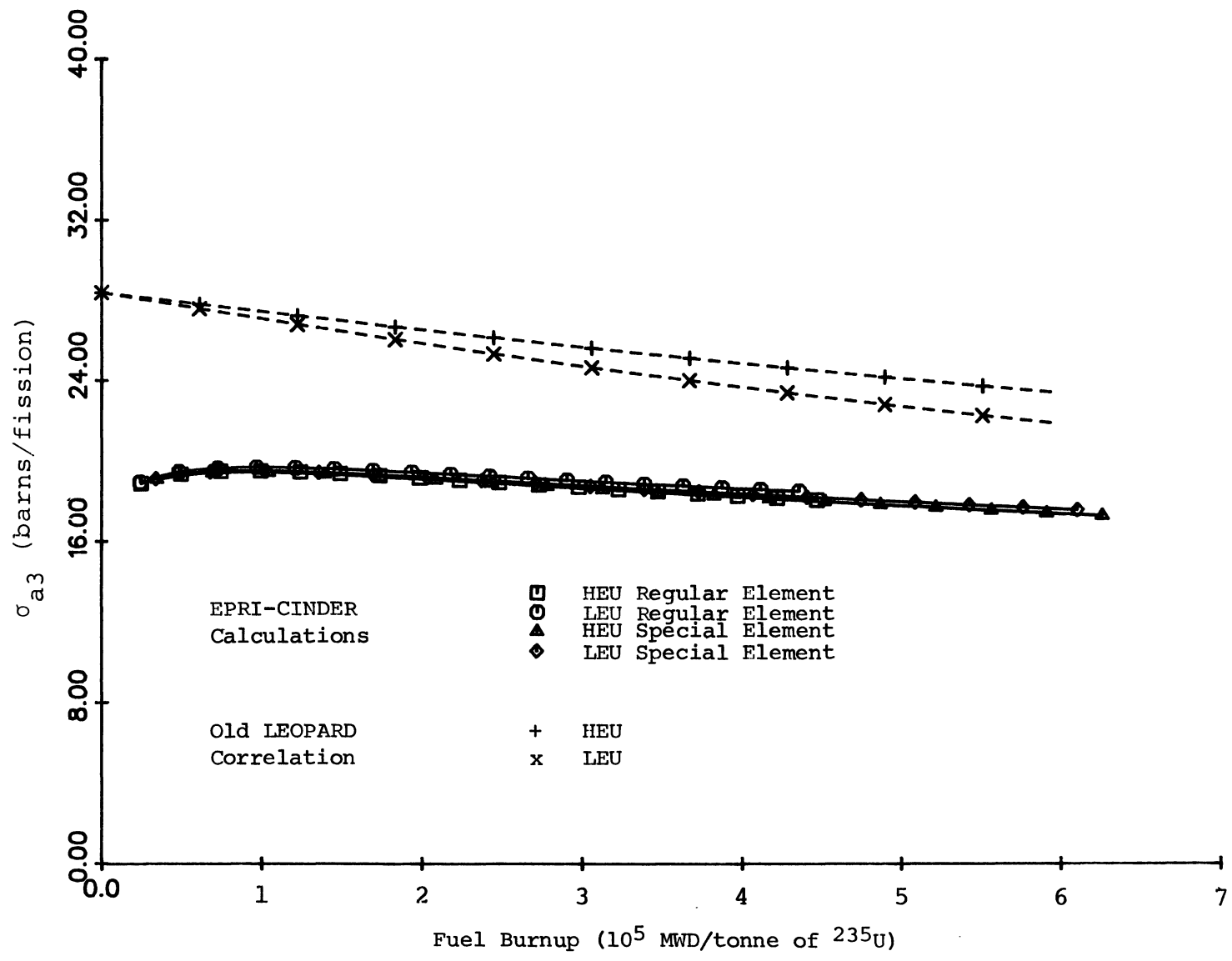


Figure 5. Fission Product Group 3 Cross Section for the FNR Fuel

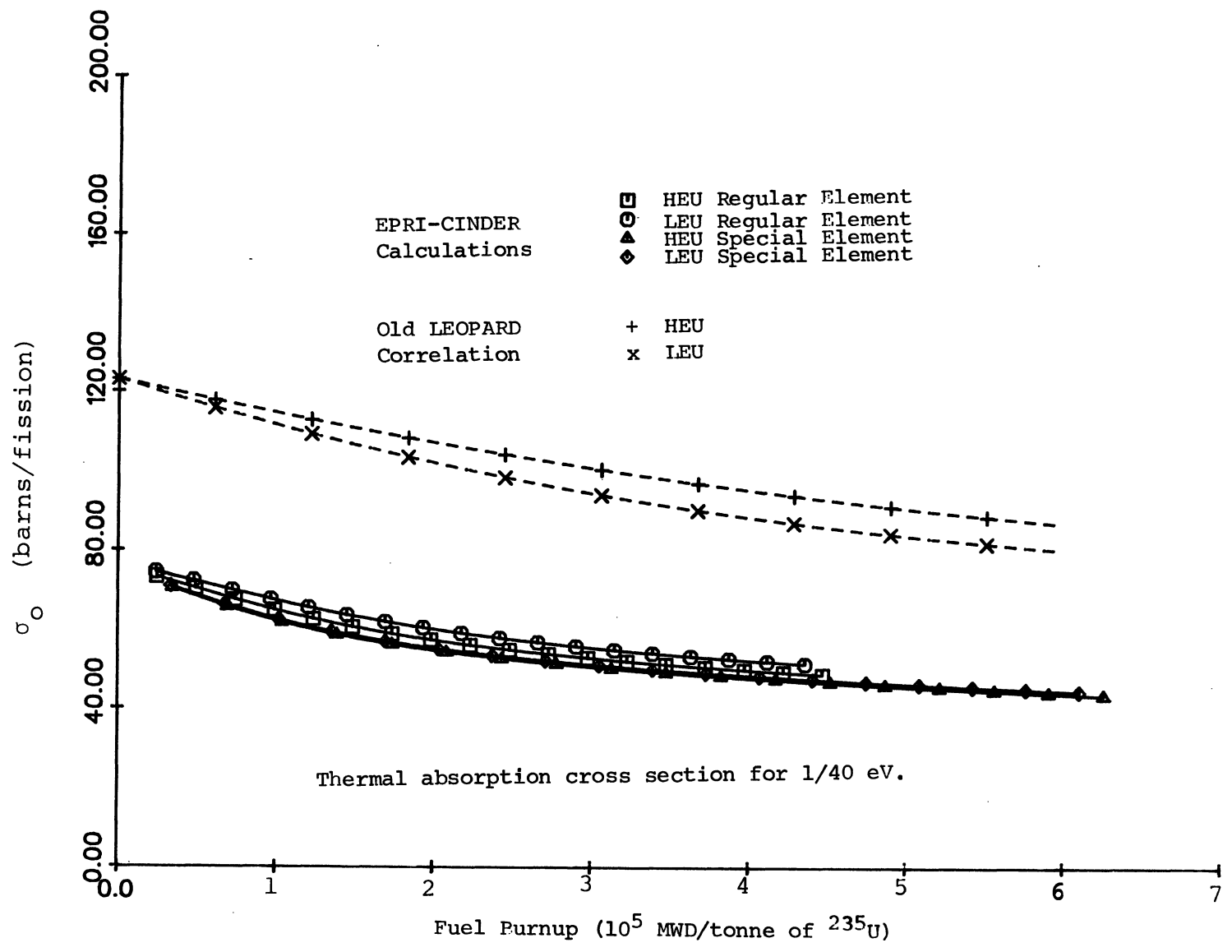


Figure 6. Fission Product Group 4 Cross Section for the FNR Fuel

fuel types were used together to derive a single correlation for each group. For the 0.025 eV cross section  $\sigma_0$ , because the differences between the fuel types are relatively large, only the data for the HEU special fuel element were used to correlate the burnup dependence. Another correlation to represent the differences between fuel types was derived by taking advantage of the different amounts of fuel and water present in the various fuel types. This correlation takes the form

$$\sigma_0(r) = \sigma_{0,HS} C_1 \{1 + C_2 \exp(-C_3 r)\}$$

where  $r$  is the ratio of hydrogen atoms to  $^{235}\text{U}$  atoms in the unit cell at beginning of life,  $\sigma_{0,HS}$  is the thermal cross section for the HEU special element obtained as a polynomial in fuel burnup in units of MWD/tonne of  $^{235}\text{U}$ , and  $C_1$ ,  $C_2$ , and  $C_3$  are derived constants. The data used in deriving these three constants were the values for  $\sigma_0$  for the four fuel types at a burnup of 100,000 MWD/tonne of  $^{235}\text{U}$ . The lumped fission product correlations derived in our study are simple but sufficiently accurate. The maximum deviation between the correlations and the EPRI-CINDER results is observed to be about 4% for low fuel burnup for the LEU regular element, with the deviations usually less than 1% for all four groups and four fuel types.

With the new fission product correlations, LEOPARD calculations were performed to generate few-group constants for the 2DB-UM code. Comparison of the eigenvalues calculated by the 2DB-UM code with those of the identical test cases with a library utilizing the old burnup correlation indicates the effect is small but significant. The test case simulated the June 1977 HEU critical experiment, with the old correlations yielding an eigenvalue of 1.0139 compared with a value of 1.0182 obtained with the new correlations.

The HEU and LEU batch core depletion tests illustrate



the differences more completely, for fuel depletion is the basis of the correlation. The difference in the eigenvalue for the two correlations increases almost linearly with fuel depletion. The eigenvalues with the new correlations are greater than those with the old as a consequence of the overprediction in the absorption cross sections by the old correlations. At the end of life at 200 days of depletion, the differences amount to 0.68% for the HEU and 0.54% for the LEU core.

The new LEOPARD fission product correlations duplicate the EPRI-CINDER results quite well for the four FNR fuel types analyzed, thus eliminating a known deficiency of the LEOPARD code. The repercussions of the modification are not dramatic but significant enough to merit further study.

### C. Thermal Flux Maps

A substantial amount of effort was made between December 1981 and October 1982 to measure the thermal flux distribution for various LEU and HEU core configurations, as described in Appendix B. As explained in Appendix B, three methods were used to measure the thermal flux, iron wire activation, rhodium wire activation, and SPND measurements. A substantial amount of effort was also made during the same period to model the measured thermal flux distributions by 2DB-UM calculations, as described in Appendix C. The methods used to calculate the thermal flux distributions are described in Appendix C.

As noted in the appendices, there are several areas of inconsistency in the measurements and the calculations, the main problem being the large difference between the wire activations and the SPND measurements in the heavy water tank. In order to resolve these inconsistencies, calculations were performed to determine the sensitivity of the thermal flux to various parameters. This study is not yet complete, but it appears at the present time that the thermal flux distribution is most sensitive to the absorption and slowing

down cross sections in the non-lattice regions of the core and in the H<sub>2</sub>O and D<sub>2</sub>O reflectors. Moreover, these particular cross sections have the most uncertainty associated with them because of the significant global spatial/spectral coupling in these regions, especially in the D<sub>2</sub>O tank. This coupling makes the traditional unit cell approach for generating cross sections somewhat uncertain.

Parametric calculations have been performed to study the thermal flux peaking in the special fuel elements and in the heavy water tank, and the sensitivity of the SPND detector in the core and reflector regions. The results of these calculations and comparisons with experiments are summarized below.

#### 1. Flux Peaking in the Special Element Water Hole

The special fuel elements contain fewer fuel plates than do the regular fuel elements, and have in place of the center fuel plates a water hole, for the insertion of control rods and sample holders. Table 1 compares the measured and calculated flux peaking in the special element at location L-57 for the April 1982 LEU core. Comparison is made here in terms of the ratio of the thermal flux at the center of the special element located at L-57 to the flux at the center of the core at L-37.

The flux distributions compared in Table 1 were obtained with the 2DB-UM code. The reference calculation, performed with a standard mesh structure of 6x6 meshes per assembly, and lattice and non-lattice cross sections generated with the LEOPARD code, underpredicts the flux peaking compared with the experimental data. In order to determine the adequacy of the 6x6 mesh structure to accurately model the flux peaking, another 2DB-UM calculation was performed with a 12x12 mesh per assembly structure. The 12x12 mesh calculation essentially had no effect on the results.

Table 1

## Thermal Flux Peaking in Special Element L-57

Measurement or Calculation	Thermal Flux Ratio L-57/L-37
SPND Data . . . . .	2.05
6x6 2DB-UM calculation with LEOPARD Non-Lattice Cross Sections . . . . .	1.65
12x12 2DB-UM calculation with LEOPARD Non-Lattice Cross Sections . . . . .	1.66
6x6 2DB-UM calculation with EPRI-HAMMER Non-lattice Cross Sections . . . . .	1.83

The cross sections for the water hole of the special elements are computed with the LEOPARD code by including a large non-lattice region (half of the total cell) and using edited non-lattice cross sections for the waterhole. In order to determine the sensitivity of the flux peak to the cross sections used in the water hole region, the cross sections for the water hole were generated with the EPRI-HAMMER code in the third calculation compared in Table 1. This resulted in a larger thermal flux peak in the special elements, as is shown in Table 1, and better agreement with experiment. However, the use of a one-dimensional transport code such as EPRI-HAMMER for this analysis may still be inadequate due to the complex geometry of the special element and surrounding fuel. Therefore, we will consider the possibility of generating accurate cross sections for the special elements using a two-dimensional transport theory code which should be capable of treating this particular geometry.

## 2. D<sub>2</sub>O Tank Flux Peaking

Thermal flux distributions in the D<sub>2</sub>O tank have been calculated with the 2DB-UM code to simulate the experimental data obtained with the SPND and wire activations. Table 2

compares the ratios of the thermal flux at position X in the D<sub>2</sub>O tank to the flux at the center of the core at L-37 for the October 1982 HEU core and for the April 1982 LEU core. The location of position X is shown in the FNR diagrams in Appendix B of Ref. 1.

Table 2  
Thermal Flux Peaking in the Heavy Water Tank

Measurements or Calculations	Thermal Flux Ratio D <sub>2</sub> O X/L-37
October 1982 HEU Core	
Iron Wire Activation . . . . .	.82
Rhodium Wire Activation . . . . .	.88
Rhodium SPND . . . . .	1.23
Calculation . . . . .	.81
April 1982 LEU Core	
Rhodium SPND . . . . .	1.61
6x6 Mesh Calculation Control Rods Out LEOPARD D <sub>2</sub> O Cross Sections	.901
12x12 Mesh Calculation Control Rods Out LEOPARD D <sub>2</sub> O Cross Sections	.904
6x6 Mesh Calculation Control Rods Out LEOPARD D <sub>2</sub> O Cross Sections Zero Axial Buckling in the Heavy Water Tank .	1.28
6x6 Mesh Calculation Control Rods In LEOPARD D <sub>2</sub> O Cross Sections	.895
6x6 Mesh Calculation Control Rods Out ANISN D <sub>2</sub> O Cross Sections .	1.26

The reference 2DB-UM calculations for both core configurations were performed with 6x6 meshes per assembly and

lattice and non-lattice cross sections generated with the LEOPARD code. From Table 2 it can be seen that the flux peak in the D<sub>2</sub>O tank measured by wire activations is significantly less than that measured by the SPND. The calculations agree well with the wire activations, but not with the SPND measurements.

A 2DB-UM calculation with 12x12 meshes per assembly was done to assess the adequacy of the 6x6 mesh structure for the LEU core, which indicates a very slight difference compared with the 6x6 mesh result. In order to determine the sensitivity of the D<sub>2</sub>O flux peak to the axial buckling in the D<sub>2</sub>O tank region, the D<sub>2</sub>O tank buckling was artificially adjusted. The results of the 2DB-UM calculation for zero D<sub>2</sub>O tank buckling is also given in Table 2. Although the increase in D<sub>2</sub>O flux is substantial, this parametric variation is quite unrealistic, and gives only an upper bound to the buckling effect.

Flux measurements are normally made with regulating rod partially inserted, but the partial insertion of control rods is difficult to model in a two-dimensional calculation. Normally, the fluxes are calculated with the 2DB-UM code with the rods assumed fully withdrawn. In order to investigate the effect of the control rod insertion on the spatial flux distribution, the flux distribution was recalculated for the LEU configuration with the rods assumed fully inserted. It is expected that the actual flux would lie somewhere between the calculation with rods withdrawn and that with rods inserted. The insertion of the control rods shifted the in-core flux away from the D<sub>2</sub>O tank, but had almost no effect on the flux within the D<sub>2</sub>O tank, as is shown in Table 2.

The D<sub>2</sub>O cross sections that have been used in the calculations were computed with the LEOPARD code, by using the method discussed in the previous section of this report. These cross sections have also been calculated with the

ANISN code,<sup>15</sup> a one-dimensional transport theory code. In this ANISN calculation, the core and reflector regions were modelled in slab geometry with a 30 group cross section set which was collapsed from a 123 group set with the XSDRN code.<sup>16</sup> The fast group absorption cross section from the ANISN code was significantly less than the LEOPARD value, and the ANISN slowing-down cross section was significantly larger than the LEOPARD value as is shown in Figures 7 and 8. The fast absorption cross section calculated by the LEOPARD code is  $4.7 \times 10^{-4} \text{ cm}^{-1}$ , an order of magnitude greater than the value calculated by the ANISN code. The ANISN calculation also showed that the D<sub>2</sub>O fast absorption and slowing down cross sections vary with penetration into the D<sub>2</sub>O tank, illustrating the spatial/spectral coupling in the D<sub>2</sub>O tank.

Flux distributions calculated with the 2DB-UM code using the heavy water cross sections from the ANISN run showed a substantially larger thermal flux peaking in the heavy water tank than the calculations with LEOPARD D<sub>2</sub>O cross sections. The use of ANISN heavy water cross sections also caused a shift in the in-core flux toward the heavy water tank, bringing the flux calculation into better agreement with the SPND measurements, but into larger disagreement with the wire activations. Comparisons of the flux distributions calculated with the 2DB-UM code using LEOPARD- and ANISN-generated D<sub>2</sub>O cross sections for the December 1981 LEU core are shown in Figures 9 and 10. The comparisons are for the thermal and fast flux distributions, respectively, in a north-south scan through the core. The ratio of the thermal flux in D<sub>2</sub>O tank position X to that at the core center obtained in this calculation with the ANISN cross sections is compared with the other calculations for the April 1982 LEU core in Table 2.

Future work in this area will involve the determination of more accurate D<sub>2</sub>O cross sections as a function of

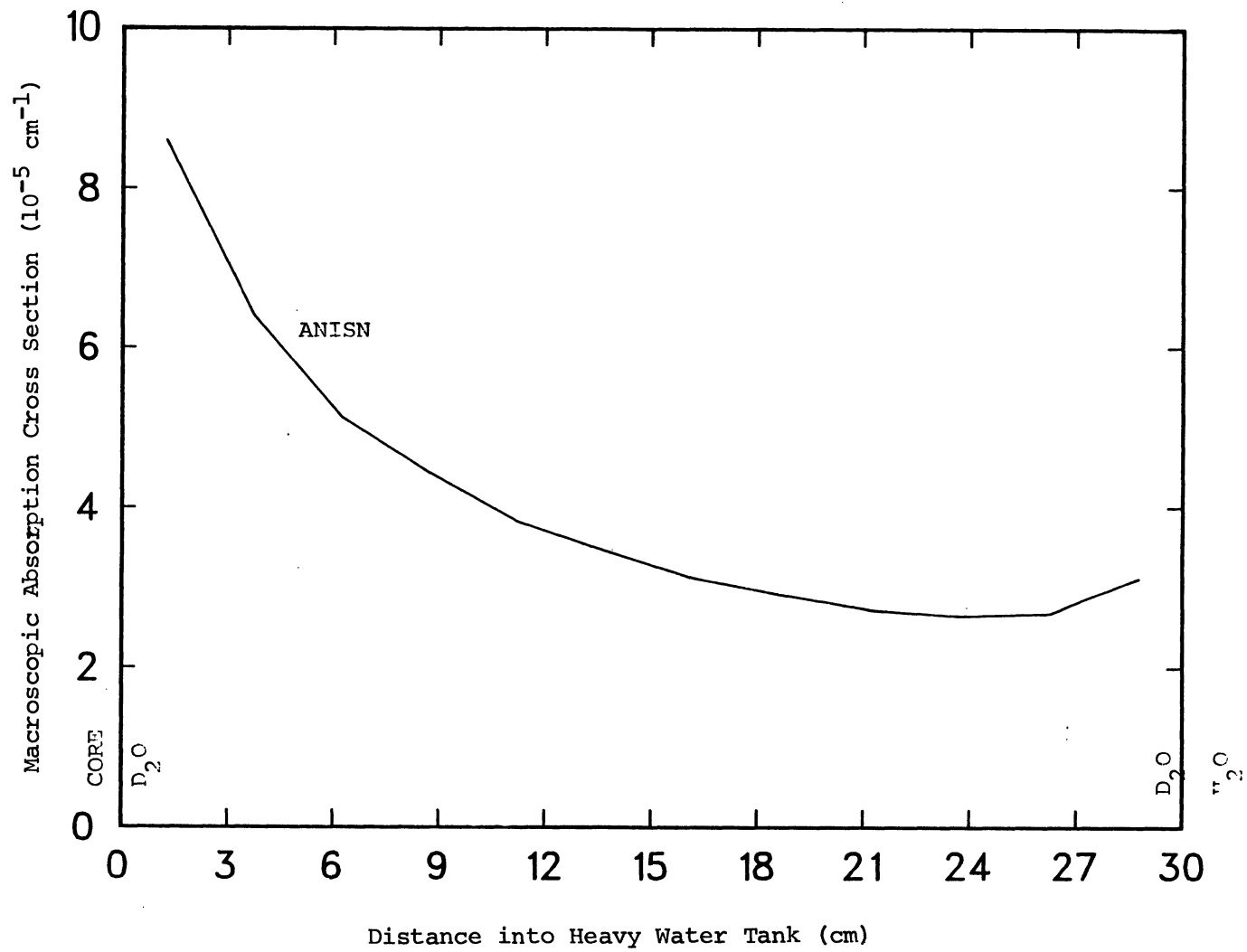


Figure 7. D<sub>2</sub>O Fast Absorption Cross Section

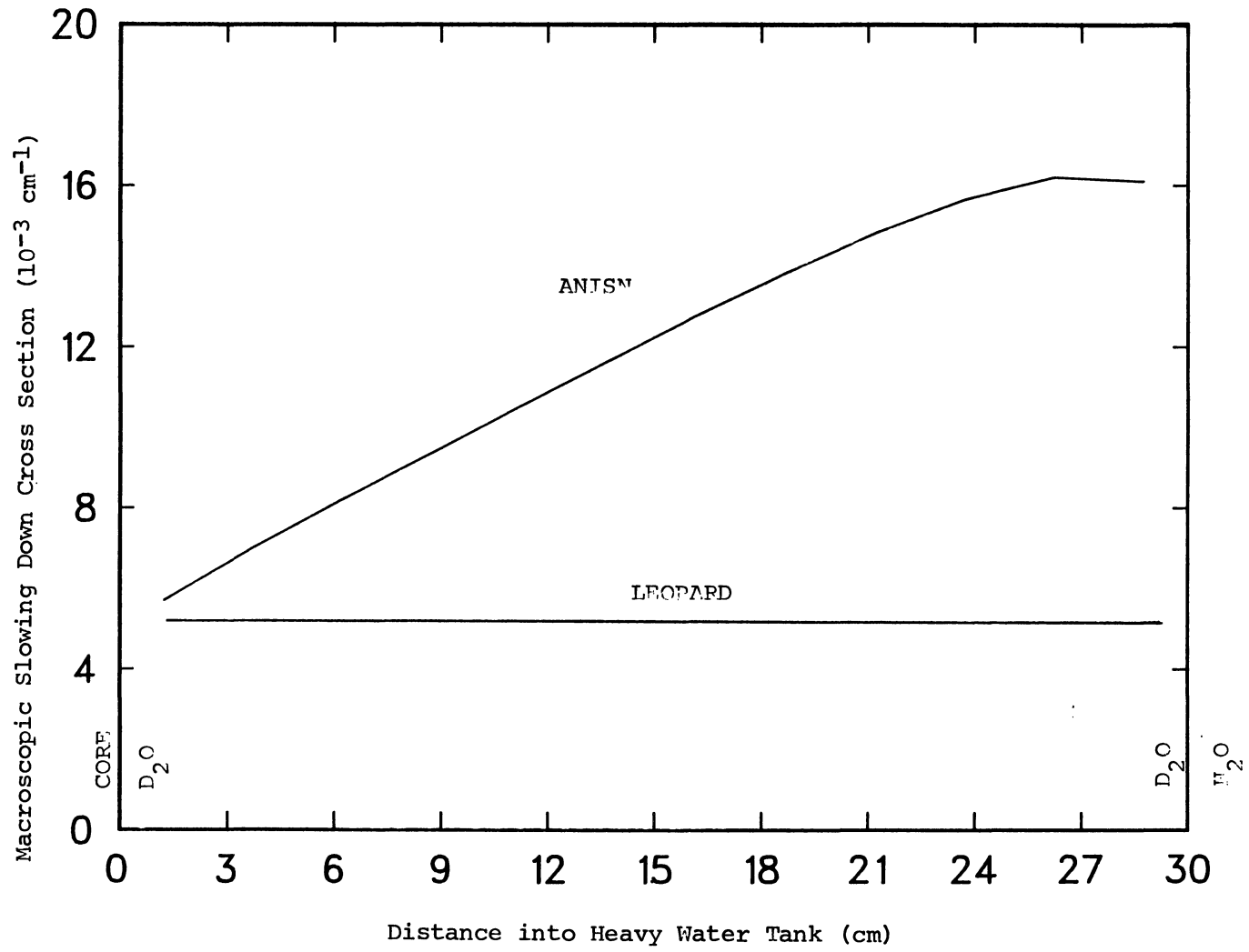


Figure 8. D<sub>2</sub>O Slowing Down Cross Section



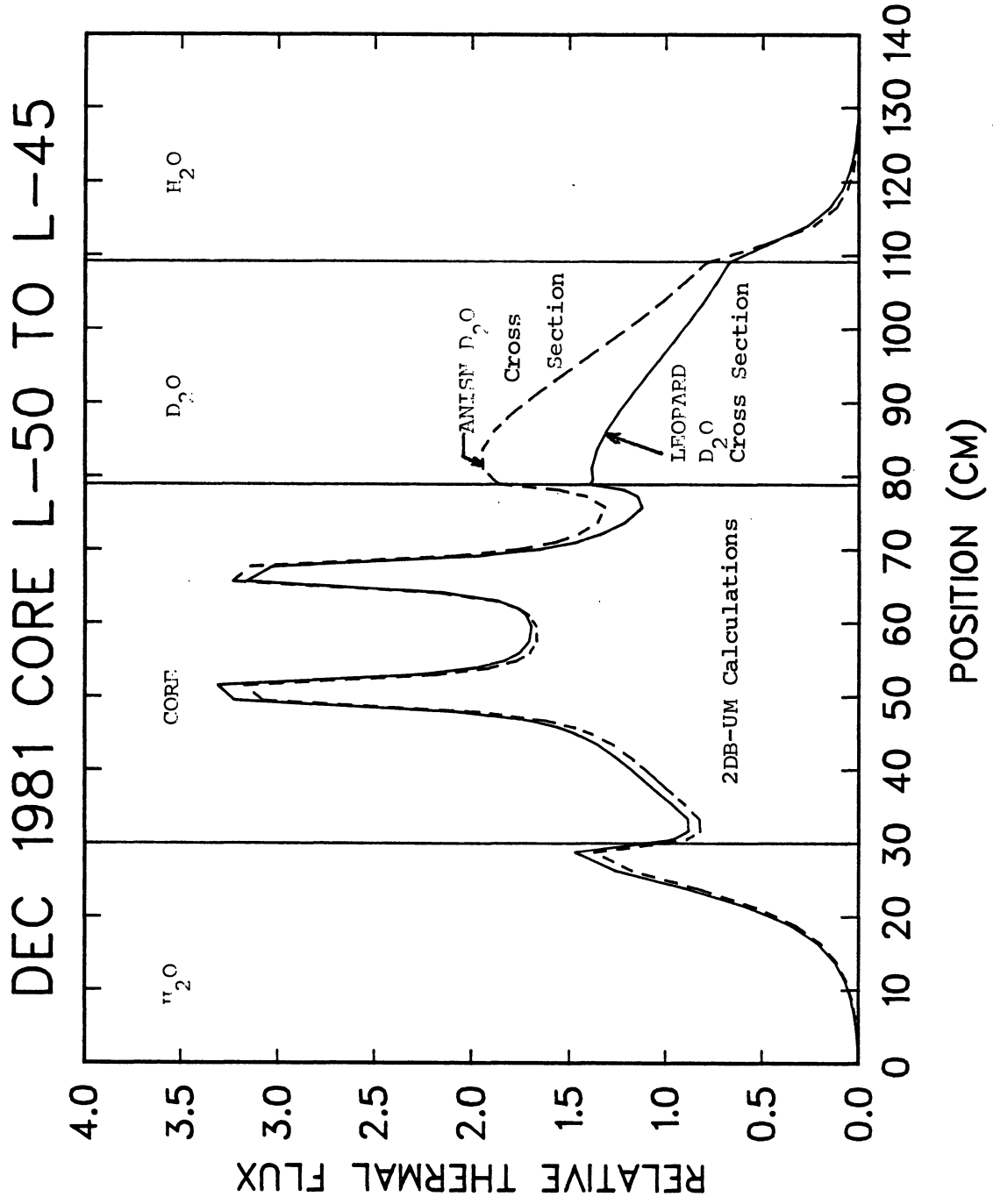


Figure 9. Thermal Flux Distribution for the December 1981 LEU Core

# DEC 1981 CORE L-50 TO L-45

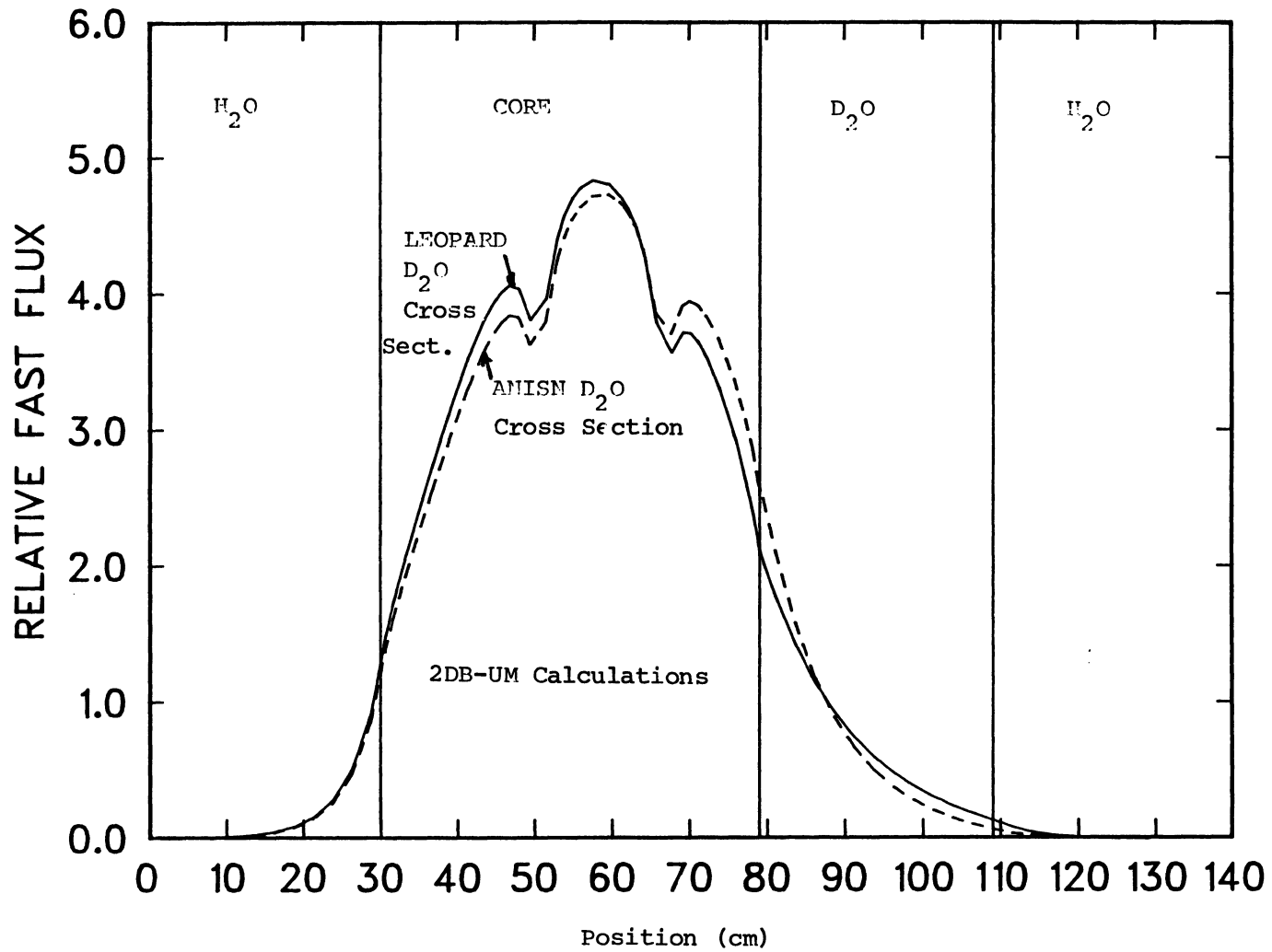


Figure 10. Fast Flux Distribution for the December 1981 LEU Core

position within the  $D_2O$  tank. This calculation is complicated by the complex geometry of the tank, which necessitates at least a two-dimensional transport code to be adequately modeled. For example, a two-dimensional transport code could be used to model the core,  $D_2O$  tank,  $H_2O$  reflector, and beam tubes in cylindrical geometry, which is still an approximate model of the actual configuration. Additional future work will include three-dimensional diffusion theory calculations in the core and reflector regions, using few group  $D_2O$  cross sections that vary axially and radially within the heavy water tank. Comparison of the diffusion theory results with other transport theory calculations (including Monte Carlo) for the heavy water tank will also be made.

### 3. SPND Detector Simulation

Modelling the SPND detector and paddle in the core, water reflector and  $D_2O$  tank has also turned out to be a difficult problem. In preliminary calculations to date, the ANISN code has been used to model the SPND and paddle in the core and reflector regions in cylindrical geometry with 30 groups. The detector is surrounded by a region of moderator material and a region of core material. A white boundary condition is used at the external boundary of the core region. The thermal flux in the SPND detector and Inconel paddle is shown in Figure 11. The flux has been normalized at the surface of the Inconel paddle.

This type of one-dimensional calculation is not a very accurate representation of the actual problem. Measurements in the  $D_2O$  tank are made in aluminum tubes filled with water that only penetrate a short distance into the heavy water tank. The measurements are made near the core-heavy water tank interface and near the axial heavy water-light water interface. The flux in the region near the detector is highly asymmetric, and the flux depression is dependent upon the three-dimensional geometry of the problem. The measure-

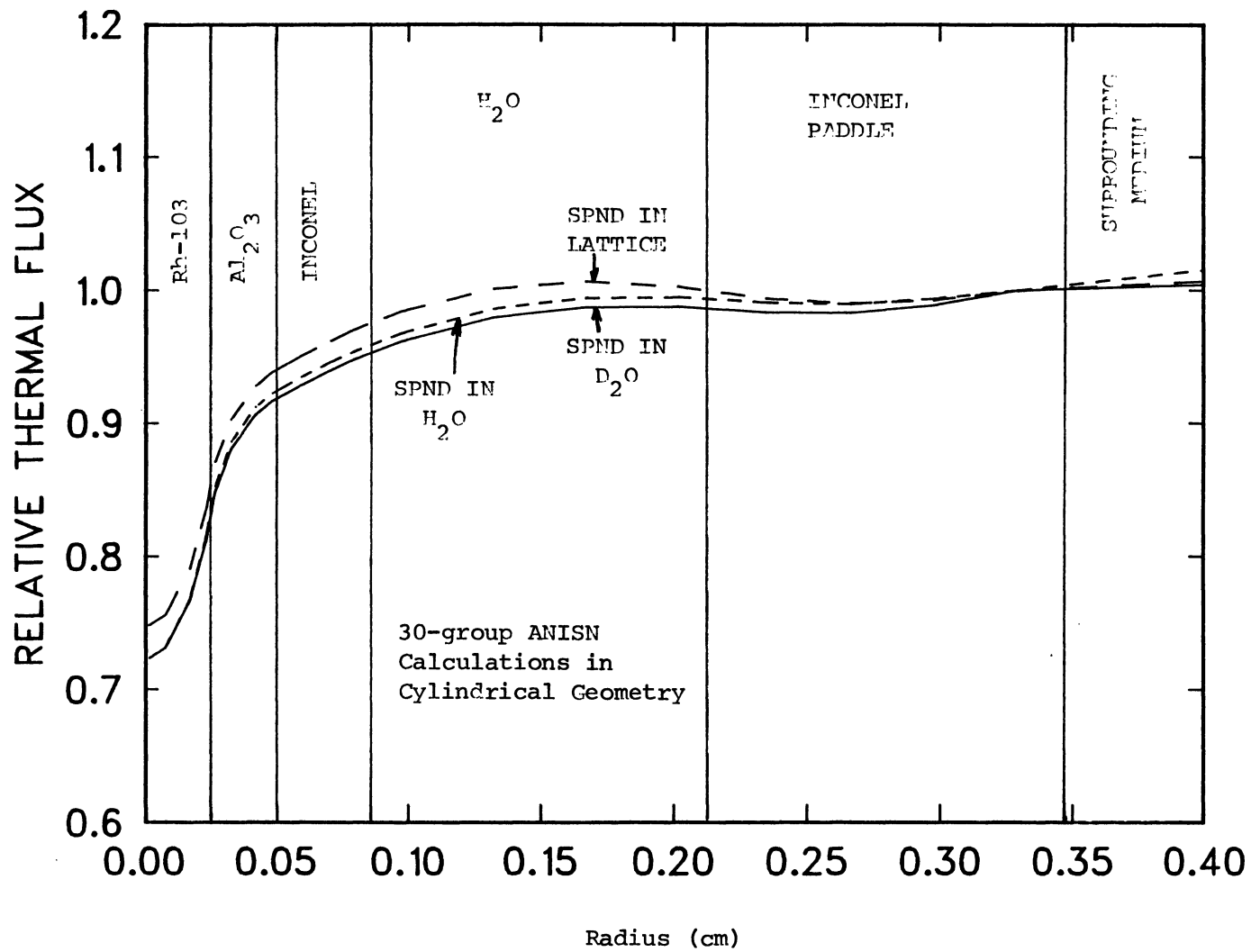


Figure 11. SPND Thermal Flux Calculated by the ANISN Code

ments within the core are made in the water gaps between the fuel plates.

It is difficult in a single calculation to model both the SPND detector and the region surrounding the detector. Because of the large resonance absorption in rhodium at 1.3 eV, a transport theory calculation is required to model the detector. The geometry of the detector is well suited for a cylindrical geometry calculation, although the modelling of the environment surrounding the detector requires different types of calculations. In the core region, a slab geometry transport theory treatment is necessary to model the fuel plates, clad, and water channels. In the heavy water tank, two or three-dimensional diffusion theory calculations are necessary to model the interface of the core, heavy water, and light water regions. Transport theory calculations are required to model the beam tubes in the heavy water tank.

Figure 11 compares three calculations done with the ANISN code in cylindrical geometry to investigate the effect of the surrounding medium on the thermal flux within the SPND detector. The rhodium emitter wire, aluminum oxide insulator, Inconel sheath, and Inconel paddle are explicitly represented. In the first calculation, the detector is surrounded by a region of core material. In the second calculation, the detector is surrounded by 16 cm of  $D_2O$  and a region of core material. In the third calculation, the detector is surrounded by 4 cm of  $H_2O$  and a region of core material. The core material in the second and third calculations provides a source of neutrons for the calculations. The three calculations are normalized at the surface of the Inconel paddle.

These calculations reveal some information about the self-shielding of the thermal flux within the SPND detector. The self-shielding factors for the SPND surrounded by a medium of core material,  $D_2O$ , or  $H_2O$  are .75, .72, .72, respectively, which are not significantly different from

each other. The bulk of the self-shielding is due to the rhodium, with only a small contribution coming from the Inconel sheath. This is reasonable, considering the large resonance in Rh-103 at 1.3 eV. Additional calculations which more accurately account for the complicated geometry of the region surrounding the detector are needed to determine the flux depression factors for the SPND detector surrounded by a medium of core material,  $D_2O$ , or  $H_2O$ . The flux depression factor is a measure of the decrease in the flux at the surface of the detector due to the presence of the detector in the medium. The sensitivity of the SPND is determined by the combined effect of the self-shielding factor and the flux depression factor.

To model the environment of the detector in the lattice region, the EPRI-HAMMER code was used in slab geometry to compute a thermal spectrum in the fuel, clad, water channel, and non-lattice region of a special element. An aluminum sample holder was inserted into the water hole of the special element to simulate the holder used to guide the detector. The spectra were analyzed by fitting a straight line to a plot of  $\log(\phi(E)/E)$  versus energy to determine a neutron temperature characterizing the Maxwellian distribution for neutron flux  $\phi(E)$ . Fits of  $\log(\phi(E)/E)$  versus energy for the HEU and LEU configurations are shown in Figures 12 and 13, respectively, indicating that the flux is nearly Maxwellian from .01 eV to .95 eV.

Figure 14 shows a plot of the neutron temperature as a function of position within the special element. The figure shows a decrease in the temperature of about 7°K in the water gaps between the plates, where the spectrum is expected to be softer, and a further drop in the water hole, and an increase in the aluminum sample holder. The calculated temperatures within the HEU and LEU fuel meat are 340°K and 347°K, respectively, indicating that the thermal spectrum in the LEU fuel is somewhat harder than in the HEU

fuel, as expected. The calculated temperatures within the aluminum sample holder in HEU and LEU fuel are 330°K and 333°K, respectively.

#### D. Ex-Core Spectrum Calculations

As part of our effort in developing models to represent the complex geometry in the FNR heavy water tank, both one-dimensional discrete-ordinates and three-dimensional Monte Carlo calculations were performed. Both scalar and angular fluxes were obtained in the ANISN calculations to compare with the flux spectra measured at the beam ports. Only preliminary Monte Carlo calculations of the scalar flux have been performed with the ANDY code<sup>18</sup> to date.

##### 1. ANISN Calculations

The crystal diffractometer measurements yield the thermal neutron spectra at selected beam ports in the D<sub>2</sub>O tank. As reported in Appendix B, an insignificant change in the neutron temperature (i.e., the temperature corresponding to the  $\log(\phi(E)/E)$  fit) at a specific port were observed between the HEU and LEU fuel; however, a large difference in neutron temperature was observed when the diffractometer was moved to a different beam port. Although this was only one set of measurements and the core configuration was the so-called "high-leakage" HEU core, the difference is large enough (40°K) to warrant additional investigation. Since this temperature difference was observed for I and J ports, which "view" the core at angles of 63° and 105° from the north-south line, respectively (hence J-port is actually looking away from the core), the thermal neutron spectrum may depend on direction, as well as distance into the D<sub>2</sub>O tank. As a preliminary attempt to simulate this geometry, a one-dimensional ANISN calculation was performed utilizing a 20-group (6 fast, 14 thermal) library collapsed from a 218-group ENDF/B-IV SCALE library<sup>17</sup>. An S8-P3 calculation was performed for a full-core north-south traverse, including the H<sub>2</sub>O reflector, core, and D<sub>2</sub>O tank. The resulting ther-

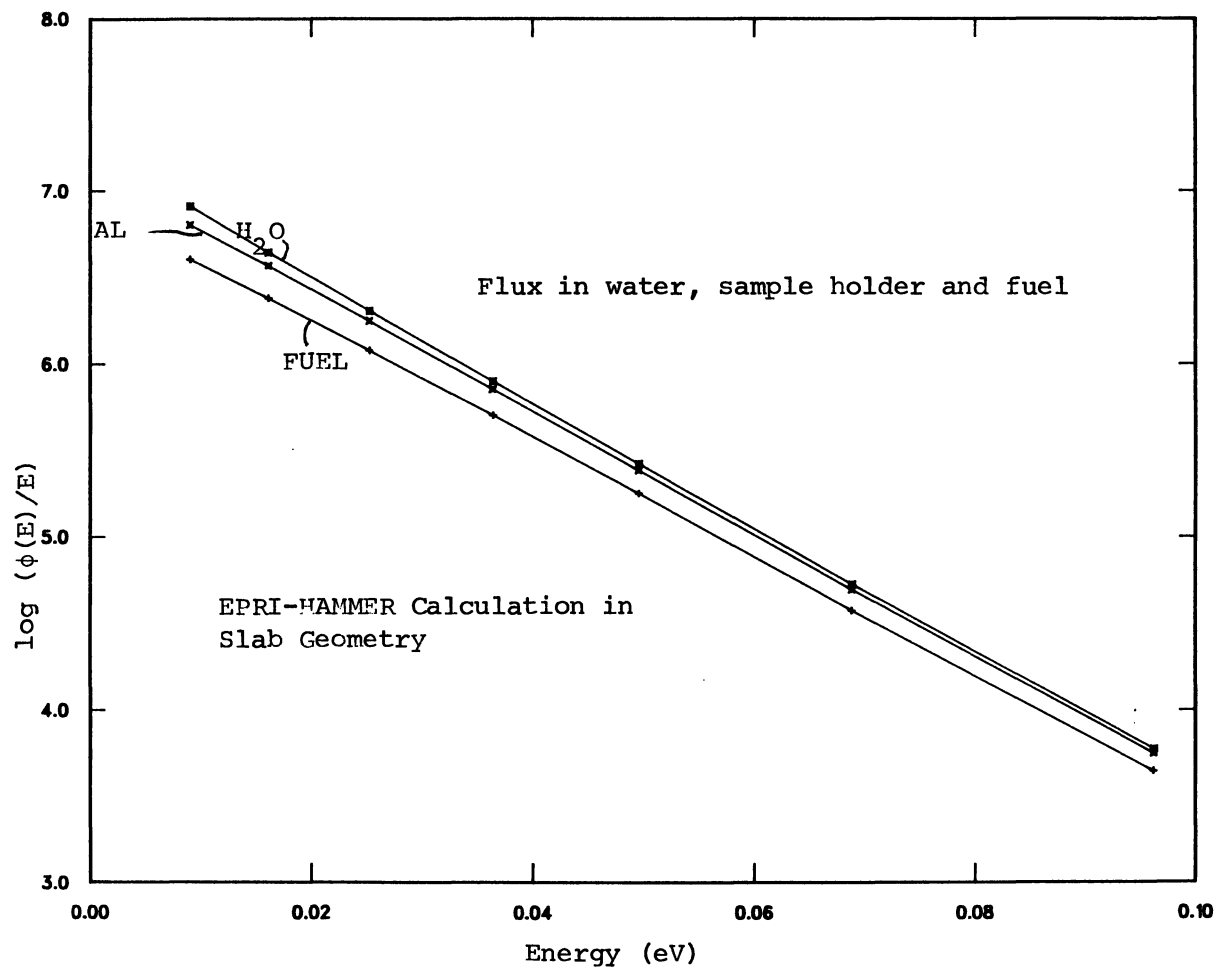


Figure 12. Linear Fit of  $\log(\phi(E)/E)$  vs. E for HEU Fuel



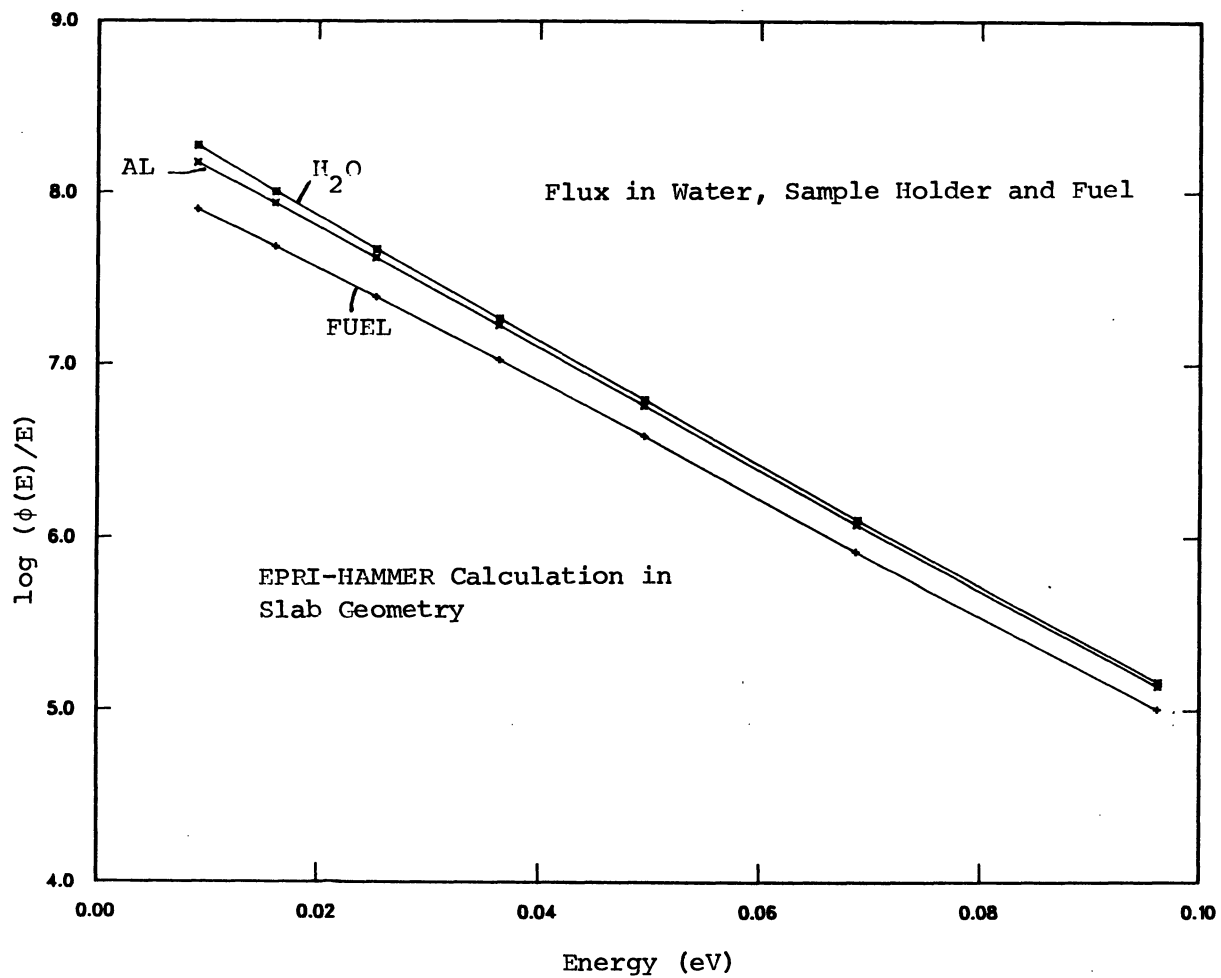


Figure 13. Linear Fit of  $\log(\phi(E)/E)$  vs.  $E$  for LEU Fuel

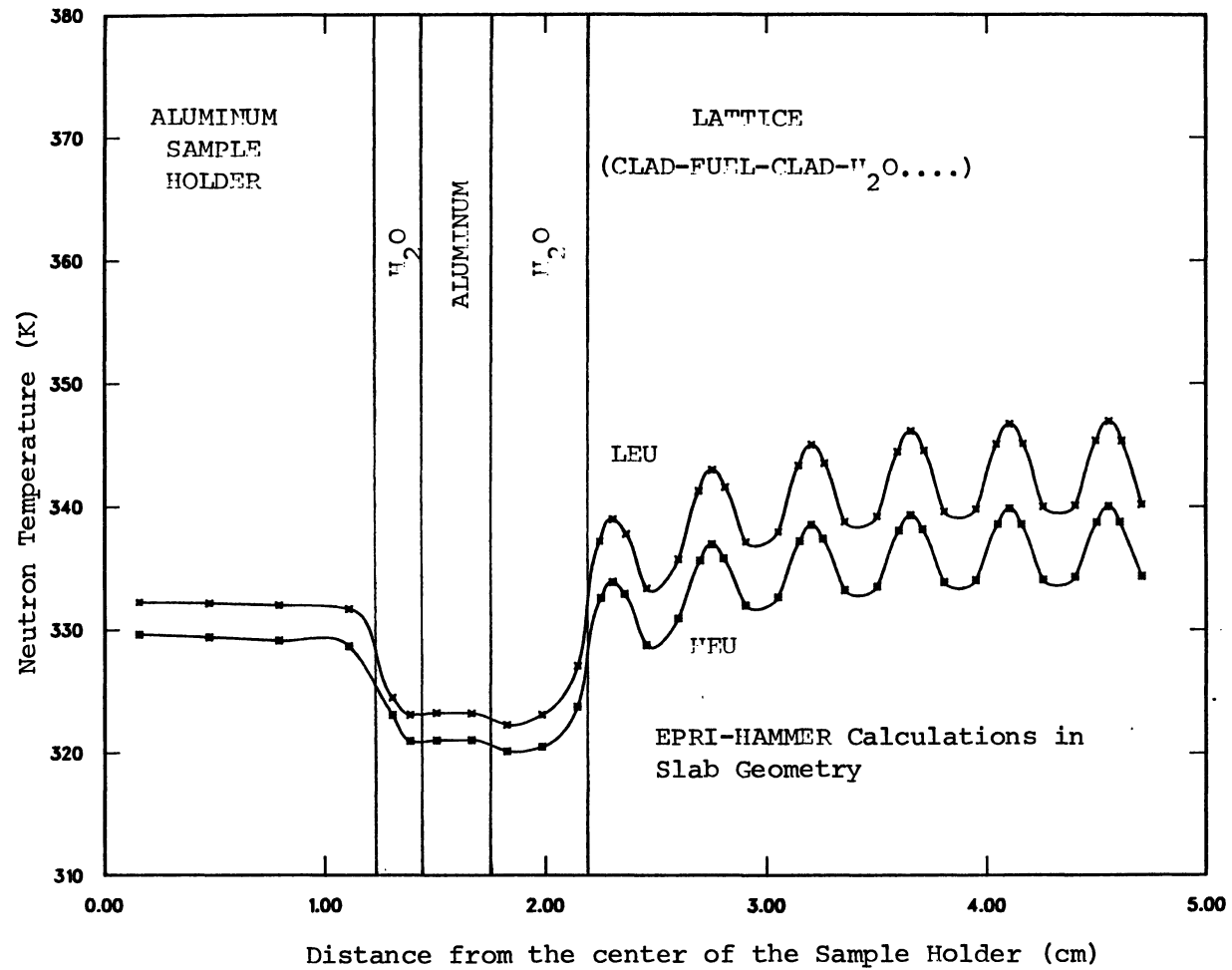


Figure 14. Neutron Temperature in the Aluminum Sample Holder in HEU and LEU Fuel

mal spectra were fit to Maxwellians and a spatially-dependent neutron temperature was then obtained. Neutron temperatures were calculated for the angular fluxes as well as the scalar flux, to ascertain whether the neutron temperature was a function of the neutron direction, as would appear to be the case for the measured spectra. The ANISN results, which must be considered preliminary, predict a temperature decrease of approximately 20°K for the angular flux at an angle of 130° from the north-south axis (hence similar to J-port) versus the angular flux at an angle of 50° from the north-south axis, which is more like I-port. The obvious drawbacks of a one-dimensional calculation for this complicated geometry force us to conclude that although there may be a directional temperature effect which appears to be consistent with experiment (and physical intuition), we would prefer to defer further quantitative conclusions for more detailed calculations (e.g., Monte Carlo or 2-D discrete ordinates). As an aside, it may be worthy of mention that the ANISN-predicted neutron temperatures within the core agreed (within 10°K or so) with completely independent THERMOS calculations of the fuel temperature, which were performed to determine the effect of the in-core sample holder on the fuel thermal spectrum.

## 2. ANDY Calculations

As part of our effort to model the complex geometry of the FNR heavy water tank, Monte Carlo calculations were performed with the ANDY code. Our effort to date has been limited to idealized simulation of a FNR geometry, with the primary purpose of estimating the degree of neutronic coupling between the core and the heavy water tank. Preliminary calculations have been performed with and without representing, in an idealized fashion, the beam tubes, as an initial effort to evaluate the impact of beam tubes on the flux distribution in the surrounding medium.

The ANDY code is a general-purpose, multi-group Monte

Carlo code, with a simple three-level topology for geometry specification. As part of the initial investigation, several test calculations were performed with the ANDY code, which compared favorably with either analytical solutions or the corresponding calculations with the ANISN code. For simulation of the FNR geometry, 27-group,  $P_0$  cross sections in the ANISN format were obtained from the SCALE package for use with the ANDY code.

The idealized FNR geometry used for our ANDY calculations is shown in Figure 15, with a beam tube extending halfway into the heavy water tank. The core is represented by a homogeneous mixture of fuel, water, and aluminum, with the 6 mm thick aluminum wall of the heavy water tank explicitly represented. The beam tube, when represented, is assumed to be vacuum. Only fixed-source calculations, with either a uniform or a cosine-shaped fission source distribution for the core region, were performed.

We present in Figure 16 fast and thermal flux distributions for the idealized FNR with a beam port, calculated for a uniform source distribution, with and without importance sampling. The flux distributions, averaged over the cross sectional area of the core and heavy water tank, and over the circular cross sectional area of the beam tubes, are plotted along a north-south scan of the core. For the case with importance sampling, the particle weight that was assigned is indicated for each region. With a limited number of particle histories simulated, the information presented in Figure 16 is of limited statistical significance. The general trend, however, appears to be reasonable. Even with a uniform source distribution for the core region, which tends to overestimate the flux in the reflector regions, thermal flux peaking in the heavy water region is not pronounced. This result needs to be, however, compared with more accurate calculations. In Figure 17, neutron flux spectra obtained with the ANDY code are plotted for a point

at the middle of the core, at the core-heavy water interface, and at the middle of the heavy water tank. The results correspond to the case without importance sampling plotted in Figure 16, and softening of the spectrum in and around the heavy water tank is clearly visible.

Unfortunately, because of poor statistics in our ANDY results, with limited numbers of particle histories simulated, neither the degree of coupling between the core and heavy-water reflector nor the effect of the beam port can be quantified. Further study is underway to perform similar calculations with a deterministic code in an idealized two-dimensional geometry to compare with the ANDY results obtained so far. Once the degree of neutronic coupling between the core and reflector regions is quantified, further Monte Carlo calculations may be performed for a more realistic geometry confined primarily to the heavy water tank.

#### E. Control Rod Worth Calculations

Full length rod worth measurements were made on the 27 element fresh LEU core in December, 1981. The fuel loading for this core is shown in Figure 18. The control rod worths for this core were calculated with the 2DB-UM code as described in Appendix C and the results are compared with the measured rod worths in Table 3. As noted in Appendix C, the 2DB calculation agrees well with the measurement for rods A and C, but the calculation overpredicts the measurement for the B rod by 14.2%.

The rod worth was calculated in each case by computing the reactivity difference between a rod-in case and a rod-out case. The calculation was done with 6x6 meshes per assembly with control rod cell cross sections obtained with the EPRI-HAMMER and TWOTRAN<sup>19</sup> codes, as discussed in earlier reports.<sup>1,2</sup> Several parametric calculations were performed to determine the sensitivity of the rod worth to various parameters. It appears that the most sensitive parameter is the slowing down cross section in the heavy water, as noted

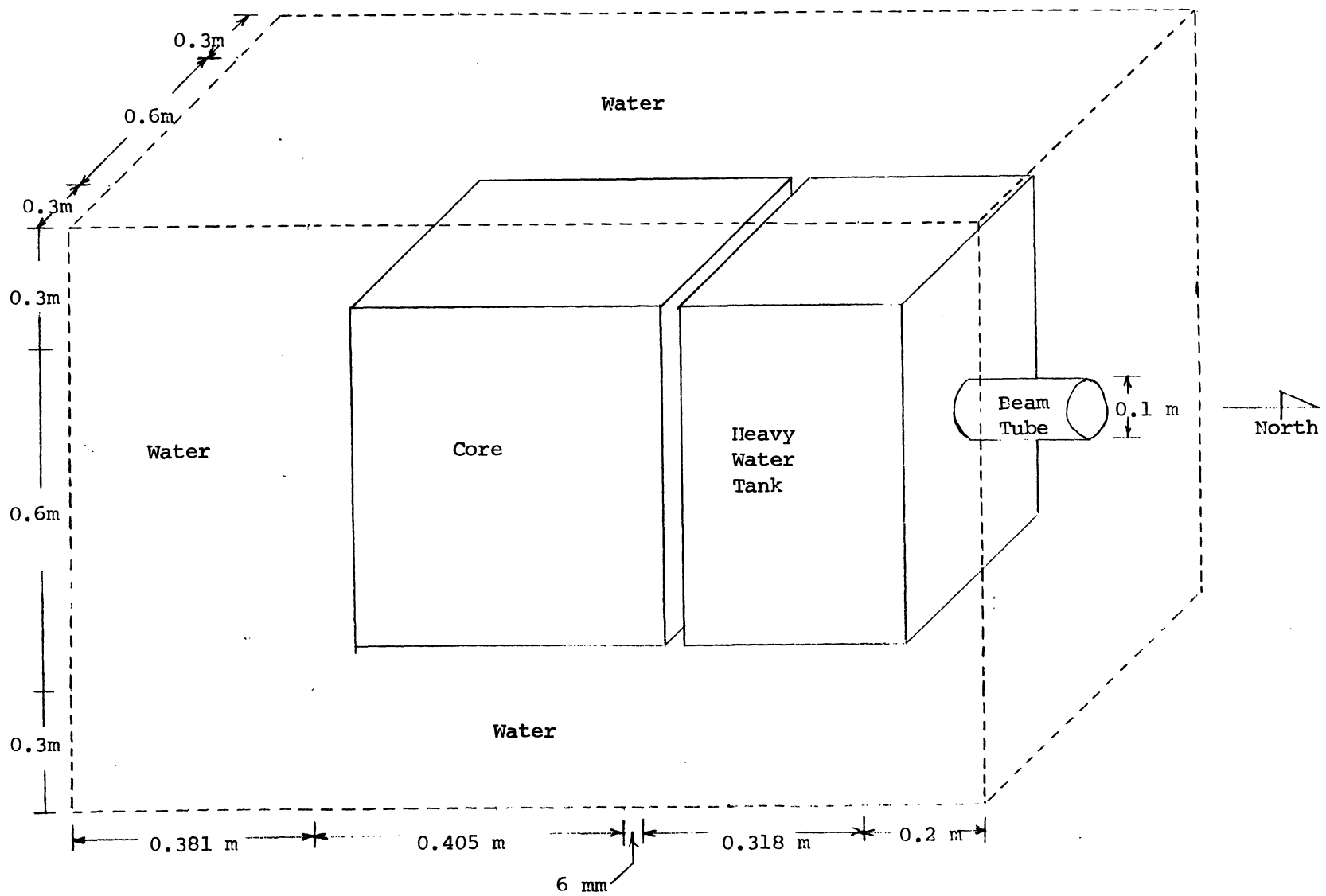


Figure 15. Idealized FNR Geometry for ANDY Calculations

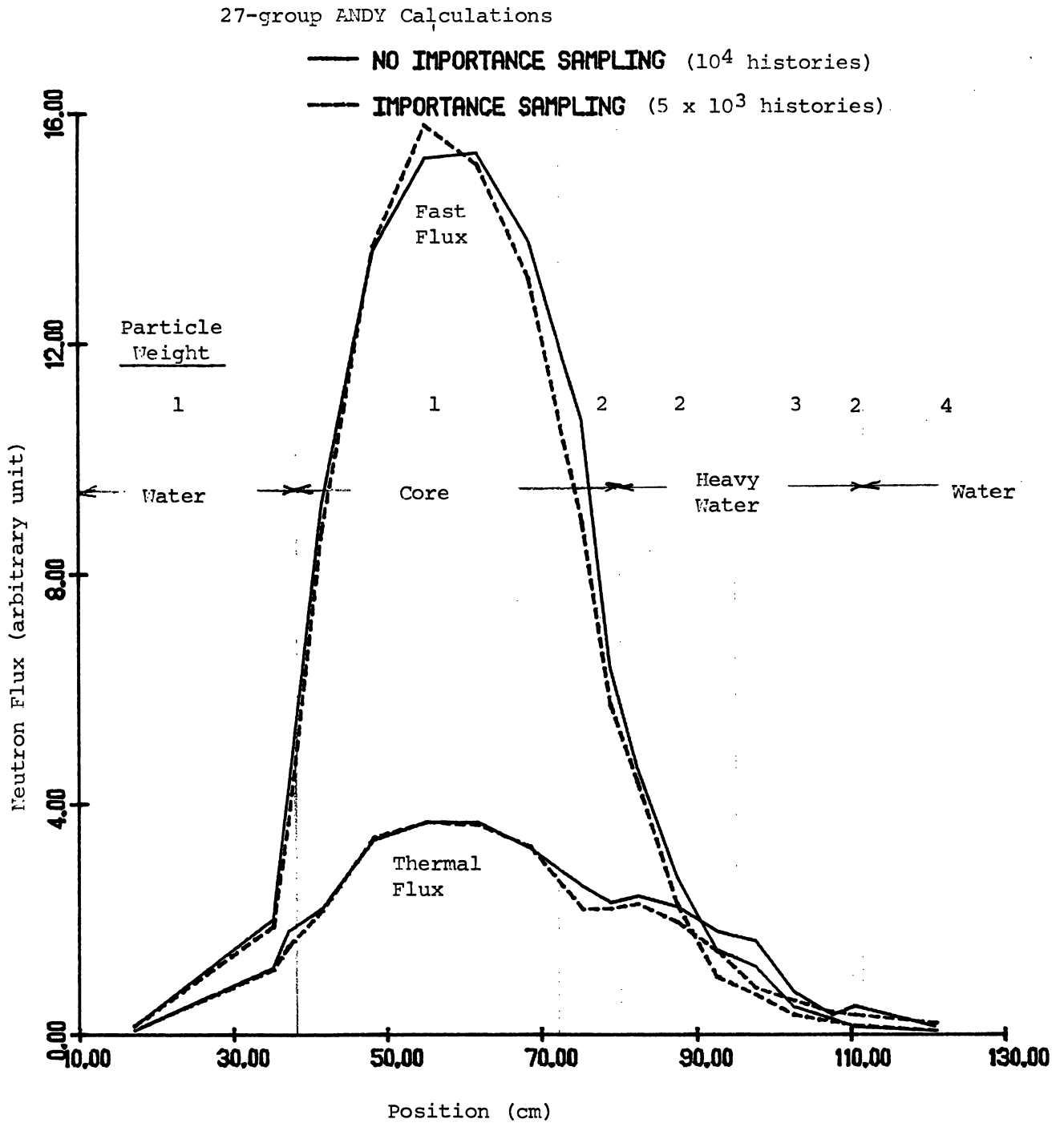


Figure 16. Fast and Thermal Neutron Flux Distributions Calculated by the ANDY Code

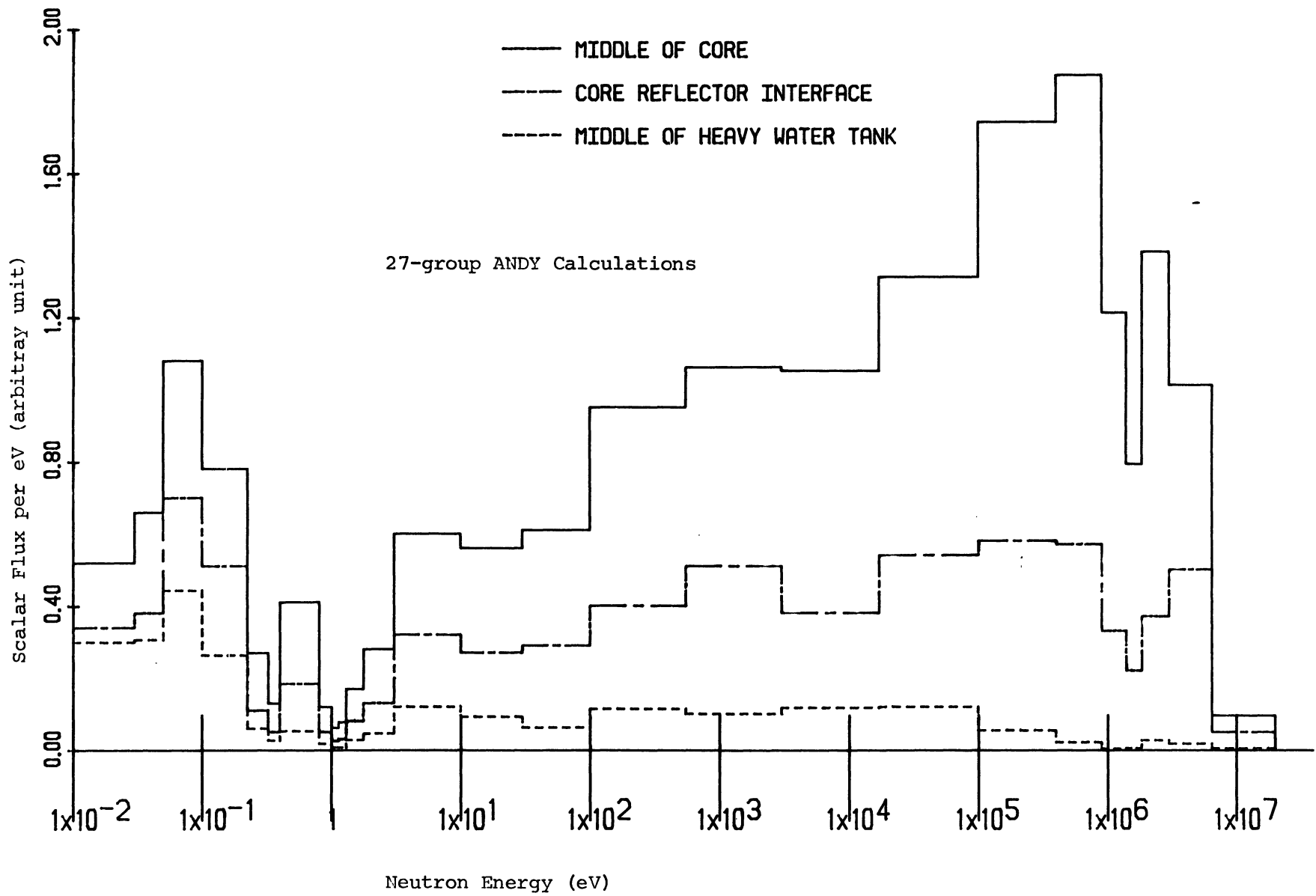


Figure 17. Neutron Flux Spectra Calculated by the ANDY Code



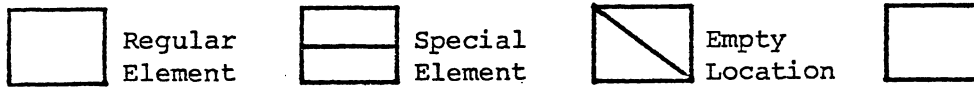
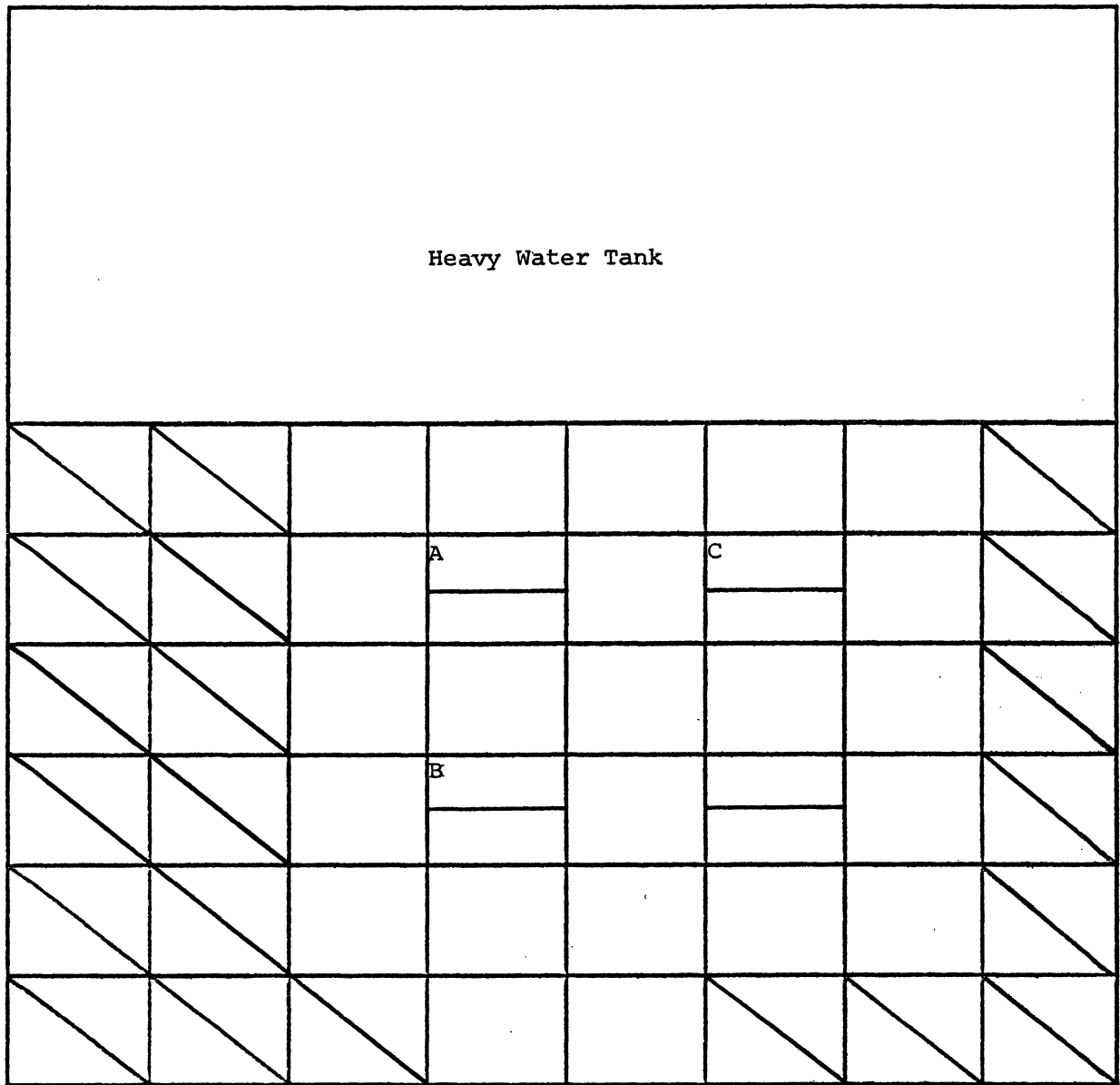


Figure 18. December 1981 LEU Core Map

Table 3

Rod Worths for the December 1981 LEU Core

Measurement or Calculation	Reactivity Worth ( $\% \Delta k/k$ )		
	A Rod	B Rod	C Rod
Experimental data . . . . .	2.22	2.32	2.28
6x6 Calculation			
LEOPARD D <sub>2</sub> O Cross Sections			
Equilibrium Xenon . . . . .	2.28	2.65	2.25
12x12 Calculation			
LEOPARD D <sub>2</sub> O Cross Sections			
Equilibrium Xenon . . . . .	-	2.81	-
6x6 Calculation			
LEOPARD D <sub>2</sub> O Cross Sections			
Zero Xenon . . . . .	2.32	2.66	2.29
6x6 Calculation			
ANISN D <sub>2</sub> O Cross Sections			
Equilibrium Xenon . . . . .	2.43	2.34	2.41

in the discussion of the parametric investigation which follows.

In order to assess the adequacy of the 6x6 mesh structure, a 2DB-UM calculation with 12x12 meshes per assembly was done to model shim rod B. This calculation yielded an inferior result compared with the measurement than the 6x6 calculation, as is shown in Table 3. This is not too surprising since the rod cross sections were computed from EPRI-HAMMER calculations specifically designed for 6x6 2DB-UM geometry. Another 2DB-UM calculation with zero xenon concentration was also done to determine the effect of xenon concentration on the rod worth. As can be seen in Table 3, the potential effect of time varying xenon concentration is quite small.

The effect of the D<sub>2</sub>O slowing down cross section on the rod worth calculations was investigated by calculating the D<sub>2</sub>O cross sections with the ANISN code, as described in Section IV.C, above. Replacing the LEOPARD-generated D<sub>2</sub>O

cross sections with the ANISN-generated cross sections had the effect of increasing the flux within the D<sub>2</sub>O tank, thus causing a shift in the flux away from the south face of the core, as discussed earlier in connection with Figures 9 and 10. The flux is shifted away from the B rod and toward the A and C rods, causing an increase in the worth of rods A and C, and a decrease in the worth of rod B.

The results of 2DB-UM control rod calculations with the ANISN-generated D<sub>2</sub>O cross sections are compared with the experimental data in Table 3. Agreement between measurement and calculation for the worth of rod B is much better with the ANISN D<sub>2</sub>O cross sections than with the LEOPARD D<sub>2</sub>O cross sections, but the agreement for A and C rods is worse with the ANISN cross sections. A comparison of the rod-in and rod-out flux profiles through rods A and B is shown for the thermal and fast flux, respectively, in Figures 19 and 20. The ANISN D<sub>2</sub>O cross sections were used in the 2DB-UM calculations to generate these plots.

The rod worth calculations at this time are not conclusive. There is, perhaps, a need for an additional full-length rod calibration on a fresh LEU core to further test the calculational capability. There is also a need for an accurate spectral calculation to determine the spatial dependence of the slowing down cross section in the D<sub>2</sub>O tank.

#### F. Mixed LEU-HEU Control Rod Worths

A limiting factor in determining the maximum allowable fuel burnup in the FNR core is the shutdown margin. In order to determine the possibility of using partially burned LEU fuel in an equilibrium HEU core, the control rod worths for various mixed core configurations have been calculated. These calculations will be useful for studying an optimal fuel management strategy for the transition from HEU to LEU fuel. Application of mathematical programming to the optimization of the fuel shuffling scheme of the FNR will require correlations to calculate the rod worth for various

# DEC 1981 CORE L-50 TO L-45

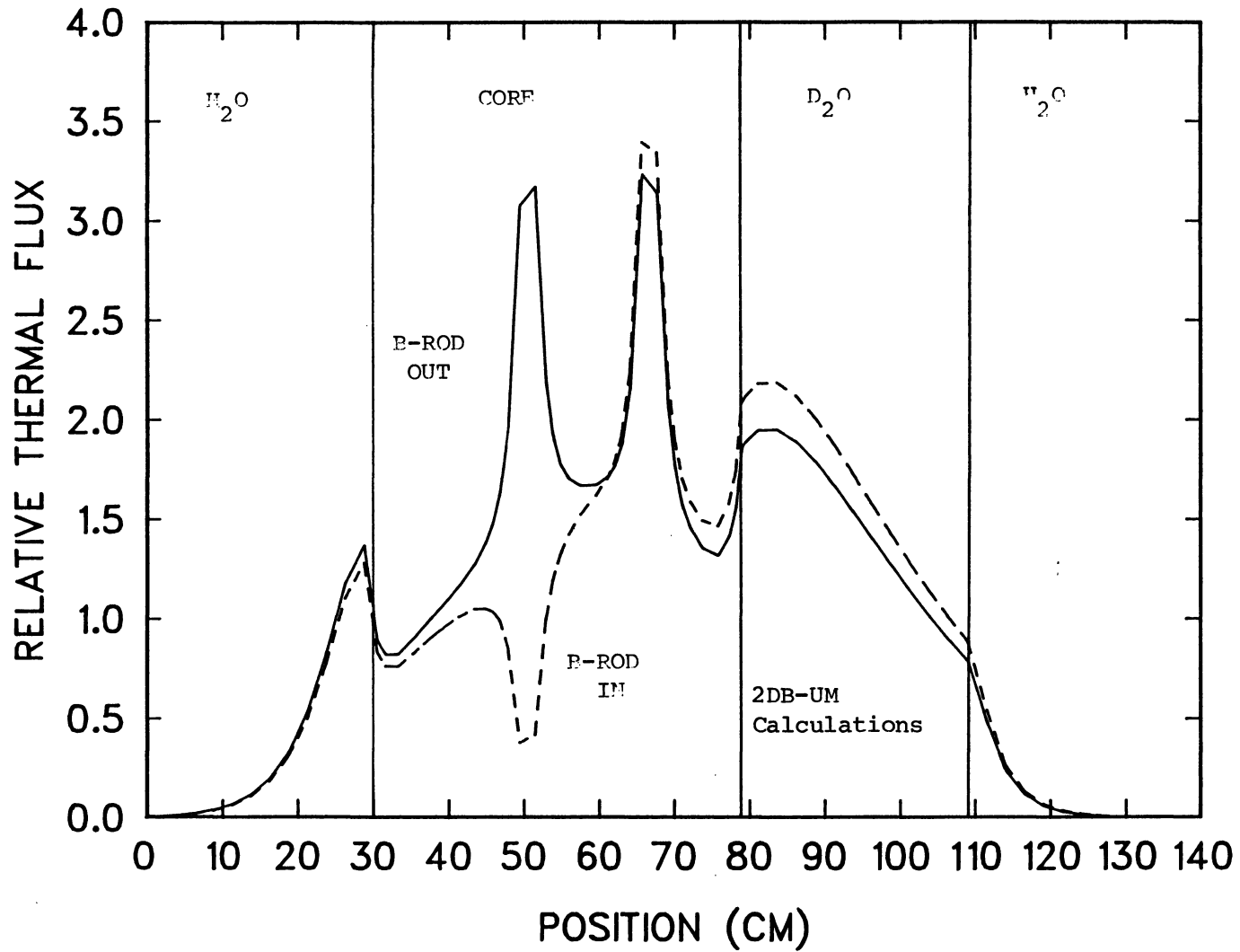


Figure 19. Thermal Flux Distributions for the December 1981 IEU Core

# DEC 1981 CORE L-50 TO L-45

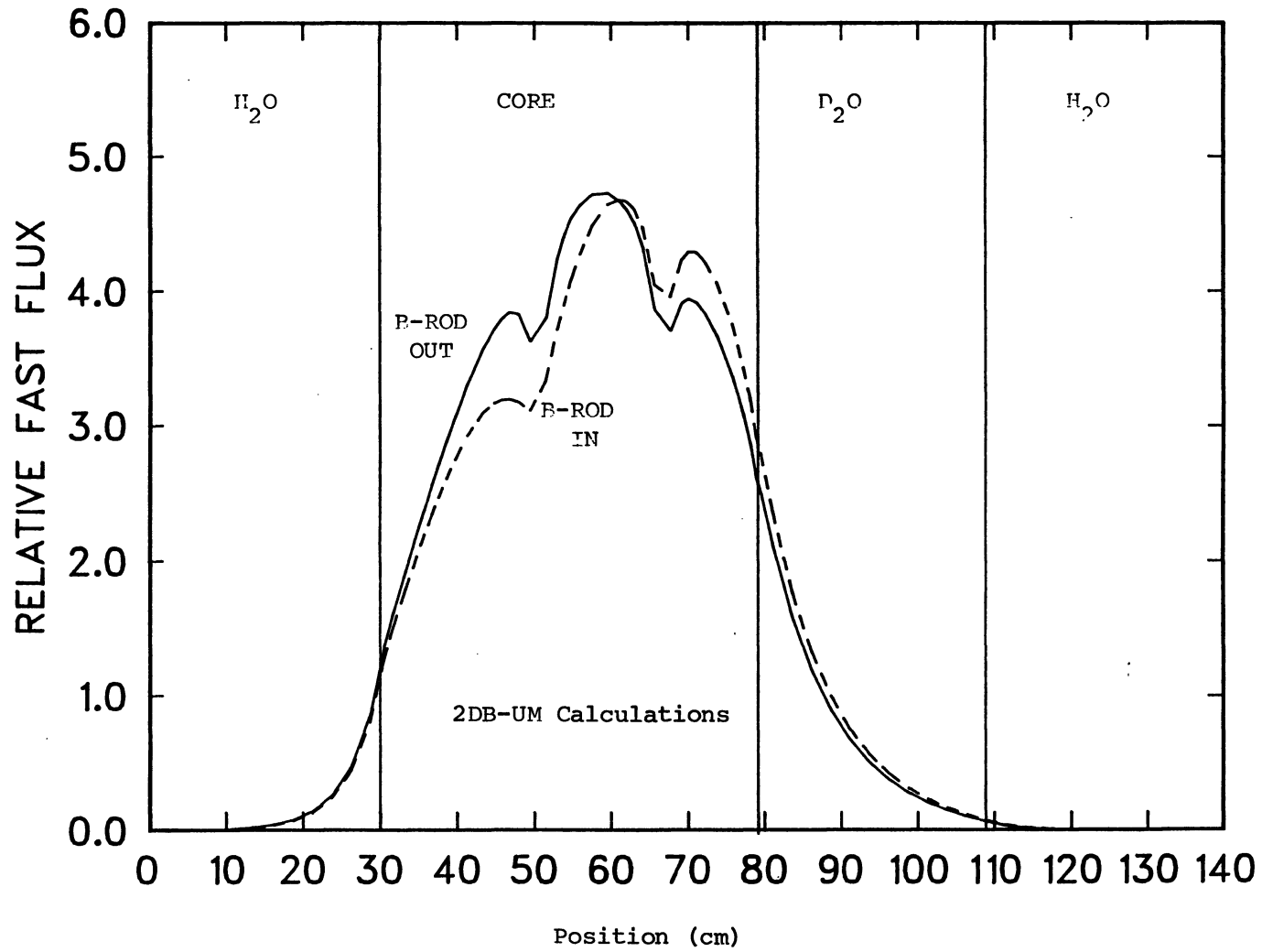


Figure 20. Fast Flux Distributions for the December 1981 LEU Core

mixed HEU-LEU core configurations. Calculations of the type reported here offer an initial step toward achieving this end. The calculations will also be useful in determining if partially burned LEU fuel from a batch core can be burned up in an equilibrium HEU cycle without violating the shutdown margin requirements. It is hoped that the partially burned LEU fuel discharged from the FNR batch LEU core can be efficiently utilized in future mixed HEU-LEU cycles. Rod worth correlations are necessary to determine the extent to which the partially burned fuel can be used, without violating the shutdown margin.

The calculations were performed by replacing the center five fuel elements in an equilibrium HEU core by LEU fuel of various burnups. The burnups of the remaining HEU fuel elements were adjusted by multiplying by a constant factor to keep the eigenvalue constant. Table 4 shows the control rod worths for FNR cycle 211B, and for the mixed cores with LEU fuel of burnups of 4%, 6%, and 8% in the center five lattice positions. Replacement of HEU fuel by LEU fuel in the center five lattice positions decreased the rod worth by several tenths of a percent. The utilization of LEU fuel with higher burnup resulted in a larger decrease in the rod worth than the lower burnup LEU fuel did. Many more calculations of this type will be required to develop sufficient correlations for an optimization study. Also, alternate methods for maintaining a constant eigenvalue might be investigated, such as adding or removing fuel from the outer region of the core.

#### G. Three Dimensional Capability for 2DB-UM

The lack of an efficient three-dimensional global analysis capability has been a serious limitation at the University of Michigan for several years. Without this capability, accurate predictions of axial flux/power shapes and control rod worths are problematical. This is especially true for the FNR with the D<sub>2</sub>O tank on one face which

Table 4

## Control Rod Worths for HEU/LEU Mixed Cores

Core Configuration	Total Rod Worth (% $\Delta$ k/k)
Reference HEU core . . . . .	6.629
4% Burnup LEU Fuel in Center 5 Elements	6.409
6% Burnup LEU Fuel in Center 5 Elements	6.366
8% Burnup LEU Fuel in Center 5 Elements	6.323

makes the problem difficult to analyze in two dimensions. Therefore, effort was initiated in August, 1982 to develop a three-dimensional capability for the 2DB-UM code. Since a primary goal of this effort was to retain the efficient macroscopic depletion capability of the 2DB-UM code (among other features installed in 2DB over the years), the decision was made to make the 2DB-UM code three dimensional rather than beginning with the three-dimensional production code 3DB<sup>20</sup> and modifying it to be consistent with the 2DB-UM code.

The major portion of this work has recently been completed and the 3DB-UM code appears to be working correctly, at least for several simple test problems, when compared with the 3DB code. In the process of incorporating the 3DB code into the 2DB-UM code, the disk input/output routines were completely rewritten with most of the storage maintained in the memory with the result that the 3DB-UM code is a factor of three faster than the 3DB code. Whether this advantage persists for the large full-core FNR problems remains to be seen. The principal work remaining on this task is to install the modifications necessary to allow the 3DB-UM code to use the identical cross section data base (cross sections parameterized as a function of fuel type, burnup, fuel temperatures, etc.) that is currently used by the 2DB-UM code.

### H. Effective Delayed Neutron Fraction

Calculation of the effective delayed neutron fraction  $\beta_{\text{eff}}$  for the FNR core was undertaken in 1981 by J. Moreira as a M.S. project.<sup>21</sup> Three different methods were used in this study: a) first-order perturbation theory, b) eigenvalue method, and c) non-leakage probability method. The eigenvalue method is based on the work of Kaplan and Henry<sup>22</sup> and the actual application of the method to the FNR configuration is described in Ref. 2.

The third method was originated in Ref. 23 and involves writing the non-leakage probability  $\mathcal{L}_f$  of fission neutrons as

$$\mathcal{L}_f = (1 - \beta) \mathcal{L}_p + \beta \mathcal{L}_d, \quad (1)$$

where  $\beta$  is the physical fraction of delayed neutrons, and  $\mathcal{L}_p$  and  $\mathcal{L}_d$  are the probabilities that the prompt and delayed neutrons, respectively, will not leak out of a given volume during slowing down. Substituting Eq. (1) into time-dependent diffusion equation for flux  $\phi$  coupled with the precursor balance equations, and taking the inner product of the terms in the resulting equations with the adjoint flux  $\phi^*$ , we obtain,

$$\beta_{\text{eff}} = \beta \frac{\langle \phi^*, \mathcal{L}_d P \phi \rangle}{\langle \phi^*, \mathcal{L}_f P \phi \rangle}, \quad (2)$$

where  $P$  is the production operator. Since the term  $P\phi$  is proportional to power, the ratio of the inner products in Eq. (2) can be interpreted as the ratio of probability of non-leakage of delayed neutrons from the core region to the corresponding non-leakage probability for any fission neutrons. Thus,  $\beta_{\text{eff}}$  can be obtained as

$$\beta_{\text{eff}} = \beta \frac{\langle \mathcal{L}_d \rangle}{\langle \mathcal{L}_f \rangle}. \quad (3)$$



Two-dimensional calculations for FNR configurations indicate that method (a) with four energy groups, underpredicts  $\beta_{\text{eff}}$  by 2~3% compared with methods (b) and (c). The results from the latter two methods are in agreement with one another to within 1%. To resolve the difference between method (a), and methods (b) and (c), further effort was undertaken in 1982 to perform the first-order perturbation calculations with a larger number of energy groups. By modifying the LEOPARD code, six-group cross sections were obtained, with the second and third groups in the standard LEOPARD structure replaced by four groups. A first-order perturbation calculation with the six-groups cross sections indicates a reduction, by a factor of two, of the difference noted earlier in the  $\beta_{\text{eff}}$  values calculated.

The values of  $\beta_{\text{eff}}/\beta$  calculated for several FNR configurations are summarized in Table 5. In addition to showing the differences due to different calculational methods, Table 5 also indicates that the ratio  $\beta_{\text{eff}}/\beta$  decrease as the core size increases. Direct eigenvalue or non-leakage probability calculations with perturbed fission spectrum, accounting explicitly for the delayed neutron spectrum, have not been performed for the 39-element equilibrium core configurations. For both the HEU and LEU configurations, in this case, first-order perturbation theory calculations were only performed. Based on the comparisons between the perturbation theory and eigenvalue results obtained for the batch core configurations, values of the correction factor,  $\beta_{\text{eff}}/\beta$ , obtainable with the eigenvalue method were estimated to be 1.139 and 1.132 for the HEU and LEU equilibrium core configurations, respectively. Based on the calculations performed to date, the effective delayed neutron fraction for the LEU core is expected to be slightly smaller than the corresponding value for the HEU core.

Table 5., Effective Delayed Neutron Fraction  
for the FNR

Core Configuration	Calculational Method	Number of Groups	$\beta_{\text{eff}}/\beta$
25-element HEU batch core	perturbation	4	1.136
	eigenvalue	2	1.164
	non-leakage probability	2	1.154
31-element HEU batch core	perturbation	4	1.123
	perturbation	6	1.136
	eigenvalue	2	1.153
	non-leakage probability	2	1.144
39-element HEU equilibrium core	perturbation	4	1.114
	eigenvalue, estimated	2	1.139
	perturbation	4	1.107
	eigenvalue, estimated	2	1.132

## V. SUMMARY AND RECOMMENDATIONS FOR FUTURE WORK

The preceding sections of this report have discussed the work performed as a part of the FNR LEU project during the 1981-82 report period. This section summarizes the current status of the project including recommendations for future effort.

The experimental portion of the project has resulted in significant advances in our ability to measure the neutronic behavior of the FNR (HEU and LEU) core. In particular, our development and testing (currently in progress) of the multiple threshold foil technique will enable accurate measurements of in-core and ex-core flux spectra, including thermal spectra as well as epithermal and fast spectra. The development of the rapid SPND measurement technique has allowed for more convenient full-core flux measurements and the determination of spatial sensitivity factors has increased the accuracy of the SPND measurements. In addition, the beam port thermal spectrum and leakage intensity measurements have contributed additional experimental data to assess the impact of the LEU fuel as well as to verify our calculational methods. Finally, of course, the successful installation and testing of the LEU core has verified that the LEU core is performing as expected, although questions remain with respect to the measurement of the thermal flux distribution, especially in the D<sub>2</sub>O tank. In addition, there remain uncertainties in the measured thermal flux spectra and intensities at the beam ports.

In the analytical area, significant achievements of the current report period include the implementation and testing of the ENDF/B-IV data base for the LEOPARD code and the successful prediction of the initial LEU configurations. Other tasks which are nearly complete include the development of the fission product correlation for MTR-type fuels for the LEOPARD code, the modification of the 2DB-UM code to incorporate a three-dimensional capability, and the determination

of the effective delayed neutron fraction for the LEU fuel. The major unresolved issues, which have already consumed a significant amount of effort during the 1981-82 report period, include the prediction of in-core and ex-core spatial flux distributions and spectra, and the prediction of control rod worths. Other items that are not resolved include the use of partially burned LEU fuel in the HEU core (or vice versa) and the optimal approach to an equilibrium LEU core.

Additional tasks in the analytical area that might be addressed in the near future include the calculation of the IAEA benchmark configuration for MTR-type research reactors and the implementation of our overall neutronic code package on a state-of-the-art microcomputer for use at other research reactor facilities.

## REFERENCES

1. W. Kerr, et. al., "Low Enrichment Fuel Evaluation and Analysis Program, Summary Report for the Period January, 1979 - December, 1979", Department of Nuclear Engineering and Michigan-Memorial Phoenix Project Report, The University of Michigan (January 1980).
2. W. Kerr, et. al., "Low Enrichment Fuel Evaluation and Analysis Program, Summary Report for the Period January, 1980 - December, 1980", Department of Nuclear Engineering and Michigan-Memorial Phoenix Project Report, The University of Michigan (March 1981).
3. D. K. Wehe and J. S. King, "FNR Demonstration Experiments Part I: Beam Port Leakage Currents and Spectra", Presented at the International Meeting on Research and Test Reactor Core Conversions from HEU to LEU Fuels, Argonne National Laboratory (November 8-10, 1982).
4. D. K. Wehe and J. S. King, "FNR Demonstration Experiments Part II: Subcadmium Neutron Flux Measurements", Presented at the International Meeting on Research and Test Reactor Core Conversions from HEU to LEU Fuels, Argonne National Laboratory (November 8-10, 1982).
5. J. A. Rathkopf, C. R. Drumm, W. R. Martin, and J. C. Lee, "Analysis of the Ford Nuclear Reactor LEU Core", Presented at the International Meeting on Research and Test Reactor Core Conversions from HEU to LEU Fuels, Argonne National Laboratory (November 8-10, 1982).
6. R. W. Hardie and W. W. Little, Jr., "PERTV-A Two-Dimensional Code for Fast Reactor Analysis", BNWL-1162, Battelle Pacific Northwest Laboratory (September 1969).
7. W. W. Little, Jr. and R. W. Hardie, "2DB User's Manual-Revision 1", BNWL-831 REV1, Battelle Pacific Northwest Laboratory (February 1969).
8. R. F. Barry, "LEOPARD-A Spectrum Dependent Non-Spatial Depletion Code", WCAP-3269-26, Westinghouse Electric Corporation (September 1963).
9. J. Rathkopf, "Development of ENDF/B-IV Cross Section Library for the LEOPARD Code", M.S. Project Report, Department of Nuclear Engineering, The University of Michigan (November 1981).

10. J. Barhen, W. Rothenstein, E. Taviv, "The HAMMER Code System", NP-565, Electric Power Research Institute (October 1978).
11. T. R. England, W. B. Wilson, and M. B. Stamatelatos, "Fission Product Data for Thermal Reactors. Part 2: Users Manual for EPRI-CINDER Code and Data", LA-6746-MS, Los Alamos Scientific Laboratory (December 1976).
12. G. J. Stankiewicz, "Time Dependent Fission Product Cross Sections for  $^{235}\text{U}$  Fuels", M.S. Project Report, Department of Nuclear Engineering, The University of Michigan (July 1981).
13. T. R. England, "CINDER--A One-Point Depletion and Fission Product Program", WAPD-TM-334, Bettis Atomic Power Laboratory (August 1962).
14. S. B. Gunst, J. C. Connor, and D. E. Conway, "Measured and Calculated Fission-Product Poisoning in Neutron-Irradiated Uranium-233", Nucl. Sci. Eng., 58, 387 (1975).
15. W. W. Engle, Jr., "ANISN, A One-Dimensional Discrete Ordinates Transport Code with Anisotropic Scattering", K-1693, Oak Ridge National Laboratory (March 1966).
16. N. M. Greene and C. W. Crave, Jr., "XSDRN: A Discrete Ordinates Spectral Averaging Code", ORNL-TM-2500, Oak Ridge National Laboratory (July 1969).
17. R. M. Westfall et al., "SCALE: A Modular Code System for Performing Standardized Computer Analysis for Licensing Evaluation," NUREG CR-0200, Radiation Shielding Information Center, Oak Ridge National Laboratory (1980).
18. D. R. Harris, "ANDYMG3, The Basic Program of a Series of Monte Carlo Programs for Time-Dependent Transport of Particles and Photons", LA-4539, Los Alamos Scientific Laboratory (1970).
19. K. D. Lathrop and F. W. Brinkley, "TWOTRAN-II - An Interfaced Exportable Version of the TWOTRAN Code for Two-Dimensional Transport", LA-4848-MS, Los Alamos Scientific Laboratory (1973).
20. R. W. Hardie and W. W. Little, Jr., "3DB, A Three-Dimensional Diffusion Theory Burnup Code", BNWL-1264, Battelle Northwest Laboratory (1970).
21. J. Moreira, "The Effective Delayed Neutron Fraction for the FNR", M. S. Project Report, Department of

Nuclear Engineering, The University of Michigan  
(July 1981).

22. S. Kaplan and A. F. Henry, "An Experiment to Measure Effective Delayed Neutron Fraction", WAPD-TM-209, Westinghouse Electric Corporation (1960).
23. P. N. Cooper, K. Firth, M. Kerridge, R. F. Mathams, A. J. Salmon and K. G. Stephens, "Some Measurements of Reactivity in a Light-Water Moderated Highly Enriched Uranium Assembly", React. Sci. Tech., 16, 65 (1962).

APPENDIX A

FNR Demonstration Experiments

Part I

Beam Port Leakage Currents and Spectra



FNR DEMONSTRATION EXPERIMENTS  
PART I: BEAM PORT LEAKAGE CURRENTS AND SPECTRA

by

D. K. Wehe and J. S. King  
Phoenix Memorial Laboratory  
University of Michigan  
Ann Arbor, Michigan 48109

Overview

The goal of the FNR-LEU experimental program has been to measure the changes in numerous reactor characteristics when the conventional HEU core is replaced by a complete LEU fueled core or by a single LEU element in the normal HEU core. We have observed comparisons in a) thermal flux intensity, spatial distribution and cadmium ratios, both in the core and in the light and heavy water reflectors, b) fast flux intensity and spectral shape at a special element within the core, c) the thermal leakage flux intensity at the exit positions of several beam ports and its spectral shape at one beam port, d) shim and control rod worths, e) temperature coefficient of reactivity, and f) xenon poison worth.

The FNR is a 2MW light water pool reactor, reflected on three faces by light water and on one face by D<sub>2</sub>O, composed of MTR plate fuel elements. Figure 1 shows a plan view of the core grid, D<sub>2</sub>O reflector tank, and beam ports. The conventional HEU fuel element contains eighteen MTR Al plates 3.0" x 24" x 0.06". The center 0.02" of each plate is 93% U-235 enriched UAl<sub>x</sub>. A normal equilibrium HEU core loading is outlined in Figure 2. Each new HEU element contains ~140 grams of U-235. The LEU low enrichment fuel retains the same plate and element geometry but the fuel is contained in a central 0.03" thick UAl<sub>x</sub> matrix with 19.5% U-235 enrichment. Each new LEU element contains ~167.3 grams U-235. In-core neutron fluxes were routinely mapped by a rhodium SPND and by many wire and foil activations. The same data, but in more restricted positions, were obtained through the light water reflector (south) and D<sub>2</sub>O reflector tank (north). Beam port leakage currents were measured during all power cycles, by transmission fission chambers at the exits of ports G, I, and J, by a BF<sub>3</sub> detector at A-port, and by a prompt  $\gamma$  detector at the F-port exit. Thermal neutron spectra for both HEU and LEU cores were measured at I port using a single crystal silicon diffractometer.

These measurements provide direct observation of the degree to which the LEU conversion alters the flux conditions for fixed

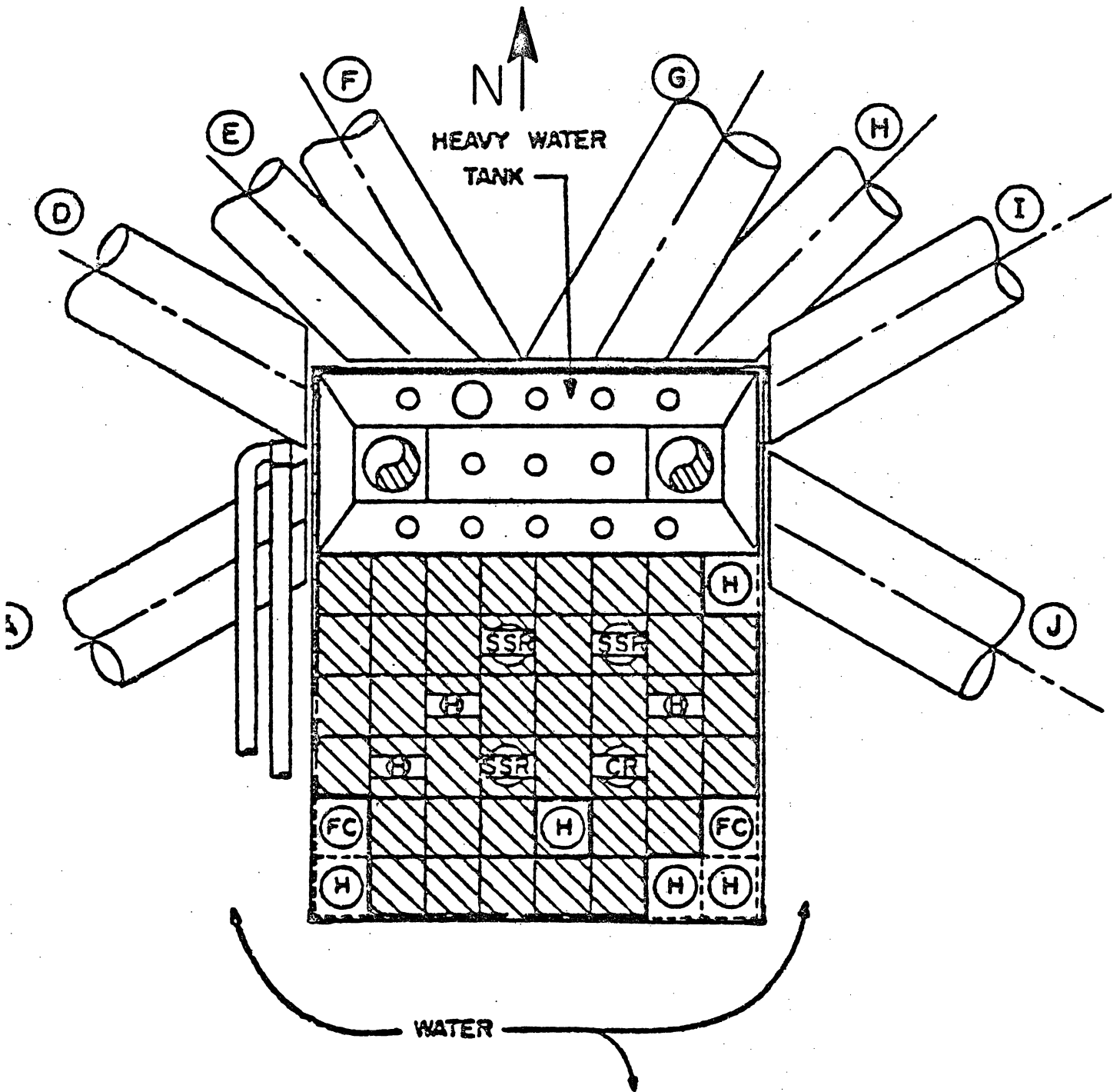
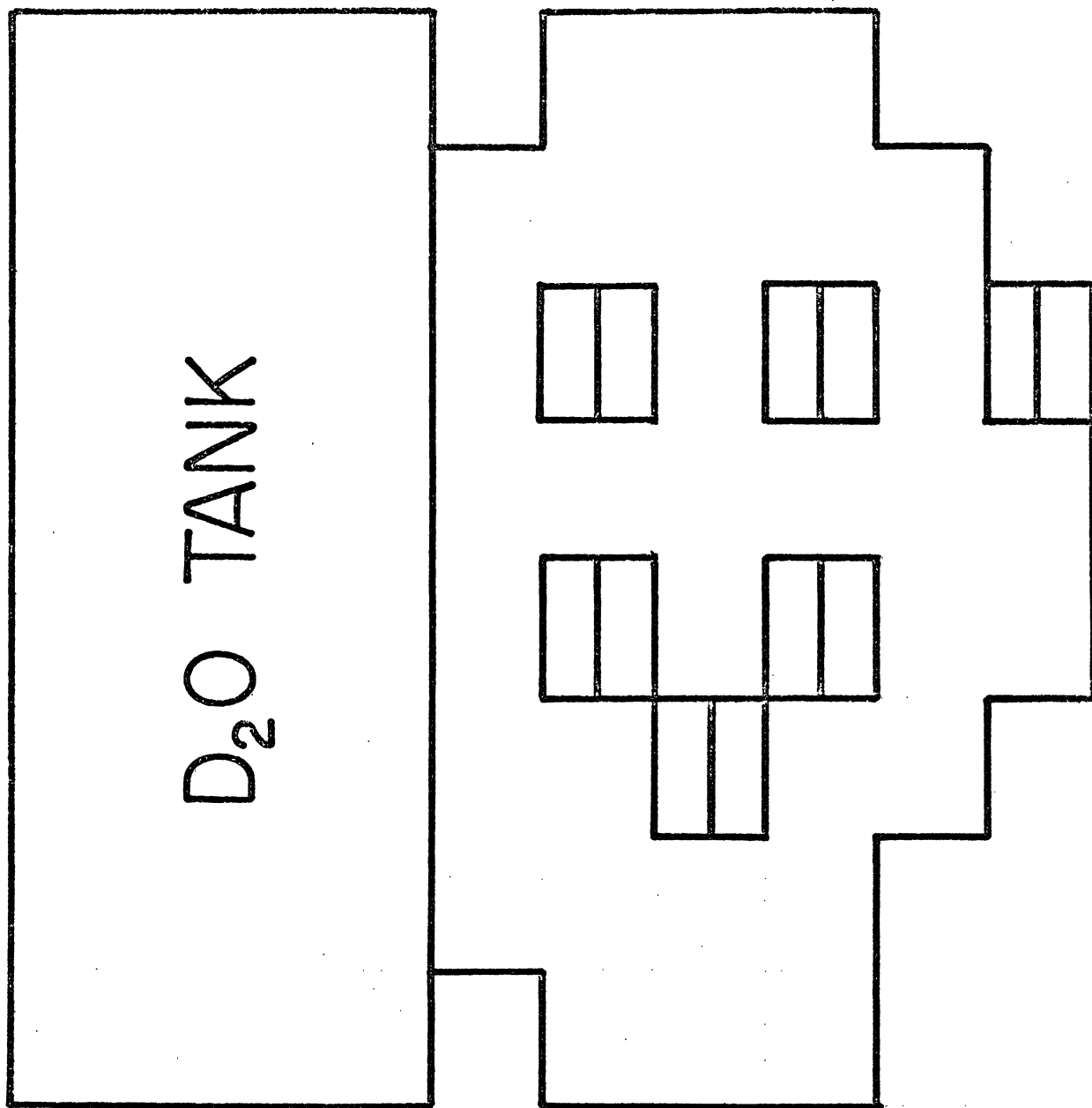



Fig. 1. FNR core geometry, showing fuel support matrix, heavy water tank, and beamports

↑N



HEU 5-29-82

Fig. 2. HEU normal core pattern. Special elements noted by .

power, and at the same time provide a data base against which model predictions can be compared.

These purposes are best fulfilled if the comparisons can be made when both HEU and LEU have approached equilibrium burn-up. Unfortunately this has not yet been possible, since only HEU conditions near equilibrium (1979-1981) have been available, while only a nearly clean, unburned ( $\sim 2.0\%$ ) LEU core has been achieved. This means that until equilibrium a relatively small (29-31 element) LEU core must be compared with the larger 38-39 element equilibrium HEU core. There is, of course, no reason in principal why this initial substantial geometry difference cannot be included in the computer modeling program. However, the difference in buckling, for the HEU and LEU cores measured, must be kept in mind in evaluating LEU/HEU changes. To show the importance of these buckling effects extensive data were obtained on special cores (which will be designated the "high leakage" HEU) which mocked up the small LEU cores as closely as possible.\* This was done by reproducing the LEU 5-row loading in the north-south direction and also the east-west dimension adjacent to the D<sub>2</sub>O tank along the north face of the core.

There were several experimental difficulties encountered in obtaining reliable data. First, the conversion from HEU to LEU and back again extended over many months. Changes of only a percent or so in count rates or detector currents become important in such a time period. During this interval in the normal life of the operating FNR, changes in core and beam port instrumentation had to be minimized and monitored. Control over beam port changes was particularly difficult. As a result of pool water leakage, G-port must be pressurized and small changes in pressure require occasional repressurization, resulting in a variable water vapor density in the port collimation. Again, unexpected changes in A-port beam geometry occurred. As a consequence G-port data is somewhat suspect, and A-port data was available for only part of the experiments.

Second, the initial conversion to the LEU core was sufficiently unpredictable in reactivity that fuel element additions were necessary during the initial LEU experiments. As a consequence three LEU cores of slightly different loading geometry are reported herein; these we designate LEU (1-5-82), LEU (1-21-82), and LEU (4-1-82). The core geometries for these are shown in

\*This experiment was suggested by Mr. Gary Cook, to whom we are indebted.

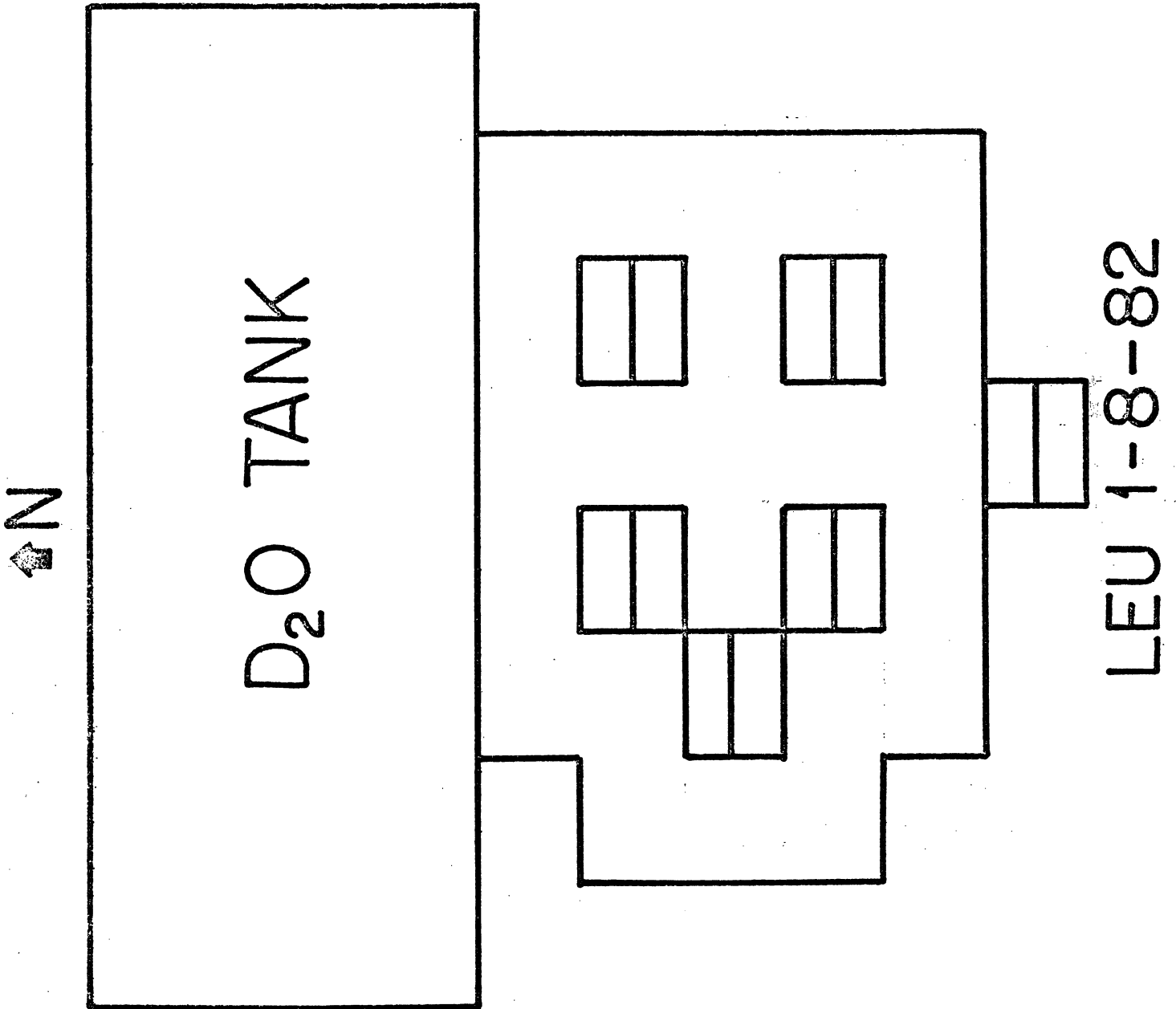


Fig. 3. LEU (1-8-82) core pattern

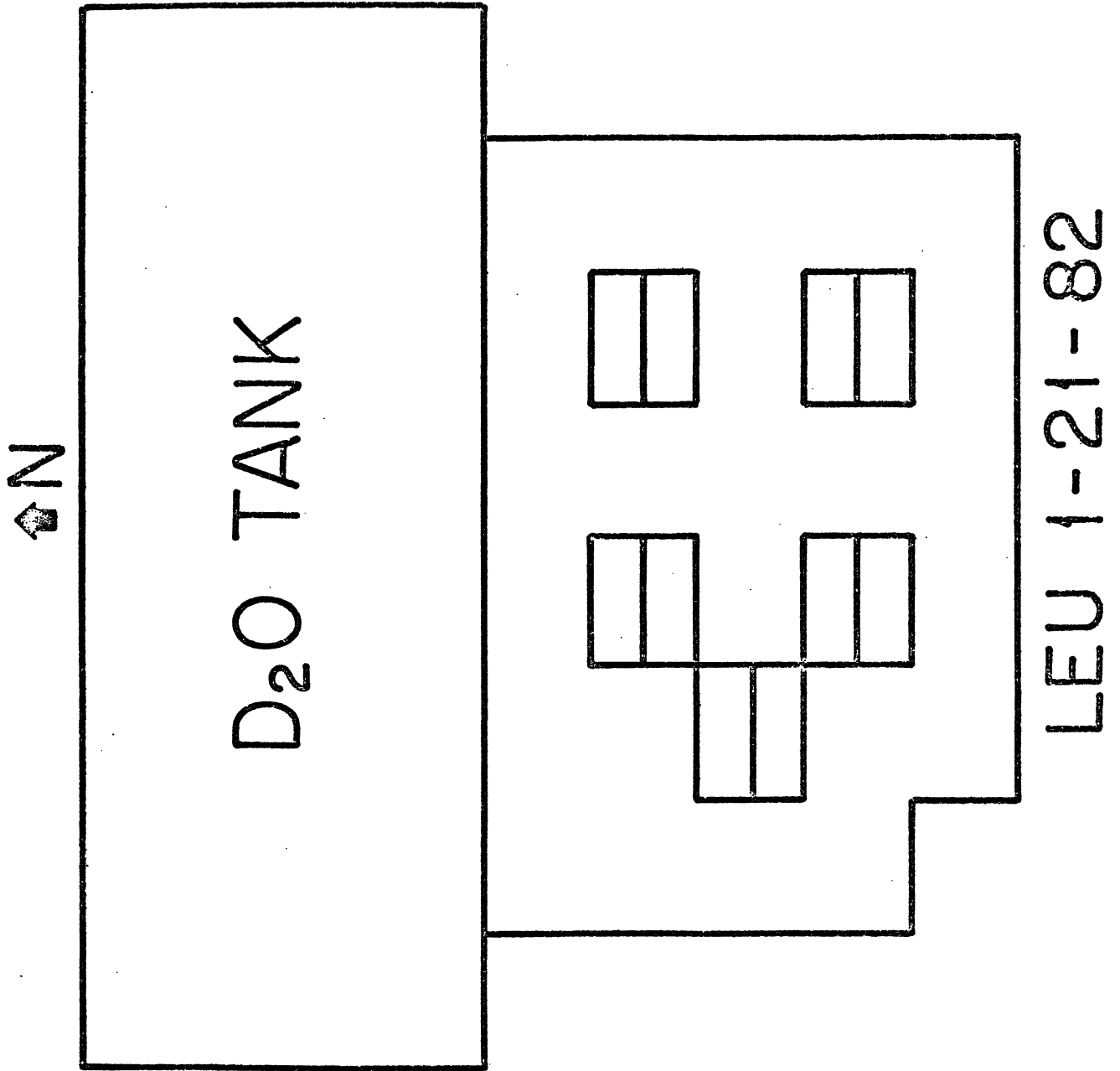


Fig. 4. LEU (1-21-82) core pattern

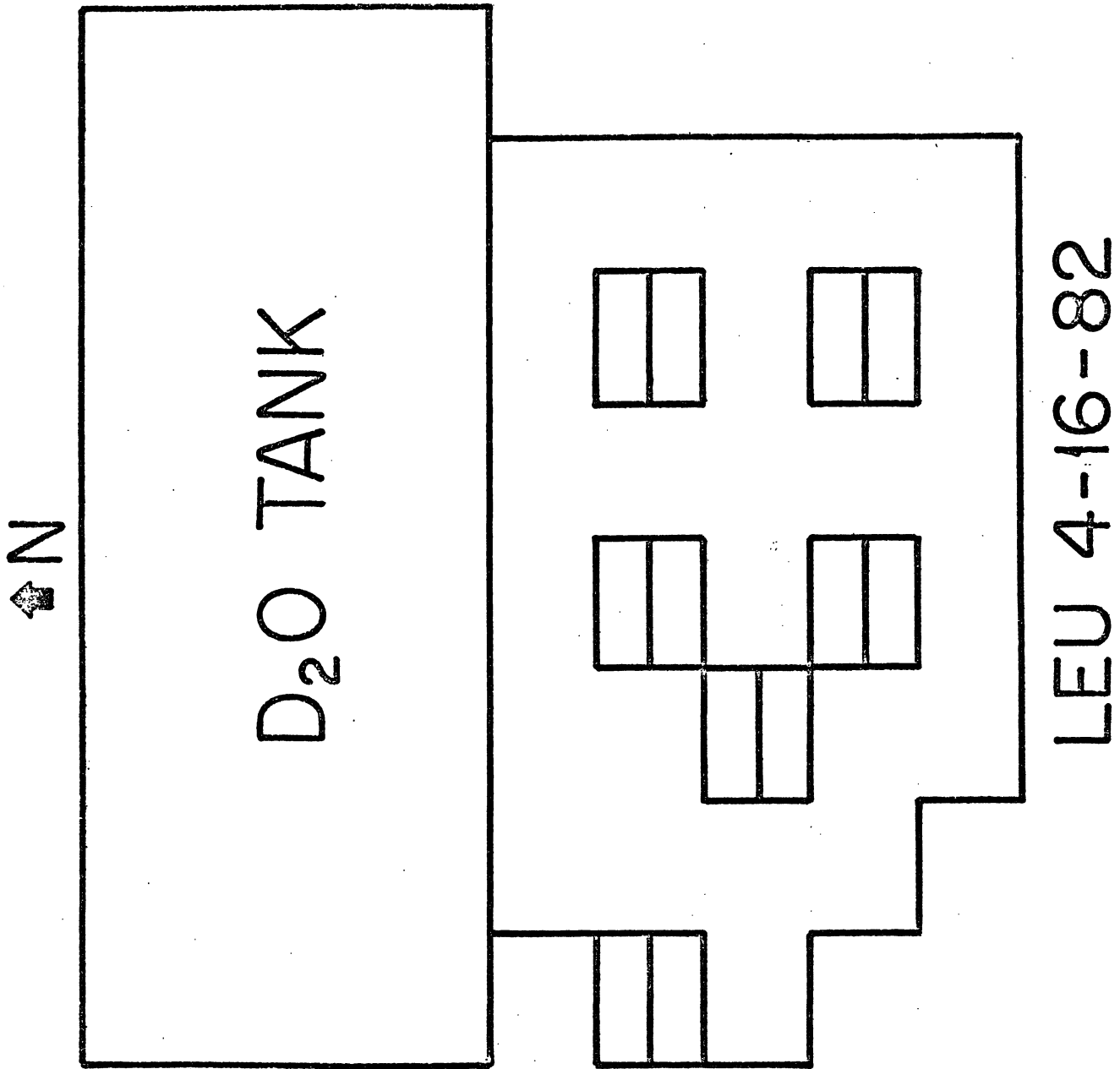


Fig. 5. LEU (4-16-82) core pattern

Figures 3,4, and 5. The major difference in these cores, as is evident in the figures, was a shift from east to west in the core loading pattern. This had a considerable effect, apparently, in shifting the beam port leakage pattern, as will be discussed below.

Third, the D<sub>2</sub>O tank has presented several special problems. Access to the volume of the tank is very limited; it is possible to reach only the upper region of the tank, the deepest penetration being 5" below the core fuel top level for the SPND detector and, 8" for wire activations. This requires a large extrapolation from a position of maximum flux gradient to predict data equivalent to core midplane. In addition there is now evidence that the rhodium SPND response in the D<sub>2</sub>O tank does not agree with either Fe or Rh wire activations when all three measurements are normalized to measurements at the same point at the center of the core.

#### Beam Port Leakage Currents

Accurate count rates were observed at the exit positions for G-, I-, and J-ports during the period 8-19-81 through 8-1-82, for A-port from 8-10-81 through 1-15-82, and for F-port from 4-14-82 through 5-19-82. Care was taken to wait for equilibrium xenon, and data were invariably used only when shim rods were within 2"-4" of full withdrawal. All of these ports have source planes either at the outer north face of the of the D<sub>2</sub>O tank (F,G,I) or are tangentially oriented 105° from north and look through reentrant voids to the central volume of the D<sub>2</sub>O tank (A,J). That is, the effective source planes for the latter are within 8" of the north-south tank center line, and within approximately 4" of the D<sub>2</sub>O south face. Port axes for A,F, and J are at core midplane, port axes for G, and I are 6" above midplane. The currents monitored at A and G are seen only after Bragg reflection at nominal specific neutron energies of 0.06 and 0.072 ev respectively, while those from J and F correspond to the full leakage spectrum. I-port currents were also monochromatic, but the intensities of all energies within the thermal leakage Maxwellian were probed. There was no indication that the effect of monochromatization influenced any of the intensity results.

The comparison of leakage currents are recorded in Tables I and II for three core loading changes. The first two are given in Table I and compare the effects of transforming from a representative HEU geometry to an LEU geometry, and then back again in reverse order. In reading Table I it is not meaningful to compare the two HEU cores or the two LEU cores because for the



TABLE I

PORT	HEU FALL 1981				LEU JAN. 1982				RATIO $\frac{\text{AVG. LEU}}{\text{AVG. HEU}}$	OVERALL RATIO	
	AUG	OCT	NOV	AVG $^{\circ}$ /s	1/8	1/21	AVG $^{\circ}$ /s	AVG.			
A			51.6 $\pm$ 1.5	51.6 $\pm$ 1.5	48.5 $\pm$ 1.5		48.5 $\pm$ 1.5	0.94 $\pm$ 0.04	0.98 $\pm$ 0.02		
F											
G	310.5 $\pm$ 6	298 $\pm$ 4	289 $\pm$ 6	299 $\pm$ 10	296 $\pm$ 4	298 $\pm$ 4	297 $\pm$ 4	0.99 $\pm$ 0.04			
I											
J	1260 $\pm$ 10	1210 $\pm$ 10	1242 $\pm$ 10	1237 $\pm$ 10	1223 $\pm$ 10	1250 $\pm$ 10	1237 $\pm$ 10	1.00 $\pm$ 0.01			
	HEU MAY 1982				LEU APRIL 1982						
PORT	5/14	5/15, 5/16	5/19	5/28	AVG $^{\circ}$ /s	4/14	4/20	4/21	AVG $^{\circ}$ /s	RATIO $\frac{\text{AVG. LEU}}{\text{AVG. HEU}}$	AVG.
F	8.1	8.0	7.95		8.01 $\pm$ 0.10			9.59 $\pm$ 0.2	9.59 $\pm$ 0.2	1.20 $\pm$ 0.03	1.11 $\pm$ 0.04
G	275.3	275.5	276.6	277.5	276.2 $\pm$ 4	324.0	326.3	322.0	324.1 $\pm$ 5	1.17 $\pm$ 0.03	
I	77.4	77.5	77.0		77.3 $\pm$ 2			87.5	87.5 $\pm$ 2	1.13 $\pm$ 0.04	
J	1249	1269	1263	1258	1260 $\pm$ 10	1181	1196	1206	1194 $\pm$ 10	0.95 $\pm$ 0.01	

TABLE II

HEU MAY 1982						"HIGH LEAKAGE" HEU JULY '82			
PORT	5/14	5/16	5/19	5/28	AVG <sup>c</sup> /s	6/26	AVG <sup>c</sup> /s	RATIO $\frac{\text{AVG H.L.HEU}}{\text{AVG.HEU}}$	OVERALL AVG.
G	275.3	275.5	276.6	277.5	276.2 <sup>±</sup> 4	290.2	290.2 <sup>±</sup> 4	1.050 <sup>±</sup> 0.021	1.062 <sup>±</sup> 0.024
J	1249	1269	1263	1258	1260 <sup>±</sup> 10	1353	1353 <sup>±</sup> 10	1.074 <sup>±</sup> 0.012	

the G-port detector a recalibration was made. Care was taken, however, to leave all detector stations untouched between the HEU to LEU conversion in both comparisons. The April to May LEU to HEU change should be most reliable since the data sets are separated by only one month in time. The first change compares data for the HEU loading taken in August, October and November, 1981, with that for the initial two loadings of LEU, shown in Figures 3 and 4, taken in January, 1982. The reverse change compares data from the LEU core of April, 1982 (Figure 5) and the reinstalled HEU core of May, 1982 (Fig. 2). The two HEU cores are closely equivalent to each other and to earlier HEU data reported from September, 1979; they differ only in the substitution of a "special" element in place of a regular element on the south face, as shown present in Figure 2. The LEU cores were somewhat different as needed to meet reactivity requirements, as noted earlier. As may be seen by comparing Figures 3, 4, and 5 there is a gradual shift toward the west face, particularly between January and April, 1982 and an increase in total number of fuel elements.

The data of Table I for the January LEU cores show that within counting statistics and reproducibility in time, there was no change in leakage intensities from all three monitor stations, the average ratios of LEU to HEU levels being  $0.94 \pm 0.04$ ,  $0.99 \pm 0.04$ , and  $1.00 \pm 0.01$ , giving an overall ratio of  $0.98 \pm 0.02$ .

By contrast, the reverse transformation of LEU to HEU which occurred between April and May, 1982 shows a significant increase in leakage for the LEU over the HEU loadings, for three of the four beam ports. These show LEU/HEU ratios of  $1.20 \pm .03$ ,  $1.17 \pm .03$ , and  $1.13 \pm .04$  for F-, G-, and I-ports. At the same time J-port shows a loss in leakage ratio of  $0.95 \pm .01$ . A crude estimate of the change in thermal flux per unit volume of the D<sub>2</sub>O tank can be obtained from the average of these four stations. This gives  $1.11 \pm .04$ . While there has been a possible question about the pulse channel electronics at J-port in April, we are inclined to believe all the data are reliable. We observe two effects; (a) a possible shift in leakage from east to west, consistent with the LEU loading pattern of April, 1982, and (b) an average increase in leakage flux from the LEU core of at least 11%. The loss of A-port data to verify the shift is particularly unfortunate.

To estimate the effect of the higher north-south buckling for the LEU cores a 5 row "high leakage" HEU, Figure 6, was compared

↕ N

D<sub>2</sub>O TANK

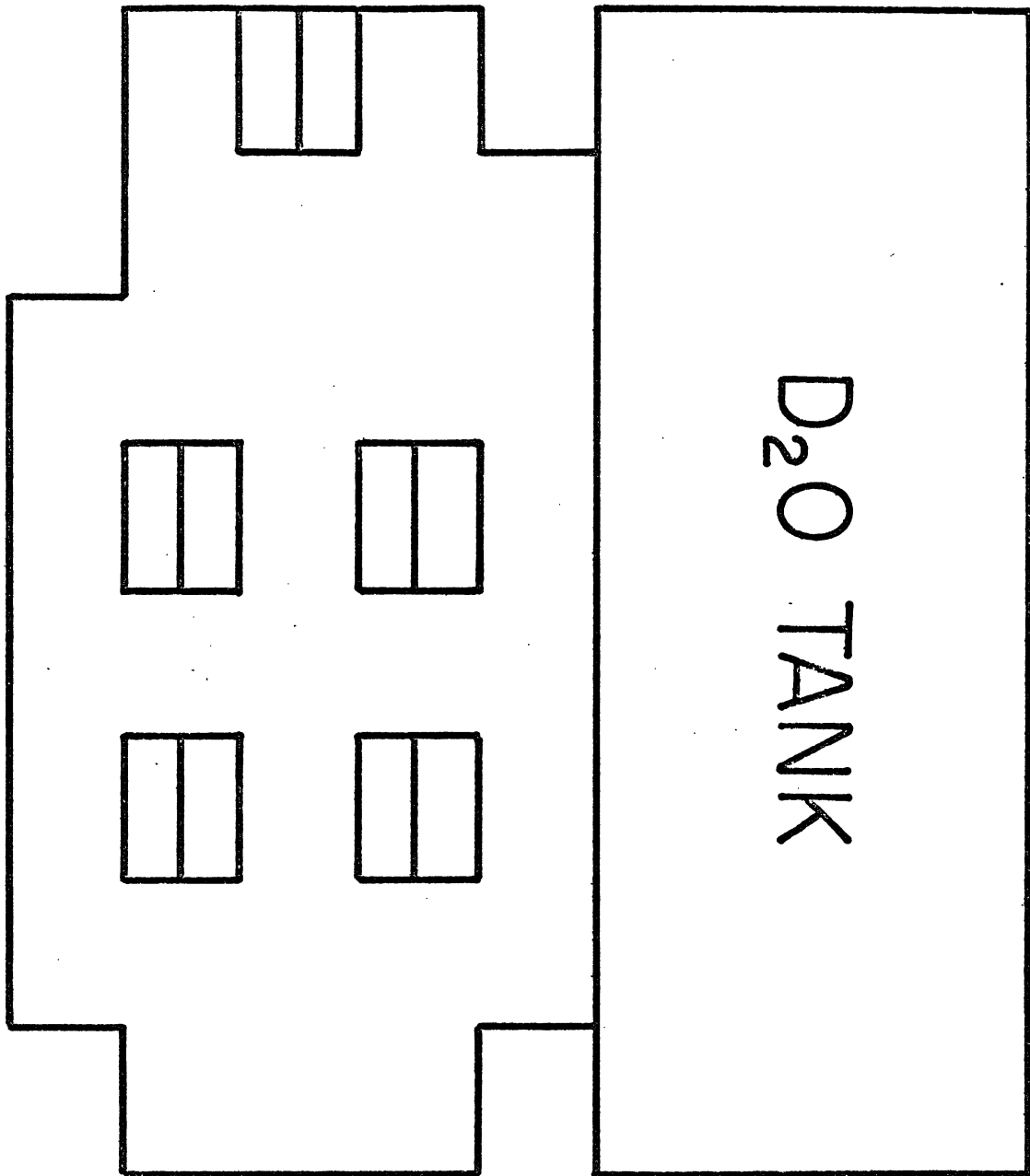


Fig. 6. "High Leakage" HEU core pattern (7-7-82)

"HIGH LEAKAGE" HEU 7-7-82

with the HEU loading of Figure 2. In addition to extensive wire activation and SPND data taken in this core, beam port leakage currents are shown in Table II. As expected an increase was found and was about 6%.

The data of Tables I and II are not simple to interpret, and the correlation with in-core data, to be discussed below, is only partially satisfactory. We draw the following tentative conclusions:

a) Installation of a full, unburned LEU core in place of an equilibrium HEU core will change beam port leakage by a factor between 0.95 and 1.15.

b) A significant fraction of this gain, perhaps the major fraction, occurs because of the enhanced north-south leakage associated with the clean LEU geometry. This gain would be expected to be reduced as the larger LEU equilibrium core is reached.

c) Interpretation of leakage currents from a D<sub>2</sub>O reflector with reentrant beam port voids is dependent both on the position and angle of beam departure from the heavy water reflector. There is evidence, for example, that J-port leakage currents closely follow in-core changes as measured in the outermost lattice position L-35 by SPND. (L-35 is the element adjacent to the D<sub>2</sub>O tank and midway, east to west, between control rod special elements). If both sets of data from the January, 1982 LEU core are normalized to unity the changes in J-port current and L-35 SPND response for successive LEU and HEU cores, as shown in Table III, are remarkably close. At the same time, the G-port current appears to compare not with in-core results, but with SPND data taken in the outer (northern) volume of the D<sub>2</sub>O tank (position D<sub>2</sub>O-S). This "correlation", though less impressive is also shown in Table III. It is evident, finally, that changes in the inner D<sub>2</sub>O position, D<sub>2</sub>O-X, do not correlate well with either J- or G-port data.

#### Beam Port Thermal Neutron Spectrum Changes

The leakage spectrum at beamport I was measured for both the equilibrium HEU core (November, 1981) and the LEU core of April, 1982. This was undertaken to determine whether any significant thermal neutron spectrum hardening of the leakage current could be detected for the low enrichment design. Measurements were made at I-port by use of a single silicon crystal diffractometer. Flux intensity as a function of energy, from E=0.02 eV to 0.140 eV, was obtained by a conventional  $\theta$ -2 $\theta$  Bragg scattering survey. A very narrow mosaic silicon crystal was used in a transmission mode; the {111} planes were used to remove second order contamination. Considerable attention was given to the crystal

TABLE III

CORE CONDITION	J-PORT	SPND L-35	G-PORT	SPND D <sub>2</sub> O-S	SPND D <sub>2</sub> O-X
LEU Jan 1982	1.0	1.0*	1.0	1.0	1.0
LEU Apr 1982	0.965	0.970	1.091	1.097	0.987
HEU May 1982	1.019	1.004	0.93	-	0.876
"H.L." HEU July 1982	1.094	1.108	0.98	-	0.934

\* LEU Jan 1982 Current for SPND in L-35 taken as the average of values measured for LEU-1-8-82 and LEU-1-21-82

collimation alignment to guarantee that all of the Bragg beam, in both the vertical and horizontal dimensions, was detected at each energy. Integral Bragg peak counts were obtained first by exact centering of the Bragg beam through very narrow vertical, then narrow horizontal slits, then opening the apertures to integrate the total Bragg beam. The detector was a transmission fission chamber of efficiency  $\xi \sim 10^{-3}$ . Such a detector allows accurate energy dependent efficiency corrections because these are simply proportional to the known fission cross section for U-235. Background was determined as the count rate when the crystal was rotated  $\pm 2^\circ$  from the Bragg condition. The flux as a function of angle, and therefore energy, was determined from the net count rate, according to

$$C.R.(\theta) = K \cdot \xi(\theta) \cdot R(\theta, \eta) \cdot \phi(\theta) \quad (1)$$

where K is a geometry constant,  $\xi(\theta)$  is the detector efficiency, and  $R(\theta, \eta)$  is the integrated reflectivity of silicon in transmission. This last term is a well known function from kinematic crystal theory which depends on crystal thickness t, silicon cell geometry, and a mosaic width parameter  $\eta$ , according to the relation

$$R(\theta, \eta) = \sqrt{\frac{\pi}{2}} \cdot \eta e^{-\tau_a t / \cos \theta} \cdot \sum_{j=1}^{\infty} \frac{(-1)^{j+1}}{j! \sqrt{j}} \left( \frac{2t\eta Q}{\sqrt{2\pi} \cos \theta} \right)^j \quad (2)$$

$$\dots Q = \frac{|F(hkl)|^2 \cdot \lambda^3 N_c^2}{\sin 2\theta}$$

$F(hkl)$  is the crystal structure factor and  $N_c$  is the number of silicon cubic unit cells per unit volume.

Although the leakage spectrum is well characterized by a Maxwellian of neutron temperature T, the weakness of the method lies in the need to calculate  $R(\theta, \eta)$ . The absolute temperature obtained is sensitive to the choice of the mosaic parameter  $\eta$ . While  $\eta$  was included as a parameter in the least square fitting of the data, it was found to have a shallow minimum and is therefore somewhat suspect. This in turn makes the absolute temperature also suspect. However, it is believed that small temperature changes are reliably detected by the method.

Data points were obtained throughout the energy interval noted above and the neutron temperature obtained by a fit to the Maxwellian function

$$\phi(E) = A \cdot E \cdot e^{-E/kT} \quad (3)$$

where A is a constant and k is the Boltzmann constant. The data is plotted as  $\ln \Phi/E$  vs  $E$ , from which  $kT$  is determined, through a least square fitting procedure, as the inverse of the slope of the plot.

Figures 7 and 8 show the resulting plots for the HEU and LEU respectively. The data are extremely well fit by straight lines between 0.02 eV and 0.13 eV. The temperatures obtained are  $373.0 \pm 2.4^\circ\text{K}$  and  $370.8 \pm 1.9^\circ\text{K}$  respectively. The difference is well within error limits, so that we are led to conclude that no apparent spectrum change is evident at I-port. The temperatures measured are not to be considered accurate on an absolute basis, but the relative values should be reliable.

It is evident that the temperature observed will depend on the effective source volume in the  $\text{D}_2\text{O}$  tank seen by the port collimation. I-port views the  $\text{D}_2\text{O}$  tank from the NE corner face. The I-port axial line extends almost diagonally from NE to SW across the tank, making an angle of  $63^\circ$  with the north axis. I-port does not have a reentrant void.

It is expected that the spectrum will soften as the port axis moves away from the normal (north). In July, 1982 (Figure 6), the diffractometer was moved to J-port where the angle of attack is  $105^\circ$ . A scan was repeated using the same geometry and systematics. The temperature observed was indeed lower and was found to be  $330 \pm 5^\circ\text{K}$ . Unfortunately, this measurement was not repeated for the standard HEU and LEU cores, so that a comparison with I-port has not yet been possible at J-port.



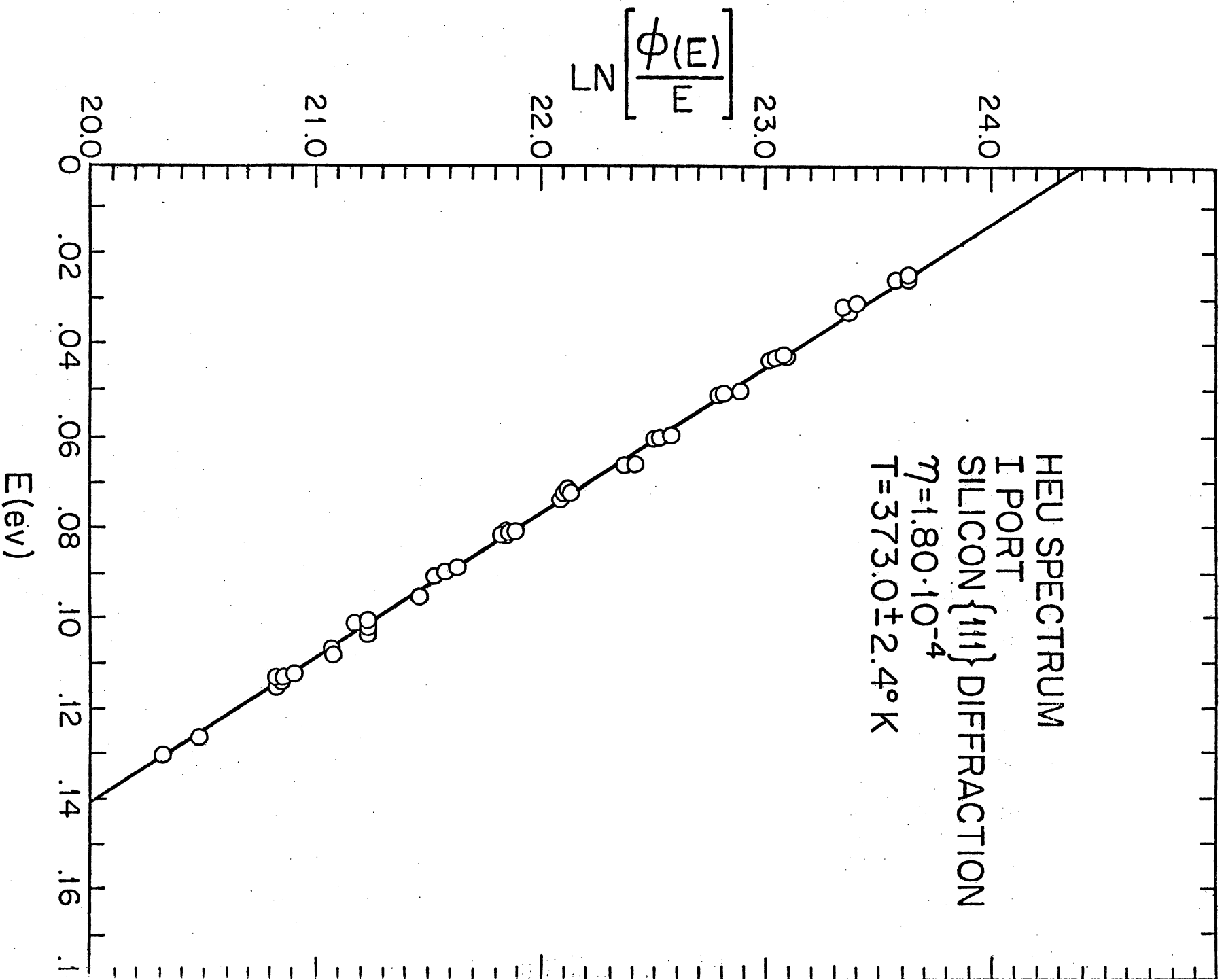


Fig. 7. HEU thermal neutron Leakage spectrum

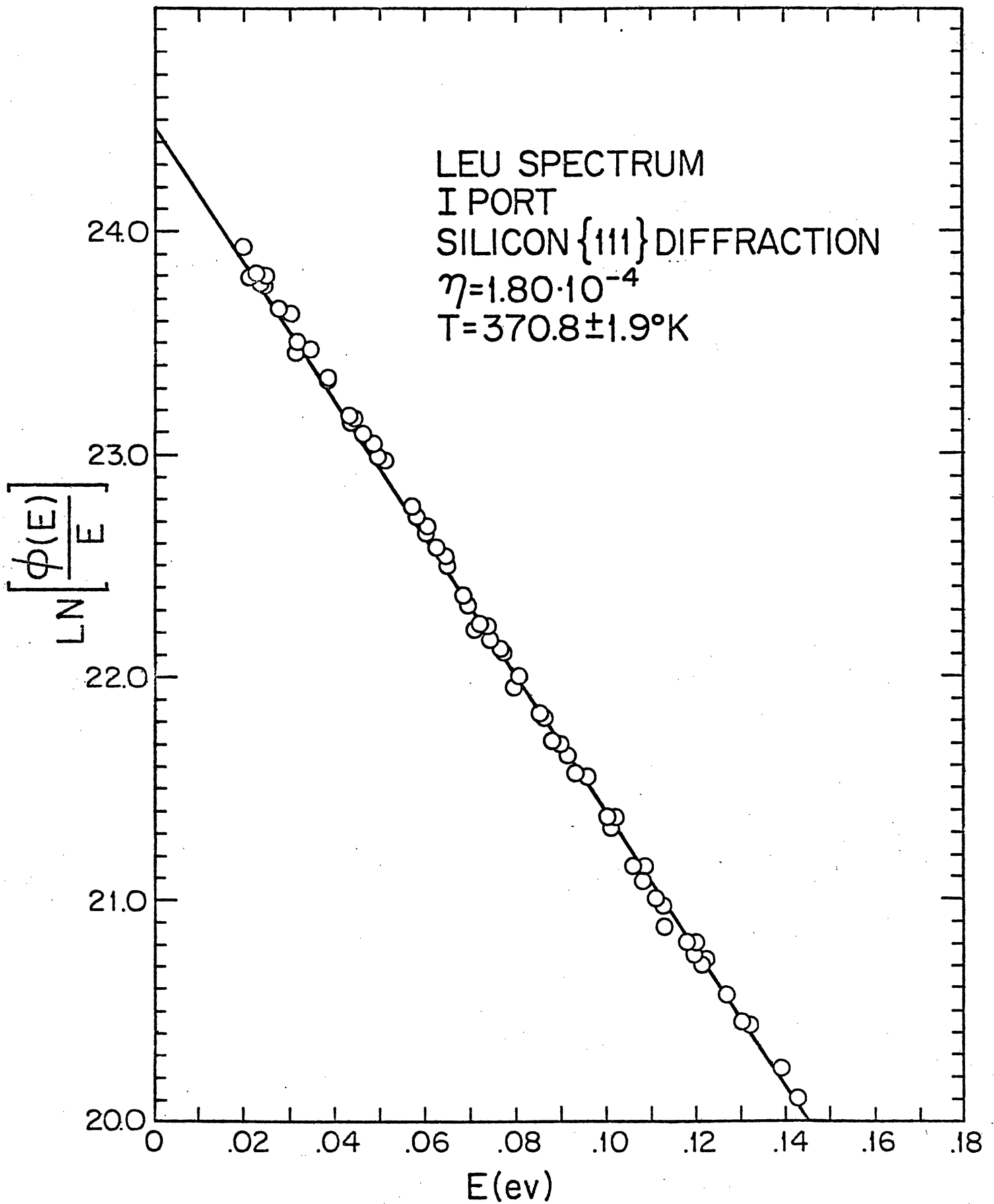


Fig. 8. LEU thermal neutron leakage spectrum

APPENDIX B

FNR Demonstration Experiments

Part II

Subcadmium Neutron Flux Measurements

FNR DEMONSTRATION EXPERIMENTS  
PART II: SUBCADMIUM NEUTRON FLUX MEASUREMENTS

by

D. K. Wehe and J. S. King  
Phoenix Memorial Laboratory  
University of Michigan  
Ann Arbor, Michigan 48109

Introduction

The FNR HEU-LEU Demonstration Experiments include a comprehensive set of experiments to identify and quantify significant operational differences between two nuclear fuel enrichments. One aspect of these measurements, the subcadmium flux profiling, is the subject of this paper. The flux profiling effort has been accomplished through foil and wire activations, and by rhodium self-powered neutron detector (SPND) mappings.

Activation Data

Techniques

The irradiation of wires and foils in and around the FNR core provides information on the reactor flux. Irradiations in the core are made by taping the probe material to a thin ( $\approx .010$ " ) aluminum paddle approximately 30" long. In some cases, samples are enclosed by .020" cadmium capsules or tubing. The bare and cadmium covered probe materials are irradiated simultaneously, mounted at the same core height, and separated in the horizontal plane by about an inch. The paddles are curved to facilitate insertion between two fuel plates (separation distance is .117"). A paddle stop rests on the top of the fuel plate and provides the axial reference point for the samples.

The heavy water tank on the north side of the core contains a dozen 1" diameter, vertical tubes which penetrate into the tank. The majority of these penetrate to 8" below the top of the fuel plate. While these tubes are filled with H<sub>2</sub>O, calculations indicate that the measurements are representative, within a few percent, of an unperturbed D<sub>2</sub>O environment. Samples are activated in these tank penetrations by first securing the material to the outside of a 5/8" diameter aluminum rod or tube, and then lowering the holder to the bottom of the tank's vertical penetration. The samples are rotated during the irradiation to ensure uniform activations. In all cases, the reactor must be subcritical during both sample insertion and removal.

## Post-irradiation Handling and Counting

After the irradiations, the handling of the samples depends upon the activity and half-life of the activated material. For long-lived isotopes, such as Mn-54, the material is normally stored in the pool until ready for counting. For short-lived isotopes, such as Rh-104m, the samples must be expeditiously and remotely prepared for counting.

The counting of the activated samples is performed using GeLi detectors. Wire samples are counted between two oppositely facing detectors multiplexed together. The sample is positioned by an automatic sample changer into a rotating, cylindrical plexi-glass holder. Pulse pileup losses are accounted for with a precision pulser fed into the GeLi preamplifier. The amplified and multiplexed signals are counted using an ND 570 ADC and fed into an ND 6620 analyzer/computer for analysis. Absolute efficiencies can be determined with NBS and Amersham mixed point source standards through a cross calibration technique at a separate GeLi detector station. Background interference is made negligible for most gamma ray energies with 2-6" lead shielding around all detectors.

The counting data is processed to give a saturated activity per unit nucleus,  $A_{satn}$ , through the relationship:

$$A_{satn} = \frac{\lambda C_{net} \left( \frac{t_r}{t_l} \right) \left\{ \frac{(\text{Pulser rate} \cdot t_L)}{(\text{Pulser counts})} \right\}}{(1 - e^{-\lambda t_i})(1 - e^{-\lambda t_r}) \epsilon (e^{-\lambda t_w}) BR \left[ m \cdot \% \cdot N_{avo} / AW \right]} \quad (1)$$

where:  $\lambda$  = decay constant  
Cnet = net counts observed  
t<sub>l</sub> = detector live time  
t<sub>r</sub> = detector real time  
t<sub>i</sub> = irradiation time  
 $\epsilon$  = absolute detector efficiency  
BR = branching ratio  
t<sub>w</sub> = time between irradiation and counting  
AW = atomic weight of element  
N<sub>avo</sub> = Avogadro's number  
a/o = atom percent of parent isotope  
m = sample weight

Once the data is converted to saturated activity per nucleus, it can be further processed to give flux data. The difficulty is that there is no unique method for translating activities into

flux. Different approaches yield fluxes which can differ substantially in their magnitudes. Two separate techniques are presented below.

1). Beckurts and Wirtz Approach. (Reference 1).

The thermal flux can be determined from bare and cadmium covered activations according to:

$$\phi_{th} = \frac{A_{satn}^{bare} - F_{cd} A_{satn}^{cadmium}}{\sigma_{2200} \frac{\sqrt{\pi}}{2} \sqrt{\frac{T_0}{T}}} \quad (2)$$

where  $F_{cd}$  is a material dependent correction to account for the epithermal activity produced below the cadmium cutoff energy. (Formal definitions of the thermal cutoff energy [ $E_{tc} \approx 0.1$  ev], and the cadmium cutoff energy [ $E_{cc} \approx 0.55$  ev], can be found in references 1 and 2).  $T_0$  and  $T$  are the temperatures corresponding to neutron velocities at 2200 m/sec and at the most probable Maxwellian energy. The flux spectrum is assumed to change smoothly from Maxwellian to  $1/E$  through the use of a joining function. The constant flux per unit lethargy expected in the epithermal region is determined from the cadmium covered irradiation, and this is used to infer the flux between  $E_{tc}$  and  $E_{cc}$ . If this flux is termed  $\phi_{it}$ , i.e. "intermediate thermal", then one can define the subcadmium flux to be:

$$\phi_{sc} = \phi_{th} + \phi_{it}$$

2). Effective Cross Section Approach.

By defining effective group cross sections, one can determine group fluxes in a conventional multi-group spectrum calculation. Define an effective activation cross section  $\langle \sigma \rangle$  by

$$\langle \sigma \rangle = \frac{\int_0^{E_{cc}} \sigma(E) \psi(E) dE}{\int_{E_a}^{E_b} \psi(E) dE}$$

where  $\psi(E)$  is a computed spectrum. Then the group flux between  $E_a$  and  $E_b$  is:

$$\phi_{E_a}^{E_b} = \int_{E_a}^{E_b} \phi(E) dE = \frac{A_{satn}^{bare} - A_{satn}^{cadmium}}{\langle \sigma \rangle}$$

The subcadmium flux is then determined by choosing the limits of integration to be 0 to Ecc.

In both approaches, some knowledge of the spectrum must be known a priori. The Beckurts and Wirtz approach was used throughout reference 2. The present paper, however, makes use of the second approach, which is believed to be an improved treatment. The spectral calculations needed to determine the effective cross sections are discussed in a separate paper presented in this conference.

#### Iron Wire Activation Data

Irradiation of iron wires in the FNR yields two useful reactions: Fe-58(n, $\gamma$ )Fe-59, and Fe-54(n,p)Mn-54. Activation data from the first reaction are used to measure flux in the thermal regime, while data from the second (threshold) reaction respond to fast flux near the fission regime. Pertinent material data are summarized in Table I. The long half lives of these daughters obviates the necessity for rapid handling. The irradiations are performed at equilibrium xenon, with the three FNR shim rods typically 85% or more withdrawn from the core. Typically, 29" lengths of bare and cadmium covered wire are irradiated at full power for an hour, then cleaned, cut into one inch segments, and coiled to simulate point sources.

To illustrate the quality of typical iron wire results, Figure 1 presents axial flux data at the center (L-37) of three different FNR cores. The three cases have been normalized to unity to emphasize the close similarity in axial profile typifying all our HEU-LEU comparisons. Error limits, both vertical and horizontal, as well as profile smoothness are also typical. Figure 2 compares some of the same iron wire results with rhodium SPND measurements to be described below. Again all profiles have been normalized to unity at the core center. The close agreement between the two techniques when normalized together is quite satisfactory, we believe.

#### Rhodium Wire Activation Data

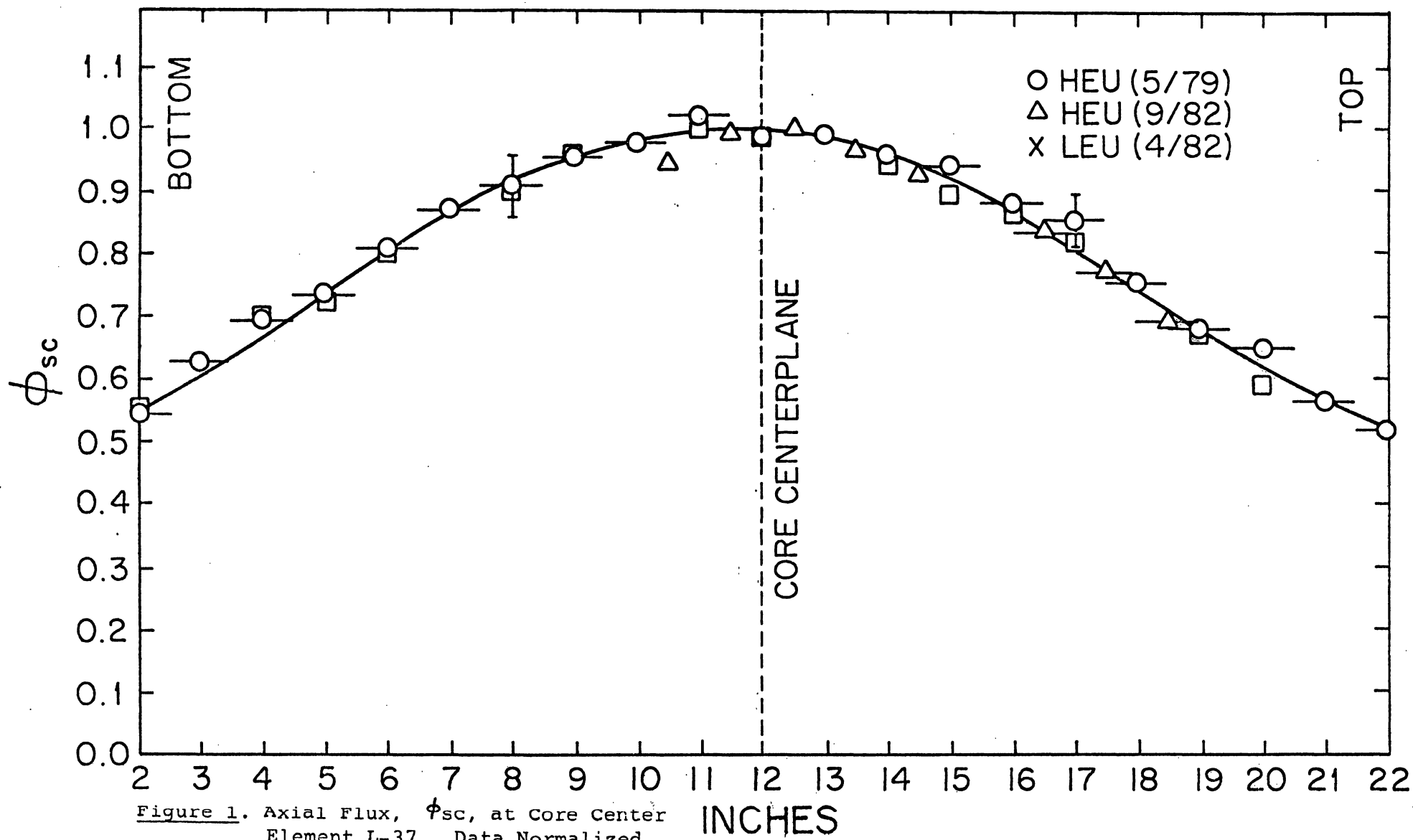
The activation and counting of rhodium wire is quite different from that of iron wire, as can be inferred from Table I. Rhodium, because of its large cross section and short half life, must be handled carefully, and yet, expeditiously. Because of lack of accurate beta counting equipment available near the reactor, and the difficulty in beta counting multiple samples quickly, the weak 555 keV gamma was used to measure the reaction.

TABLE I  
Activation Material Data

Reaction	Atomic Weight	Isotopic Abund.	Gamma Energy (kev)	Branch Ratio	Half Life	Effective Subcadmium Cross Section $\langle \sigma \rangle$ barns *			Normal Diameter	IRRAD. Time	IRRAD. Power
						Core Center	D <sub>2</sub> O (X)	H <sub>2</sub> O Reflect.			
$^{58}\text{Fe} \rightarrow ^{59}\text{Fe}$	55.85	0.29%	1099	56.5%	44.56 days	.911	.976	-	.020"	1 hr.	2MW
$^{54}\text{Fe} \rightarrow ^{54}\text{Mg}$	55.85	0.29%	835	100%	312.2 days	-	-	-	.020"	1 hr.	2MW
$^{103}\text{Rh} \rightarrow ^{104}\text{Rh}$	102.91	100%	555	2.0%	43 sec.	104.5	109.4	112.5	.020"	30 min.	20kW
$^{103}\text{Rh} \rightarrow ^{104\text{m}}\text{Rh}$	102.91	100%	-	-	4.28 min.	8.58	8.98	9.23	.020"	30 min.	20kW

\*These values are based on preliminary spectral calculations and are subject to refinement.





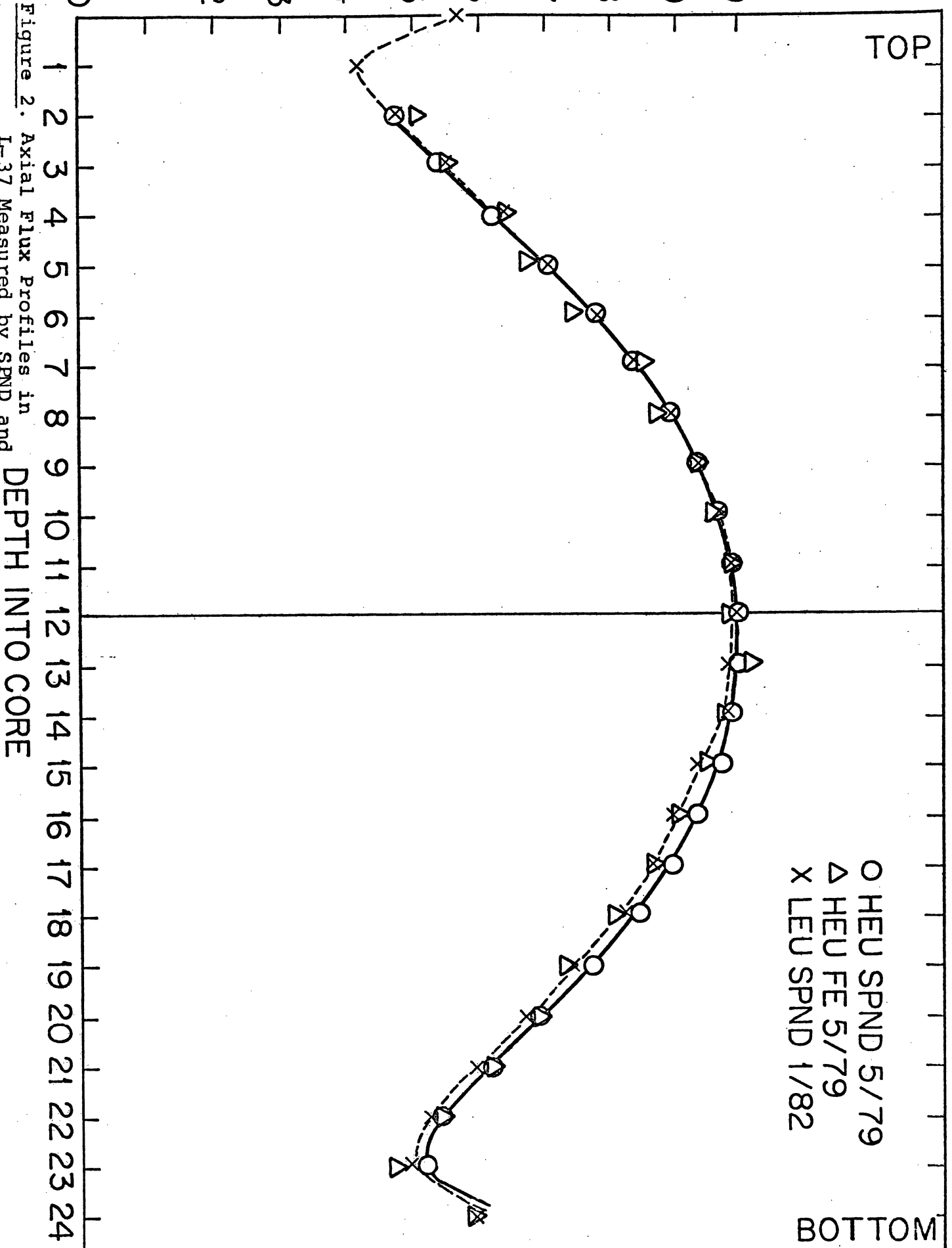


Figure 2. Axial Flux Profiles in L-37 Measured by SPND and Wire Activation. Data

DEPTH INTO CORE

O HEU SPND 5/79  
 Δ HEU FE 5/79  
 X LEU SPND 1/82

TOP

BOTTOM

$\phi_{sc}$

The rhodium wire dimensions were chosen to match the emitter dimensions of Rh SPND.

Typically, one inch lengths of 99.99% pure, bare and Cd-covered wires were irradiated at 20 kW for 30 minutes, in and around the core. Power normalizations were determined by monitoring the leakage flux at beam port J. (The beam port geometry is described in Part I of this paper.) In several separate experiments, the observed leakage intensity at J-port (and G-port as well) showed remarkable agreement with reactor power (as determined by the FNR operational fission chambers) from 20 kw to 2 MW. Post irradiation handling involved removing and cutting the wires into 1/4" segments remotely, drying the samples, and transporting them to the counting facility. All times were calibrated to a single clock.

1). Activation Kinetics.

The rhodium activation and simplified decay scheme is summarized in figure 3.

Defining:  $\sigma$  = effective production cross section,  
 $N$  = isotopic number density per Rh-103 nucleus,  
 $A$  = activity,  
 $\lambda$  = decay constant

and using subscripts g and m to refer to the ground and metastable states, one finds that:

a) during the irradiation:

$$N_m(t) = \frac{\sigma_m \phi}{\lambda_m} (1 - e^{-\lambda_m t}) \quad (3)$$

$$N_g(t) = \frac{\sigma_g \phi}{\lambda_g} (1 - e^{-\lambda_g t}) + \sigma_m \phi \left\{ \frac{1}{\lambda_g} (1 - e^{-\lambda_g t}) - \left( \frac{e^{-\lambda_m t} - e^{-\lambda_g t}}{\lambda_g - \lambda_m} \right) \right\} \quad (4)$$

Equations 3 and 4 show that for an irradiation of 30 minutes, both the ground and metastable states are saturated.

b) after the irradiation:

$$N_g(t) = \phi \left\{ \left[ \left( \frac{\sigma_m + \sigma_g}{\lambda_g} \right) - \left( \frac{\sigma_m}{\lambda_g - \lambda_m} \right) \right] e^{-\lambda_g t} + \frac{\sigma_m}{\lambda_g - \lambda_m} e^{-\lambda_m t} \right\}$$

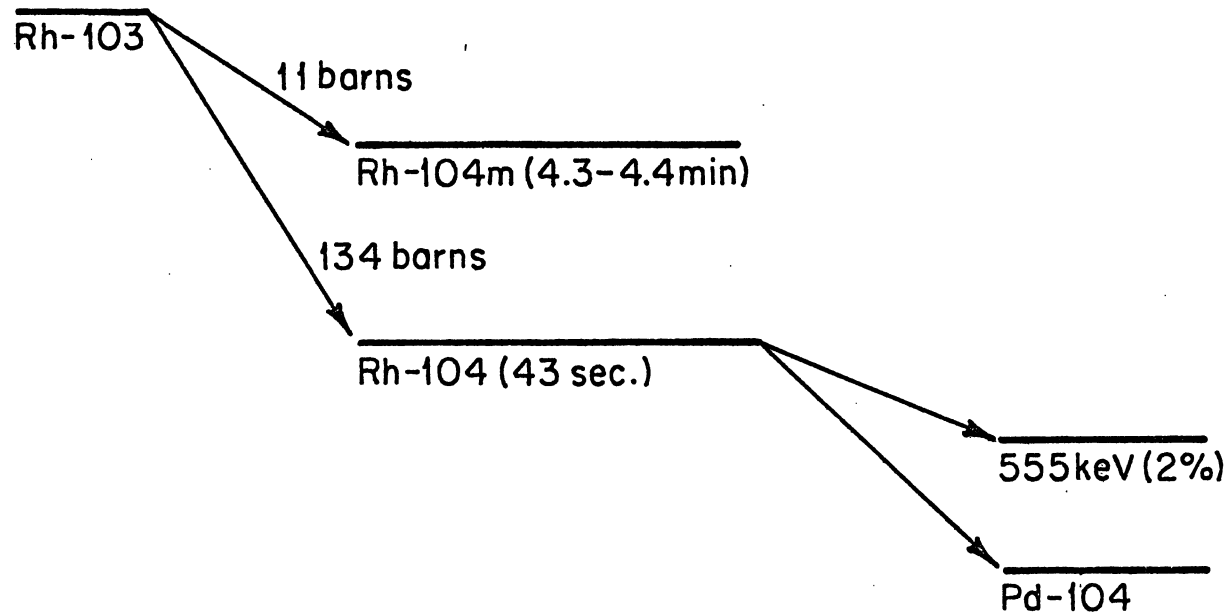


Figure 3. Rhodium Decay Scheme.

Since the minimum wait time is 10 minutes, the contribution from the ground state term is negligible, so that

$$A_g(t) = \frac{\lambda_g}{\lambda_g - \lambda_m} \cdot \sigma_m \phi \cdot e^{-\lambda_m t}$$

Thus, although the ground state decay is detected, the decay is governed by the half life of the metastable state. Furthermore, the effective cross section must be defined as:

$$\langle \sigma_{sc} \rangle = \frac{\lambda_g}{\lambda_g - \lambda_m} \left\{ \frac{\int_0^{E_{cc}} \sigma_m(E) \psi(E) dE}{\int_0^{E_{cc}} \psi(E) dE} \right\}$$

which we have assumed to be equivalent to:

$$\langle \sigma_{sc} \rangle = \frac{\lambda_g}{\lambda_g - \lambda_m} \cdot \frac{\sigma_m(E_0)}{\sigma_m(E_0) + \sigma_g(E_0)} \cdot \left\{ \frac{\int_0^{E_{cc}} (\sigma_m(E) + \sigma_g(E)) \psi(E) dE}{\int_0^{E_{cc}} \psi(E) dE} \right\} \quad (5)$$

where  $E_0$  is a fixed energy in the thermal spectrum. This cross section is shown in Table I for different media.

## 2). Epithermal Correction Factors for the Rhodium SPND

As is discussed later, the rhodium SPND responds to neutrons of all energies. If the subcadmium flux is desired, then it is necessary to know the detector current corresponding to subcadmium neutrons. This is accomplished by measuring the rhodium subcadmium fractions,  $f_{th}$ , for rhodium wire with the same diameter as that in the rhodium SPND. The results are shown in Table II for locations in and around the equilibrium HEU and fresh LEU cores. The data indicate that the flux is harder for the LEU fuel.

## 3.) Rhodium Subcadmium Flux Measurements

Rhodium activation data can also be used to determine the subcadmium flux intensity and thus provide an independent check on other profile methods. This is more difficult because of the problems of self-shielding (estimated to be 20-30%) and flux depression (calculated to be of order 5%), as discussed in reference 3. Even for relative fluxes, differences in the self-shielding are medium dependent and must be considered. However, between the D20 reflector and the central core region, this difference is calculated to be only about 5%. Relative subcadmium fluxes from rhodium wire activations are presented below.

TABLE IIMEASURED SUBCADMIUM CORRECTION FACTORS,  $f_{th}$ 

	<u>Position</u>	<u><math>f_{th}</math><sub>HEU</sub></u>	<u><math>f_{th}</math><sub>LEU</sub></u>
L-35	Regular Fuel Element (Core Boundary, North Face)		.786
L-37	Regular Fuel Element (Core Center)	.791	.749
L-39	Regular Fuel Element (LEU South Face)		.795
L-40	Regular Fuel Element (HEU South Face)	.830	
L-67	Regular Fuel Element (Second Column from West Face)	.830	
L-57	Regular Fuel Element (Third Column from West Face)		.860
H <sub>2</sub> O	Water Reflector, Second Channel (Center Plane, South Face)	.930	.914
D <sub>2</sub> O	Heavy Water Reflector (Position X) (Center Plane, North Face)	.895	.892
L-39	Special Fuel Element (waterhole)	.913	

## Rhodium Self-Powered Neutron Detector Data

### Rhodium SPND Characteristics

The rhodium SPND has served as the primary flux profiling tool at the FNR. The detector probe, shown in Figure 4 uses a 20 mil diameter, one inch rhodium emitter insulated from the 1/16" outer diameter inconel sheath with aluminum oxide. A parallel background lead, not shown in the figure, is used to correct for background effects. The probe is mounted on an inconel 600 paddle (.093" x .625" x 36") with a 1/4" x 1.5" hole around the emitter section to minimize flux perturbations. The probe can be positioned at any height in either of two water channels in any fuel assembly. Special adapters have been fabricated to permit measurements in H2O and D2O reflectors.

While rhodium has the largest sensitivity to thermal neutrons of any commercially available SPND, it also possesses two principal disadvantages:

(i) it responds significantly to epithermal neutrons because of its 5000 barn resonance at 1.25 eV, and

(ii) the presence of a metastable state (4.3-4.4 minute half life) requires waiting several minutes before an equilibrium signal can be measured.

The first of these problems is overcome by measuring the subcadmium contribution to the detector reaction rate, as described above and evaluated in Table II. As shown in reference 4, the subcadmium flux can be calculated from:

$$\phi_{sc} = \frac{f_{th} I_{net}}{S} \quad (6)$$

where:  $f_{th}$  = subcadmium fraction of the detector current,  
 $I_{net}$  = net detector current  
 $S$  = detector sensitivity to subcadmium neutrons.

The detector sensitivity can be calculated using the methods described in reference 5, or calibrated through the use of the activation data described earlier. The sensitivity is related to the emitter reaction rate per unit incident flux, so that if  $k$  is a proportionality constant, we may define a sensitivity factor

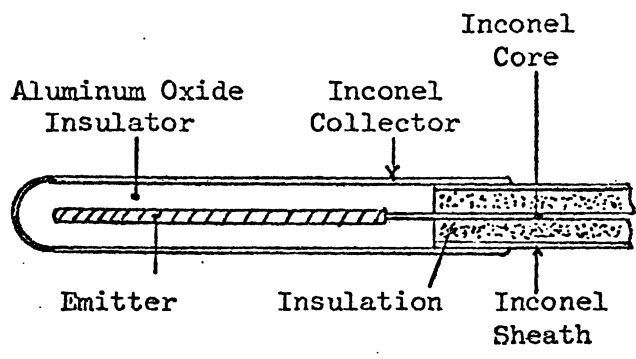


Figure 4. SPND Construction



which is applicable to any given spatial volume (core, D20 or H2O reflector)

$$S \sim k \left\{ \frac{\int_V \int_0^{E_{cc}} \psi_d(\underline{r}, E) \sigma(E) dE d\underline{r}}{\int_V \int_0^{E_{cc}} \psi_0(\underline{r}, E) dE d\underline{r}} \right\} \quad (7)$$

where  $\psi_d$  is the depressed and shielded flux in the detector,  $\psi_0$  is the flux present without paddle or detector, at the volume position being measured, and the integration is over the emitter volume. A term similar to the one in brackets is calculated in a manner described in a later paper presented at this conference.

It should be noted that there are many physical factors, such as  $\beta$  and  $\gamma$  behavior in the detector and detector leads, included in the constant  $k$ . These factors may not be identical for core, D20, and reflector regions. We assume, for the present, these differences are small. Regardless of such possible variations, as well as the differences in flux depression defined by equation (7), we have elected in this paper to present all SPND results using the constant value of  $S = 3.0 \cdot 10^{-21}$  amps/nv, recommended by the manufacturer, reference 7.

The second obstacle, the delayed response of the detector, can be handled through the use of analytic techniques described in reference 6. All of the data presented in this paper were obtained from an equilibrium detector signal.

The quality of SPND profiles is illustrated by two of the curves of Figure 2. There is generally greater smoothness than for the activation data, but nearly the same axial resolution. The latter is fixed by the 1.0" emitter length.

## Experimental Results and Interpretations

### Single LEU Element Replacement

In a single element replacement experiment fresh HEU and LEU elements are alternately placed at the core center in an equilibrium HEU core. Iron wire activations were made along the full axial length of the elements, but for this experiment only bare wire activations were made. Figure 5 shows the core geometry used. For operational convenience the fresh elements were simply interchanged between core center (L-37) and core edge (L-40).

↑N

D<sub>2</sub>O TANK

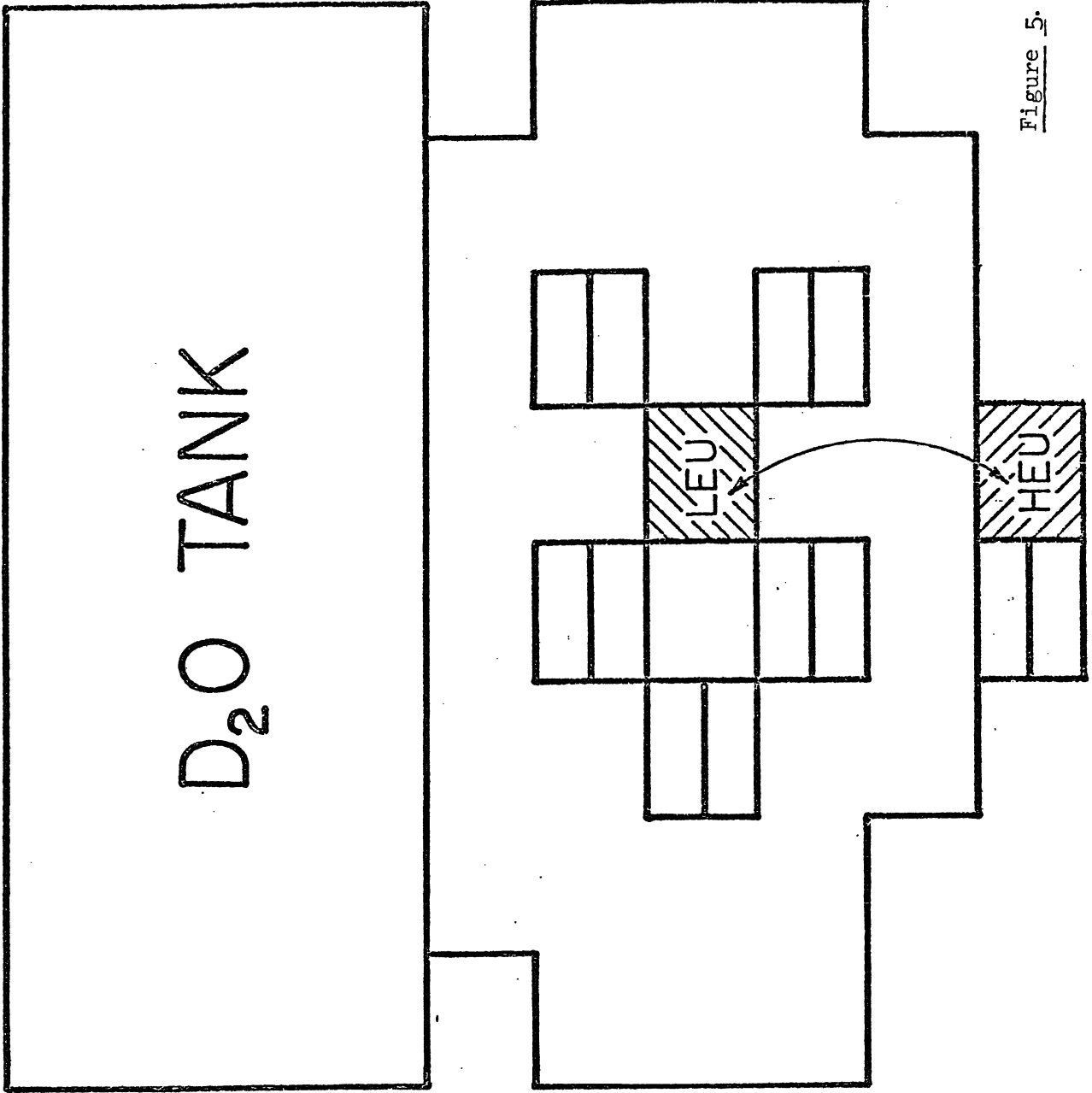


Figure 5. Core Geometry Single Element Replacement

HEU 10-15-81

The reactivity change associated with this interchange is discussed in a separate paper in this conference. An average was made of the saturated activities of the six one inch wire segments symmetric about the core midplane, for both the HEU and LEU elements. Table III gives the ratio of these averages for both iron wire reactions. The (n,p) threshold reaction responds to fast neutrons and suggests very little change in fission rate. The (n, $\gamma$ ) ratio is consistent with the degradation in low energy neutron intensity expected for the higher U-235 loading in the LEU element. This reaction has a small episcadmium contribution, not removed by cadmium covered activations. Since it is anticipated that the LEU spectrum is somewhat harder than that of HEU, it may be observed that, if anything, the HEU/LEU thermal flux ratio is larger than 1.19. However, it is to be noted that the measured ratio is almost exactly equal to the U-235 ratio.

#### Rhodium SPND Flux Profiles

Many SPND maps have been obtained during the HEU/LEU comparison program. These have included partial or full profiles in the core, in the south H2O reflector and in accessible positions of the D20 north reflector. Activation results from Fe and Rh wires have been used to verify SPND profiles at specific points in both core and reflector. This verification has been particularly significant in a) comparing profile intensities from one core type to another, and b) comparing the core versus D20 peak intensities in the profile of any given core.

Although absolute intensities based on wire activation calibration could have been presented, we have elected to present the extensive SPND results as they were measured according to equation (6) with fixed sensitivity, of  $3.0 \cdot 10^{-21}$  amps/nv throughout all regions measured. Improvements can be applied by interested readers for the absolute value of S and its variation with position. The reasons for this choice are several: the SPND data is most easily reproducible, smooth without activation error fluctuations. Perhaps most important is the existence of a significant discrepancy in the ratio of D20 peak flux to core peak flux, as measured on the one hand by the SPND and on the other by Fe wire activation. When this measured discrepancy is resolved S will be calibrated by both Fe and Rh wire activities. For the present paper all wire activations will be normalized to the core center SPND value for each core investigated.

TABLE III  
SINGLE ELEMENT REPLACEMENT  
IN EQUILIBRIUM HEU CORE

Reaction	Ratio	$\frac{\text{HEU Activity}}{\text{LEU Activity}}$
Fe-58 (n, $\gamma$ ) Fe-59		1.19 $\pm$ 0.036
Fe-54 (n, p) Mn-54		1.02 $\pm$ 0.031

As reviewed in Part I of this paper there are three sets of cores that have been mapped; a) the large equilibrium HEU cores of dates 5/79, 9/79, 8/10, 11/81, and 5/82. These cores should be closely equivalent in flux profile since loading patterns (Figure 2, Part I) are essentially identical; b) three small LEU cores identified according to loading dates 1-8-82, 1-21-82, and 4-16-82 (Figures 3, 4, and 5, Part I). The April LEU core is somewhat larger than the January LEU and shifted in East to West in loading geometry; c) the so-called "high leakage" HEU cores of 7, 8, 9, 10/82 (Figure 6, Part I). These have the narrow five row North-South loading of the LEU cores and are intended to mock-up the LEU leakage conditions as nearly as possible. These will be designated simply as HL-HEU cores in this paper.

As described earlier, the geometry of the D20 tank precludes making measurements beyond 8" below the top of the fuel plates. Furthermore, the SPND can extend down to only 5" below the top of the fuel plates because of its design. For mapping in a given horizontal plane fluxes must be extrapolated 1" to yield a 1/4-height value, and 7" for the quoted core midplane value. While there is a significant uncertainty in the value of the D20 tank flux extrapolated to core midplane, the ratio of the core to D20 tank fluxes should be reliable for the core 1/4-plane height. Since the back row of tank penetrations (i.e., farthest north, M-Q) do not extend as far into the tank, this data should be viewed with some suspicion. The D20 tank penetrations are shown in Figure 6.

In the light water reflectors, special assemblies were designed to allow SPND measurements at four fixed distances radially away from the core. These adapters were designed to fit snugly against adjacent fuel assemblies. But because the fuel plates are curved away from the SPND adapters, the radial position of the detector channels must be defined carefully. The geometry of the adapter is shown as an insert in Figure 7. The 1/8" aluminum face plate and 1/16" slot position separators have been treated as voids, and the H2O thickness dimensions are consistent with this assumption. No adjustments to the data are made for the effect of the aluminum sideplates.

In the core, the detector probe is designed to fit into water channels 11/32" on either side of the center bail. The data is plotted to reflect the actual radial position whenever it is known. Otherwise, the detector is assumed to be positioned radially at the center of the fuel assembly.

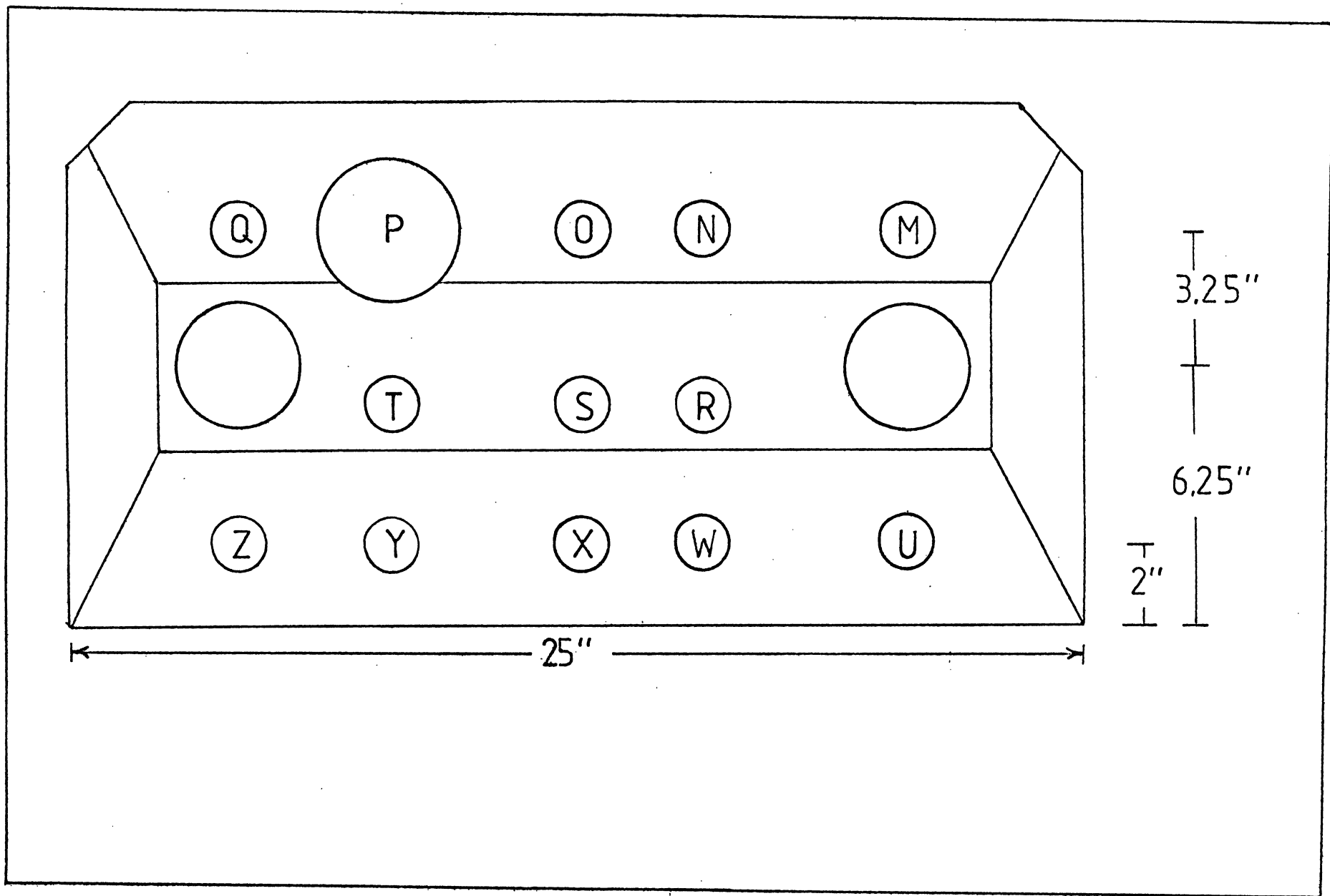


Figure 6.  $D_2O$  Tank Penetration Geometry

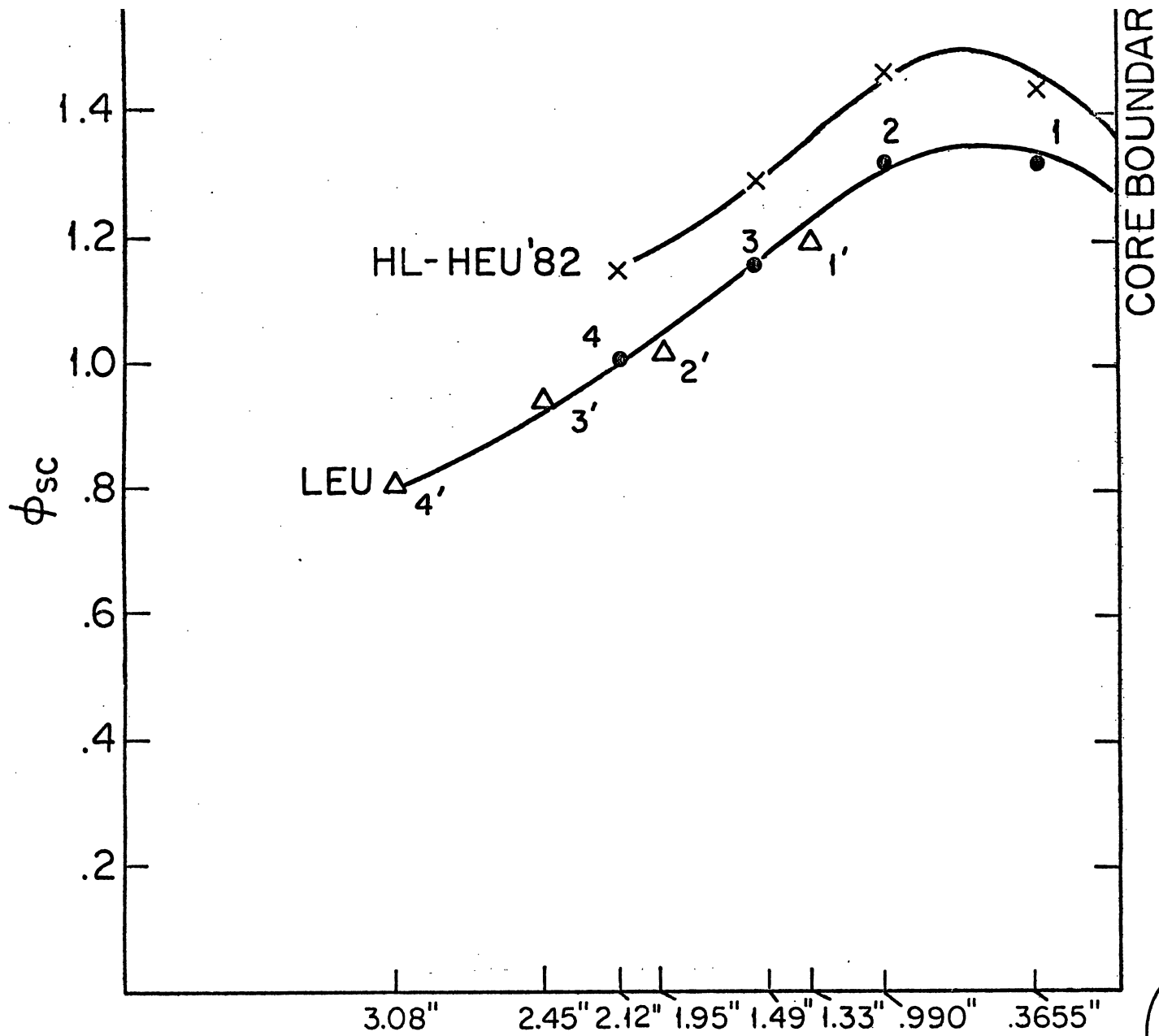


Figure 7. H<sub>2</sub>O Reflector Flux Profiles and Adapter

The SPND subcadmium flux maps from six core loadings are given in Tables IV-IX. The tables are arranged so that the 1/4, 1/2, 3/4 height fluxes are arranged in vertical descending order in each lattice position. (Figure 8 gives the grid plate lattice designations). All flux values are in units of  $10^{13}$ . Table X lists the values of  $f_{th}$  used for each lattice or reflector position, as interpolated from the measurements in Table II. The format of Table X gives a single value of  $f_{th}$  for each lattice position; the upper number applies to HEU cores, the lower to LEU cores. No axial variation is assumed. In the D20 tank, extrapolated data are presented with the 1/4-height flux above that for the core midplane. The positions of the typed data on the figure approximate the actual D20 positions measured.

The H20 reflector data is presented in the same format as for the core. The primed (e.g., 1', 2', 3', 4') H20 reflector channels shown in Table VI refer to measurements made at radial positions further into the reflector than the normal positions (e.g., 1, 2, 3, 4). The relative distances are shown in the H20 profiles given in Figure 7. In this figure the two sets of points were plotted from the two different LEU cores of Tables VI and VII but appear to fit smoothly together. The H20 peaks for equilibrium HEU cores fall considerably below the LEU peak, but in Figure 7 it is evident that the peak is slightly higher for the HL-HEU loading.

Figures 9 and 10 are plots of the SPND data given in Tables IV and VII, comparing the normal equilibrium HEU core with the nearly fresh LEU core of 4/82. The plots are North-South and East-West profiles both passing through the core center element L-37. Differences in core size and burnup make easy assessment of the effect of LEU fuel replacement difficult. Reflector peaking in both H20 and D20 are clearly greater in the smaller North-South geometry of LEU. The westerly shift in the LEU loading is also evident in Figure 10. The LEU flux in L-37 is 13.5% lower than for the same position in HEU. The large peaking at the special element, L-57, is nearly the same for both cores. Because of differences in East-West loading symmetry the maximum core flux, seen in Figure 10, is 10.7% lower for the LEU core, rather than the 13.5% for L-37.

Figure 11 provides a comparison between the normal HEU core and the high leakage cores typified by HL-HEU (7/82). The latter shows the effect on the North-South leakage pattern associated with the smaller 5-row core. Although the core center flux is nearly the same for both cores, the considerably larger H20 and D20 reflector peaking of the smaller core is quite similar to the effect



D <sub>2</sub> O		0	Π
		<u>.635</u>	<u>.644</u>
		<u>.813</u>	<u>.824</u>
	†	S	Γ
		<u>1.16</u>	<u>1.05</u>
		<u>1.48</u>	<u>1.35</u>
	X	W	
	<u>1.46</u>	<u>1.43</u>	
	<u>1.87</u>	<u>1.83</u>	

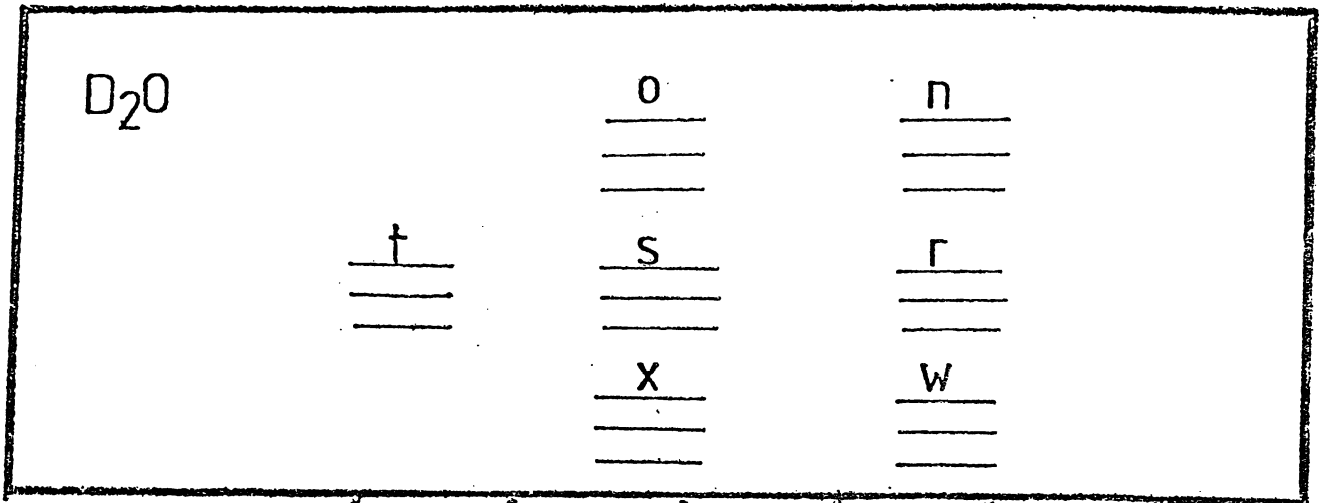
				.933			
	.821	1.01	1.22	1.20	1.12	.915	
				.948			
			A		C		
			*	1.45	*		
				1.17			
.683	.950	*	1.49	1.48	1.45	1.29	.944
				1.18			
			B		CR		
			*	1.37	*		
				.928			
	.837	.984		1.07	1.02	.884	
				.829			
				.717	.678		

\* special

H<sub>2</sub>O

Channel	1	.859
Channel	2	.843
Channel	3	.727
Channel	4	.612

Table IV. HEU SPND Data from 9/27/79 core.



			.896		.579
			1.15		.749
			.972		.647
		A	1.08	C	
		*	1.38	*	
		*	1.15	*	
.627	*	1.07	1.13	.939	.717
.789		1.38	1.43	1.26	.926
.657		1.15	1.17	1.10	.774
		B	.948	CR	
		*	1.24	*	
		*	1.04	*	
.554	.697	.708	.639	.480	
.684	.861	.880	.800	.604	
.575	.731	.755	.673	.504	
		*			

\* special

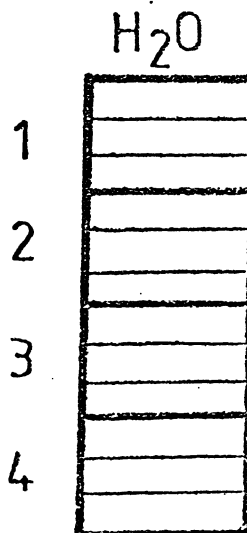


Table V. LEU SPND  
Data from 1/8 core.

D <sub>2</sub> O		<u>0</u>	<u>n</u>
		<u>    </u>	<u>    </u>
		<u>    </u>	<u>    </u>
	<u>t</u>	<u>S</u>	<u>r</u>
	<u>    </u>	<u>1.21</u>	<u>1.13</u>
	<u>    </u>	<u>1.55</u>	<u>1.45</u>
	<u>X</u>	<u>W</u>	
	<u>1.77</u>	<u>1.70</u>	
	<u>2.26</u>	<u>2.18</u>	

.574	.781	.935	.878	.770	.542
.713	1.00	1.20	1.16	1.00	.707
.605	.873	1.02	.993	.870	.618
.643	.908	A		C	.653
.820	1.15				.843
.705	.945	*		*	.720
	*				.659
					.846
					.717
.513	.718	B		CR	.585
.645	.930				.758
.530	.780	*		*	.665

\* special

	H <sub>2</sub> O
Channel 1	1.04
	1.19
	1.10
Channel 2	.926
	1.12
	1.02
Channel 3	.792
	.941
	.850
Channel 4	.667
	.807
	.737

Table VI. LEU SPND  
Data from 1/21 core

D <sub>2</sub> O		<u>0</u>	<u>n</u>
		<u>    </u>	<u>    </u>
		<u>    </u>	<u>    </u>
	<u>†</u>	<u>S</u>	<u>Γ</u>
	<u>    </u>	<u>1.33</u>	<u>1.18</u>
	<u>    </u>	<u>1.70</u>	<u>1.51</u>
	<u>X</u>	<u>W</u>	
	<u>1.74</u>	<u>1.65</u>	
	<u>2.23</u>	<u>2.12</u>	

				.820		
	.788	1.04	1.16	1.12	.954	.679
				.946		
*			A	.932	C	
				1.23		
			*	1.02	*	
	.684	*	1.02	1.08	.842	.642
	.861	2.63	1.33	1.28	1.13	.824
	.717		1.11	1.05	1.01	.699
			B	.850	CR	
				1.10		
			*	.923	*	
	.628	.753		.595	.660	.498
				.783		

\* special

H<sub>2</sub>O

Channel 1	1.09
	1.32
Channel 2	1.08
	1.32
Channel 3	1.00
	1.16
Channel 4	.861
	1.01

Table VII. LEU SPND  
Data from 4/16/82  
core.

D <sub>2</sub> O		O	n
	†	S	Γ
		X	W
	1.55	1.48	
	1.98	1.90	

				.907			
				1.16			
				.947			
			A	1.16	C		
				1.45			
			*	1.20	*		
.553	.858	2.21	1.16	1.24	1.12	.960	.719
.692	1.09	2.80*	1.47	1.56	1.45	1.24	.913
.526	.844	2.25	1.19	1.27	1.19	.987	.747
			B	1.15	CR		
				1.48			
			*	1.21	*		
				.960			
				1.24			
				1.00			
					*		

\* special

H<sub>2</sub>O

1	
2	
3	
4	

Table VIII HEU SPND  
Data from 5/29/82  
core.

D <sub>2</sub> O		0		n			
		t		S		r	
		X		W			
		1.65					
		2.11					
		1.28					
		A		C			
		*		1.53		*	
*				1.57			
		B		CR			
		*		1.43		*	
				1.01			

\* special

		H <sub>2</sub> O	
Channel 1	1	1.14	
		1.43	
		1.15	
Channel 2	2	1.15	
		1.46	
		1.21	
Channel 3	3	1.03	
		1.29	
		1.04	
Channel 4	4	.893	
		1.14	
		.939	

Table IX. HL - HEU SPND Data from July 7, 1982 core

Heavy Water Tank							
L-76	L-66	L-56	A Rod	L-36	C Rod	L-16	L-6
L-77	L-67	L-57	L-47	L-37	L-27	L-17	L-7
L-78	L-68	L-58	B Rod	L-38	Control	L-18	L-8
	L-69	L-59	L-49	L-39	L-29	L-19	
		L-60	L-50	L-40	L-30		



Figure 8. Key to Lattice Positions

D<sub>2</sub>O

0  
.895

п  
.895

†  
.895

S  
.895  
.892

Г  
.895  
.892

X  
.895  
.892

W  
.895  
.892

	.820	.820	.820	.800	.820	.820	
	L-65	L-55	L-45	L-35	L-25	L-15	
	.786	.786	.786	.786	.786	.786	
			<b>A</b>	.800	<b>C</b>		
L-76	L-66	L-56	*	L-36	*	L-16	L-6
	.750	.750		.750		.750	
.830	.830	*	.800	.791	.800	.800	.830
L-77	L-67	L-57	L-47	L-37	L-27	L-17	L-7
	.749	*	.749	.749	.749	.749	
			<b>B</b>	.800	<b>CR</b>		
L-78	L-68	L-58	*	L-38	*	L-18	L-8
	.750	.750		.750		.750	
		.830	.800	.800	.800	.830	
		L-59	L-49	L-39	L-29	L-19	
		.795	.795	.795	.795	.795	
				.830	.830		
			L-50	L-40	L-30		

\*special

HEU = .913  
LEU = .860

Values are presented as:

HEU
L-#
LEU

H<sub>2</sub>O

1	
2	.930
3	.914
4	

Table X  
Values of  $f_{th}$   
used in calculation  
of  $\phi_{sc}$ .



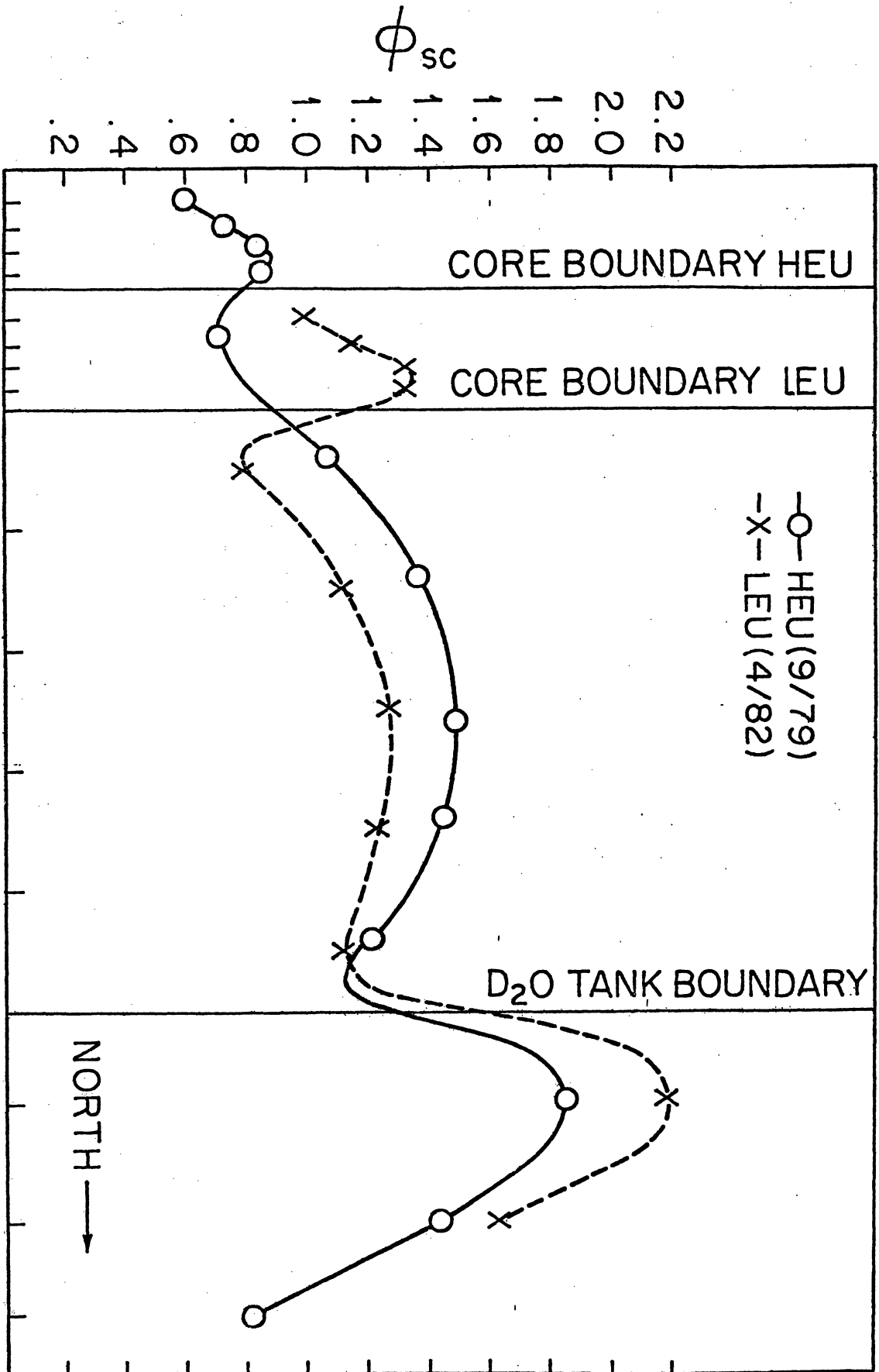


Figure 9.  $\phi_{sc}$  Core Midplane, LEU (4-19-82) vs HEU (9-27-79).  
North-South Traverse

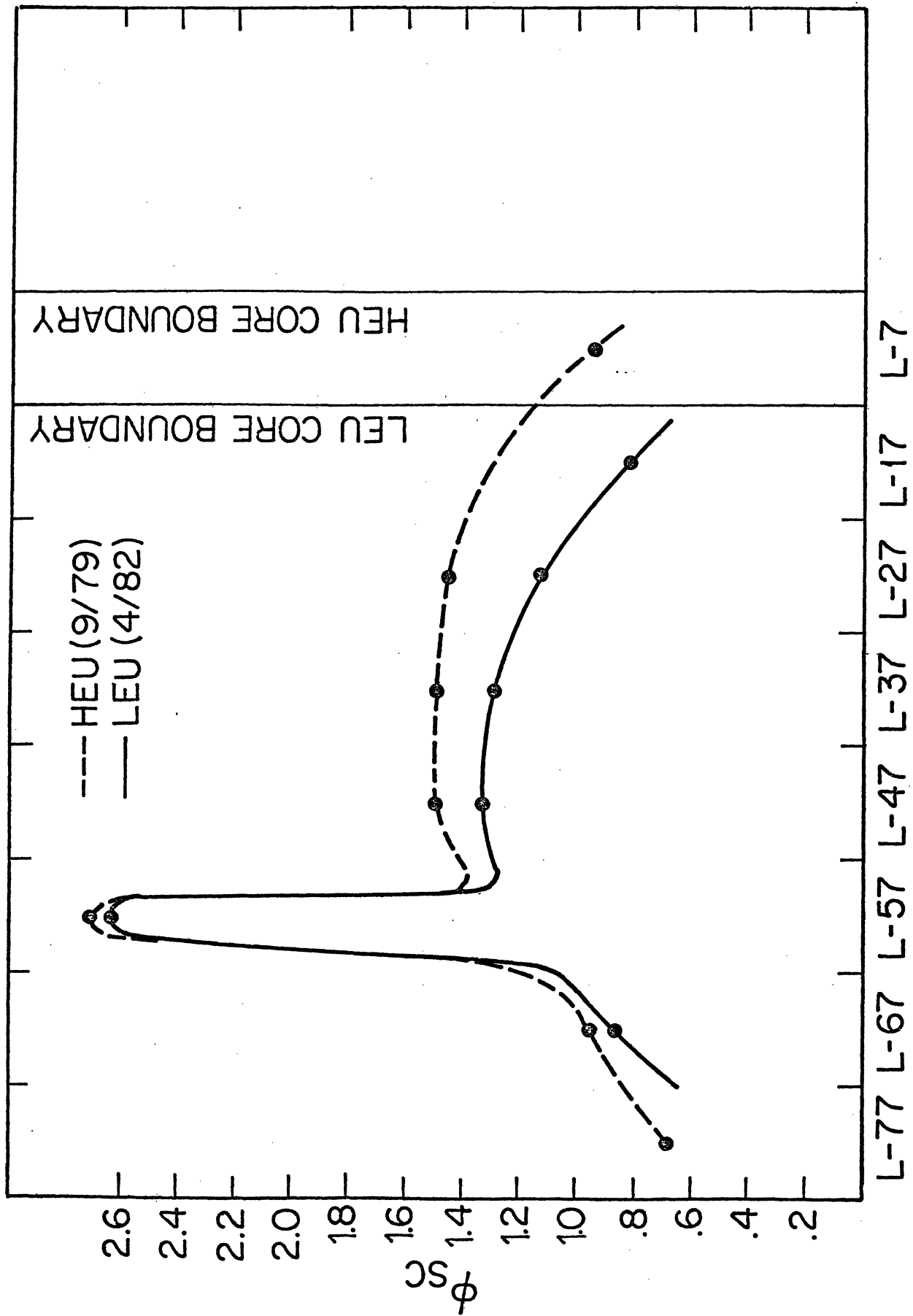


Figure 10.  $\phi_{sc}$  Core Midplane, LEU (4-16-82) vs HEU (9-27-79). East-West Traverse

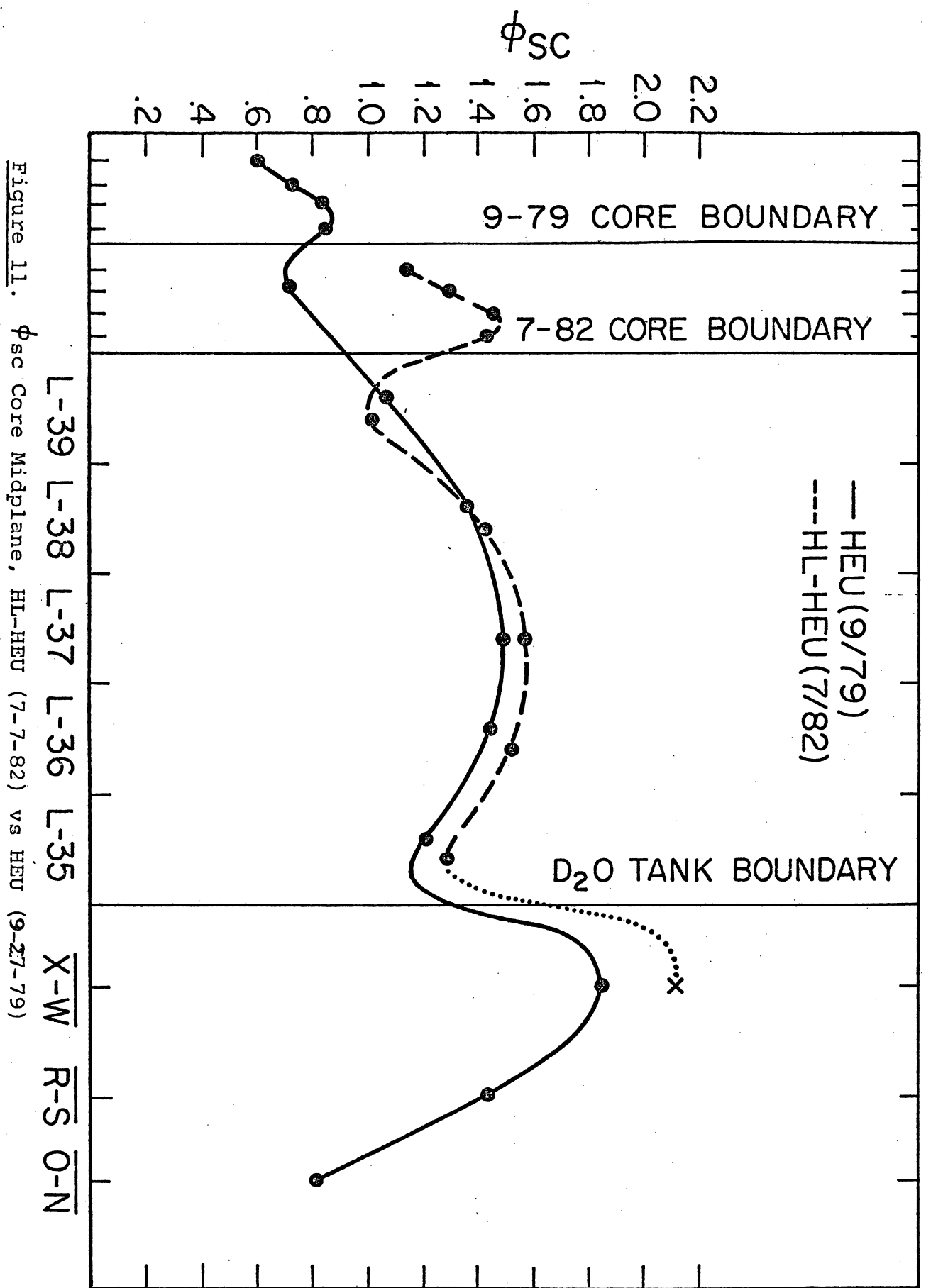


Figure 11.  $\phi_{sc}$  Core Middplane, HL-HEU (7-7-82) vs HEU (9-27-79)

from the LEU comparison of Figure 9. The change in both cases is dominantly due to the larger buckling of the two small cores.

#### Comparison of Rhodium SPND and Wire Activation Data

The HL - HEU cores were deliberately designed to have the same small North-South core dimension and core - D20 interface geometry as for the LEU (4/82). The purpose for these cores was two-fold; first, to compare fluxes for equal geometries, and second, to compare experimental results when all measurement methods are made at the same time and same detector position. Figure 12 reveals several important answers to these questions. First, the similarity in reflector peaking for equal core dimensions is dramatically demonstrated. The dominating effect of large buckling, inferred from Figure 11, is clearly evident. The LEU reflector peaks differ from the same peaks in the HL - HEU only by +6% in D20 and -7.7% in H20. Second, despite this similarity, the central LEU flux is depressed by 18.5%. This difference, in fact, easily accounts for the already small difference in H20 reflector peaking. Third, it is clearly evident that a gross disagreement exists in the D20 tank between SPND and wire activation data, when both sets of data are normalized at the reactor core center.

This disagreement remains a source of serious concern and until resolved provides no useful benchmark for the proper cross sections to be modeled in the D20 tank. Small improvements of order 15% can be anticipated from several sources such as more rigorous evaluation of the sensitivity factor in equation (6) but the disagreement in Figure 12 is much greater than this. Peaking ratios of D20 flux to core center flux are given in Table XI for all detectors in each of several core types. The ratios from SPND data compare very poorly with those from both Fe and Rh activations. Unfortunately no wire data was obtained from the LEU loadings. Particular care was exercised in determining the actual axial depths at which measurements were made simultaneously in both core and D20 tank. It is worth noting that the D20 depths (the lowest possible) are not the same in wire and SPND cases. The flux ratios given in the last column are extrapolated from the measured positions to correspond to the 6" or 1/4 core depth. This extrapolation is believed to be reliable since it is easily seen from the axial data points very near 6". The ratios correspond to the midcore flux values given in Tables IV, VII, VIII, and IX and in Figures 9, 11 and 12, since the D20 midcore values are just those at 6" multiplied by a constant determined by an in-core axial profile such as shown in Figure 1 or 2.

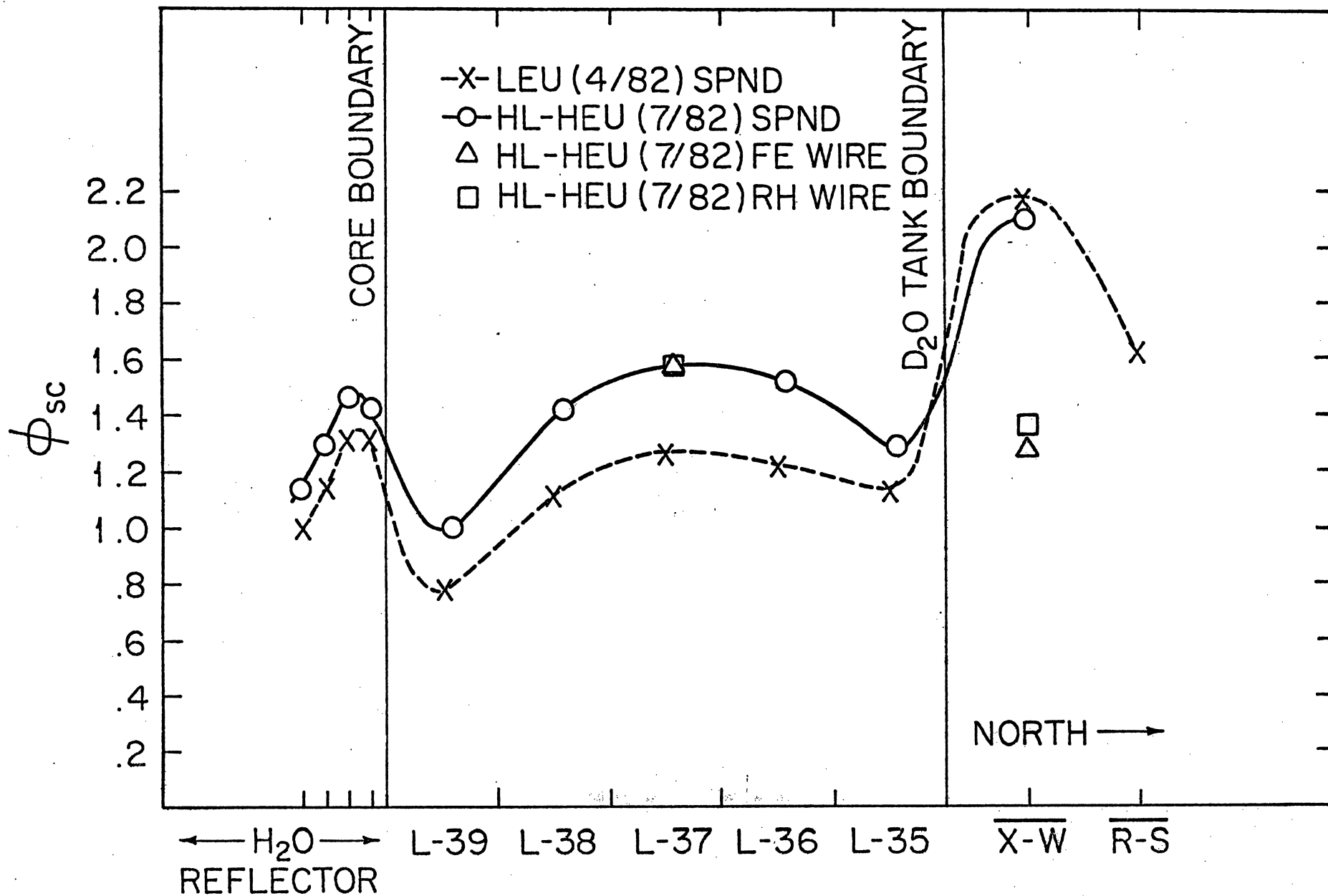


Figure 12.  $\phi_{sc}$  Core Midplane, LEU (4-19-82) vs HL-HEU (7-7-82)

TABLE XI  
RATIO OF D<sub>2</sub>O TO CORE CENTER FLUXES

Core	Date	Detector	Actual Depth measured*	Flux Ratio (D <sub>2</sub> O-X/L-37)
HL - HEU	10/1/82	SPND	5.0"	1.23
HL - HEU	10/1/82	Fe	7.5"	.82
HL - HEU	10/1/82	Rh	7.5"	.88
HL - HEU	8/25/82	Fe	7.5"	.83
HEU	5/ /79	Fe	7.5"	.73
HEU	9/ /79	SPND	5.0"	1.25
HEU	5/ /82	SPND	5.0"	1.25
LEU	4/ /82	SPND	5.0"	1.61

\* The flux ratios shown in the last column result from axially extrapolating the measurements at these depths, to the 6" or 1/4 core depth.

A somewhat different summary of core and reflector peaking at midplane is presented in Table XII for all representative cores. Relative SPND numbers from core to core should be reliable and reproducible to perhaps 2-3%. Since the method of calorimetric power calibration was the same in all details for all cores, except HL-HEU (7/82), it is believed that no significant error exists from this source [calibration thermocouples were replaced just prior to HL-HEU (7/82) and their calibration and positioning may have introduced some minor but unknown systematic error for HL-HEU (7/82)]. It is to be noted that the first two cores should closely agree since both are equilibrium HEU loadings. The 5/82 core appears to show 2.0% to 5% higher levels than the equivalent 7/79 numbers. We have no ready explanation for this difference other than possible burn-up differences. However, the five element "cross" at core center presents the most reliable comparison and for this the disagreement is 2.0% - within experimental uncertainty.

#### Summary Conclusions

Within the experimental limitations discussed in the sections above, the program to measure subcadmium flux profiles leads to the following conclusions:

(1) Replacement of a single fresh HEU element by a fresh LEU element at the center of an equilibrium HEU core produces a local flux depression. The ratio of HEU to LEU local flux is  $1.19 \pm .036$ , which is, well within experimental uncertainty, equal to the inverse of the U-235 masses for the two elements.

(2) Whole core replacement of a large 38 element equilibrium HEU core by a fresh or nearly unburned LEU core reduces the core flux and raises the flux in both D20 and H20 reflectors. The reduction in the central core region is 4.0% to 10.0% for the small fresh 29 element LEU core, and 16% to 18% for a 31 element LEU core (4/82) with low average burnup ( $< 3\%$ ). These changes are consistent with the total core U-235 inventory. The increases in reflector peaking are dominated by the reduced core dimension in the North-South direction associated with the smaller LEU cores.

(3) Special "high leakage" HEU cores, which reproduce the smaller LEU North-South geometry exhibit reflector flux increases similar to the LEU cores, and at the same time show a core center (L-37) flux 18.5% to 20.5% greater than the LEU (4/82) core.

(4) There is no observable change in axial profiles between HEU and LEU cores.

(5) Magnitudes of the D20 reflector fluxes relative to core fluxes as measured by SPND with a fixed value of sensitivity,  $S$ , are in gross disagreement with the same flux ratios measured by

TABLE XII

HEU-LEU MIDPLANE FLUX SUMMARY

<u>FUEL</u>	<u>DATE</u>	<u>TOTAL ELEM'T</u>	<u># SPEC'L</u>	<u>H2O SPND</u>	<u>L-37 SPND</u>	<u>D20-X</u>		<u>CENTRAL SPND FLUX</u>			<u>COMMENTS</u>
						<u>SPND</u>	<u>WIRE</u>	<u>5 AVE.</u>	<u>3 AVE.</u>	<u>MAX.</u>	
HEU	9/79	38	5	.859	1.48	1.87	1.08	1.45	1.43	1.49	Slight flux tilt west.
HEU	5/82	38	6	----	1.56	1.98	----	1.48	1.50	1.56	Flux center L-37.
HL-HEU	7/82	35	5	1.43	1.57	2.11	1.28	----	1.51	----	Five tiered core. Not standard equilib. HEU.
LEU	1/8/82	29	6	----	1.43	----	----	1.34	1.35	1.43	} Cores differ: Special in L-40 moved to regular in L-65. Flux moves west. Batch core.
LEU	1/21/82	29	5	----	----	2.26	----	----	----	----	
LEU	4/82	31	6	1.32	1.28	2.23	----	1.21	1.20	1.33	Fuel added to west face. Flux shifts west.

NOTES:

- (1). Wire data in D20 normalized to SPND L-37 flux. Data taken on a similar core.
- (2). "5 AVE" is average of L-36, L-37, L-38, L-27, and L-47.
- (3). "3 AVE" is average of L-36, L-37, and L-38.
- (4). "MAX" is the maximum value of the core subcadmium SPND flux (excluding flux traps in special fuel elements).



Fe and Rh wire activations. Space dependent refinements of S are calculated to give some improvement in the discrepancy but the major part of the correction remains to be resolved.

#### Acknowledgements

The authors would like to acknowledge the work of Gerald Munyan, Sheila Melton, Keith Flint, and Michael Bacovcin who have diligently acquired and reduced much of the data presented in these two papers. Their dedicated efforts have contributed significantly to the experimental program. Special thanks should also be given to Mr. Gary Cook, Assistant Reactor Manager, and Mr. Frank Bernal, Senior Reactor Operator, for their advice, cooperation, and skilled handling of the reactor and experiments.

### References

- (1). K. H. Beckurts and K. Wirtz, Neutron Physics, Springer-Verlag (1964).
- (2). "The RERTR Demonstration Experiments Program at the Ford Nuclear Reactor," Proceedings of the International Reduced Enrichment for Research and Test Reactor Program Symposium, November 1980. (unpublished)
- (3). W. Jaschik and W. Seifritz, Nuc. Sci. Eng., 53, p. 61-78, (1974).
- (4). Low Enrichment Fuel Evaluation and Analysis Program, University of Michigan Department of Nuclear Engineering Technical Report, January 1980.
- (5). H. D. Warren, Nuc. Sci. Eng., 48, p. 331 (1972).
- (6). "Inverse Kinetic Analysis of Rhodium SPND for Thermal Flux Mapping," Trans. Am. Nucl. Soc., 35, p. 571 (1980).
- (7). Neutron Detector Data Sheet, Reuter-Stokes Canada LTD., RSN-202, Serial number LC-0511. Also, Reuter-Stokes publication, "Self-Powered, In-Core Neutron Detector," RSN-202-M2.

APPENDIX C

Analysis of the Ford Nuclear Reactor

LEU Core

## ANALYSIS OF THE FORD NUCLEAR REACTOR LEU CORE

J. A. Rathkopf, C. R. Drumm, W. R. Martin, and J. C. Lee  
Department of Nuclear Engineering  
The University of Michigan  
Ann Arbor, Michigan 48109

### Introduction

The University of Michigan Department of Nuclear Engineering and the Michigan-Memorial Phoenix Project have been engaged in a cooperative effort with Argonne National Laboratory to test and analyze low enrichment fuel in the Ford Nuclear Reactor (FNR). The effort was begun in 1979, as part of the Reduced Enrichment Research and Test Reactor (RERTR) Program, to demonstrate on a whole-core basis, the feasibility of enrichment reduction from 93% to below 20% in MTR-type fuel designs.

The low enrichment uranium (LEU) core was loaded into the FNR and criticality was achieved on December 8, 1981. The critical loading followed one-for-one replacements of high enrichment uranium (HEU) fuel elements with LEU fuel elements in the center and periphery of the FNR core. Following the critical loading, approximately six weeks of low power testing of the LEU core was performed including measurement of control rod worths, full core flux maps, and spectral measurements in-core and ex-core. This was then followed by 2 months of high power testing (2MW), during which similar measurements were taken. These measurements were performed as part of the demonstration experiments portion of the overall FNR LEU testing and are described in two companion papers<sup>1-2</sup> to be presented at this meeting. The focus of this paper is the analysis of the LEU core and prediction or simulation of the various measurements, such as critical mass, control rod worths, relative worths of LEU vs. HEU elements, and relative flux profiles in-core and ex-core. Comparisons between measured and calculated values are included wherever possible.

Previous reports<sup>3-5</sup> have described the demonstration experiments program and the analytical effort to develop and verify the calculational methods used for analyzing the FNR HEU and LEU configurations. In particular, Section VI of Reference 5 compares the FNR LEU and HEU cores with respect to relative flux/power distributions, control rod worths, various reactivity coefficients, and fuel cycle parameters. Noting that these comparisons are strictly valid only for the FNR HEU/LEU comparison, we summarize the important effects below. (These comparisons are for fresh LEU versus fresh HEU cores.)

- (1) The in-core thermal flux level in the fuel is expected to decrease 15-20% due to the increase in fissile loading.
- (2) The D<sub>2</sub>O tank thermal flux is expected to decrease approximately 4-8%. This decrease is less than that in the

in-core flux due to the fact that the slowing-down source is nearly constant.

- (3) The control rod worths are predicted to decrease approximately 4-5% (relative).
- (4) The cycle length increases approximately 50%.
- (5) The shutdown margin decreases approximately 4-5% (relative).

The validity of these predictions can only be inferred from comparisons of predicted versus measured values on the equilibrium (depleted) HEU core and the fresh LEU core since it will take a considerable time to reach an equilibrium LEU configuration (at least 2 years) and a fresh HEU core was not available. The purpose of this report is to give the status of such comparisons and indicate the areas of uncertainty which we are investigating at the present time.

### Calculational Methods

In this section we will describe very briefly the calculational methods used to perform the FNR HEU/LEU analyses. References 4 and 5 provide additional detail if needed.

#### Cross Section Generation

The cross sections that are used in the global diffusion theory analyses are generated via an extensively modified version of the LEOPARD code<sup>6</sup> suitable for slab lattices and enrichments characteristic of HEU and LEU MTR-type fuel. The LEOPARD code is a zero-dimensional spectrum code employing the MUFT code<sup>7</sup> in 54 fast groups and the SOFOCATE code<sup>8</sup> in 172 thermal groups. A critical buckling search is included to maintain the lattice cell critical throughout the core lifetime and depletion is accounted for. Within the past year we have incorporated an ENDF/B-IV data base into the LEOPARD code, as discussed below.

The EPRI-HAMMER code<sup>9</sup> is also used to generate cross sections, but primarily for control rod calculations. The EPRI-HAMMER code is a one-dimensional integral transport code which includes a 30-group thermal calculation and a 54-group fast calculation with an ENDF/B-IV data base. Although EPRI-HAMMER does not include depletion, a link between the LEOPARD and EPRI-HAMMER codes does allow for HAMMER-generated control rod cross sections as a function of depletion (of the fuel in the rodded element).

#### Global Calculations

An extensively modified version of the 2DB code<sup>10</sup>, 2DB-UM, is utilized for all global calculations for flux and power distributions in the FNR. The 2DB code is a standard finite difference code for solving the neutron diffusion equation. The 2DB-UM code accounts for burnup via a macroscopic burnup method

that is based on the interpolation of macroscopic cross sections for a particular mesh as a function of the local depletion. The burnup library is constructed from a LEOPARD depletion run for the particular fuel type. The key to this method is efficiency and ease of use--it is quite easy to simulate several years of FNR operation, accounting for the bi-weekly startups and shut-downs and accompanying fuel shuffles. We have also used the VENTURE code<sup>11</sup> for 3-D calculations to obtain space and group dependent bucklings for the 2DB-UM code. The PERTV code<sup>12</sup> is also employed for perturbation calculations for various reactivity calculations. It interfaces with the 2DB-UM code.

### Control Rod Analysis

Reference 5 should be referred to for a detailed description of our overall method for performing control rod worth calculation. Basically, the EPRI-HAMMER code is used to generate cross sections for the TWOTRAN code<sup>13</sup> which is a two-dimensional discrete-ordinates transport theory code. The TWOTRAN code generates reaction rate ratios which are then matched with the 2DB-UM code by adjusting the fast and thermal absorption/removal cross sections for the control rod region. We have found that the adjusted control rod cross sections are independent of the fuel environment; therefore, only one set is needed for the HEU fuel and one set for the LEU fuel.

### Ex-Core Calculations

The ANISN<sup>14</sup> and ANDY<sup>15</sup> codes have been used to calculate fluxes in the D<sub>2</sub>O and H<sub>2</sub>O reflectors and the beam ports. The ANISN code is a one-dimensional discrete-ordinates code and ANDY is a general purpose multi-group Monte Carlo code. Cross sections for these codes are generated via the AMPX system.

### ENDF/B-IV LEOPARD Library

Disagreement between macroscopic constants generated by the HAMMER and LEOPARD codes have been attributed to differences in their respective cross section data base<sup>4</sup>. The HAMMER code uses ENDF/B-IV data while the LEOPARD code used an early industrial cross section library. Inspection of microscopic cross sections generated by the two codes shows serious disagreement for several important isotopes including oxygen, aluminum, and <sup>235</sup>U. In order to remedy this discrepancy a library for LEOPARD was assembled from MUFT and SOFOCATE compatible libraries obtained from the Westinghouse Electric Corporation.<sup>16</sup> Implementation of the new library required modification of the LEOPARD code to accommodate the additional data contained in the ENDF/B-IV library.

Verification of the ENDF/B-IV library included simulations of critical experiments, comparisons with established benchmark codes such as the HAMMER code, and modeling of the depletion of fissile fuel in pressurized water reactor fuel. Table 1 shows some important microscopic cross sections obtained by the LEOPARD

code with its two libraries and the HAMMER code. The disagreement between HAMMER and LEOPARD results with the old library is not present for the ENDF/B-IV library. This is expected because, as mentioned earlier, the HAMMER code also uses ENDF/B-IV as its data base. The disagreement on the macroscopic level between HAMMER and LEOPARD results has not been completely eliminated, as seen in Table 2. In fact, for some parameters the old library's values are closer to those of HAMMER than are the new library's. The serious discrepancies, such as the fast fission cross section, have been reduced by the use of the LEOPARD ENDF/B-IV library.

Table 1. Comparison of Some HAMMER and LEOPARD Microscopic Cross Sections for MTR-Type Fuel

Element	Cross Section	HAMMER	LEOPARD			
			old library		ENDF/B-IV library	
			value	% diff.	value	% diff.
$^{16}\text{O}$	$\sigma_{a1}$	$1.16\text{-}2^*$	$34.4\text{-}2$	+3124.	$1.14\text{-}2$	-1.72
$^{27}\text{Al}$	$\sigma_{a3}$	$1.08\text{-}2$	$2.80\text{-}2$	+159.	$0.997\text{-}2$	-7.69
$^{27}\text{Al}$	$\sigma_{a1}$	$6.80\text{-}3$	$9.74\text{-}3$	+47.24	$6.36\text{-}3$	-6.18
$^{27}\text{Al}$	$\sigma_{a2}$	$3.06\text{-}3$	$3.50\text{-}3$	+14.38	$3.02\text{-}3$	-1.31
$^{235}\text{U}$	$\nu\sigma_{f1}$	3.07	3.12	+1.63	3.39	+10.42
$^{235}\text{U}$	$\sigma_{a3}$	39.3	37.0	-5.85	39.7	+1.02
$^{235}\text{U}$	$\nu\sigma_{f3}$	63.9	59.3	-7.20	63.6	-0.47

\*  $1.16\text{-}2$  represents  $1.16 \times 10^{-2}$

Although the ENDF/B-IV LEOPARD library does not provide perfect agreement with benchmark codes, it can be used with more confidence than the old data set. Differences between LEOPARD calculated results and those of either benchmark codes or experiment can now be attributed primarily to LEOPARD's methodology rather than its data base.

#### Analysis and Comparison with Experiment

##### HEU/LEU Single Element Exchange

Table 2. Comparison of HAMMER and LEOPARD  
Two-Group Macroscopic Constants for  
MTR-Type Fuel

Parameter	HAMMER	LEOPARD			
		old library		ENDF/B-IV library	
		value	% diff.	value	% diff.
HEU					
$k_{\infty}$	1.76447	1.76302	-0.03	1.76610	+0.00
$\phi_1/\phi_2$	3.6736	3.8063	+3.61	3.8311	+4.20
$\Sigma_{a1}$	3.8131-3*	3.8860-3	+1.04	3.7620-3	-1.34
$\Sigma_{f1}$	2.1050-3	2.0138-3	-8.20	2.1608-3	-1.10
$\Sigma_{a2}$	0.10832	0.11312	+4.43	0.11370	+5.05
$\Sigma_{f2}$	8.1130-2	8.4828-2	+4.56	8.5249-2	+5.08
LEU					
$k_{\infty}$	1.65980	1.66196	+0.13	1.66368	+0.23
$\phi_1/\phi_2$	4.6196	4.7911	+3.71	4.8317	+4.59
$\Sigma_{a1}$	6.9685-3	6.9712-3	+0.04	6.8765-3	-1.32
$\Sigma_{f1}$	2.7718-3	2.5600-3	-7.64	2.7390-3	-1.18
$\Sigma_{a2}$	0.12643	0.13252	+4.82	0.13327	+5.41
$\Sigma_{f2}$	0.0958	0.10063	+5.04	0.10111	+5.54

\* 3.8131-3 represents  $3.8131 \times 10^{-3}$

In order to examine some of the performance differences of the LEU and HEU elements as well as to provide additional opportunity for analytical methods verification, an experiment was performed on September 15, 1981. The experiment consisted of the substitution of a fresh LEU fuel element for a fresh HEU element in an equilibrium HEU FNR core. The substitution was first made at the center of the core. Then, after returning the core to its original configuration, the exchange was repeated at the edge of



the core. After each substitution the relative reactivity of the LEU element was measured.

The reactivity of the exchange at the center of the core was determined from the resulting positive period. At the edge, the effect of the change was so small, however, that the period was too long to accurately measure. Thus, in this case, the reactivity effect was deduced from the change in the critical position of the regulating rod. The configuration of the HEU core is shown in Figure 1. The center position is marked 37; the edge position is 40. The results of the experiment are summarized in Table 3.

Table 3. Reactivity Effect of HEU/LEU Exchange

Location of Exchange	$\Delta k/k$ (%)		
	Experiment	Analytic	
		2DB-UM	PERTV
Center (37)	-0.1176	-0.1301	-0.1105
Edge (40)	+0.011	+0.0036	+0.010

The HEU core and its three variations (LEU in the center, HEU on the edge, and LEU on the edge) were simulated by the 2DB-UM code. In the calculations each fuel element was approximated by an 8x8 mesh. From the calculated eigenvalues, reactivity effects of the two exchanges were determined. These values are presented in Table 3 as are those calculated by the PERTV code which uses forward and adjoint fluxes from the 2DB-UM code to calculate changes in eigenvalue. For the center exchange, where the reactivity effect is large, both analytical methods provide satisfactory results. On the other hand, the perturbation technique simulated the edge exchange much better than did the 2DB-UM code. This is because the small reactivity effect strains the eigenvalue convergence criteria in the 2DB-UM code.

The differences between the two elements are less apparent on the edge of the core than at the center simply because of the lower flux in that region. The reason why the LEU element is less reactive than the HEU at the center of the core but more reactive at the edge is more subtle. Infinite medium calculations shed some light on this phenomenon. In particular, the LEU element is less reactive in an infinite medium ( $k_{\infty}(\text{LEU}) < k_{\infty}(\text{HEU})$ ) but for a finite core, the LEU fuel is more reactive

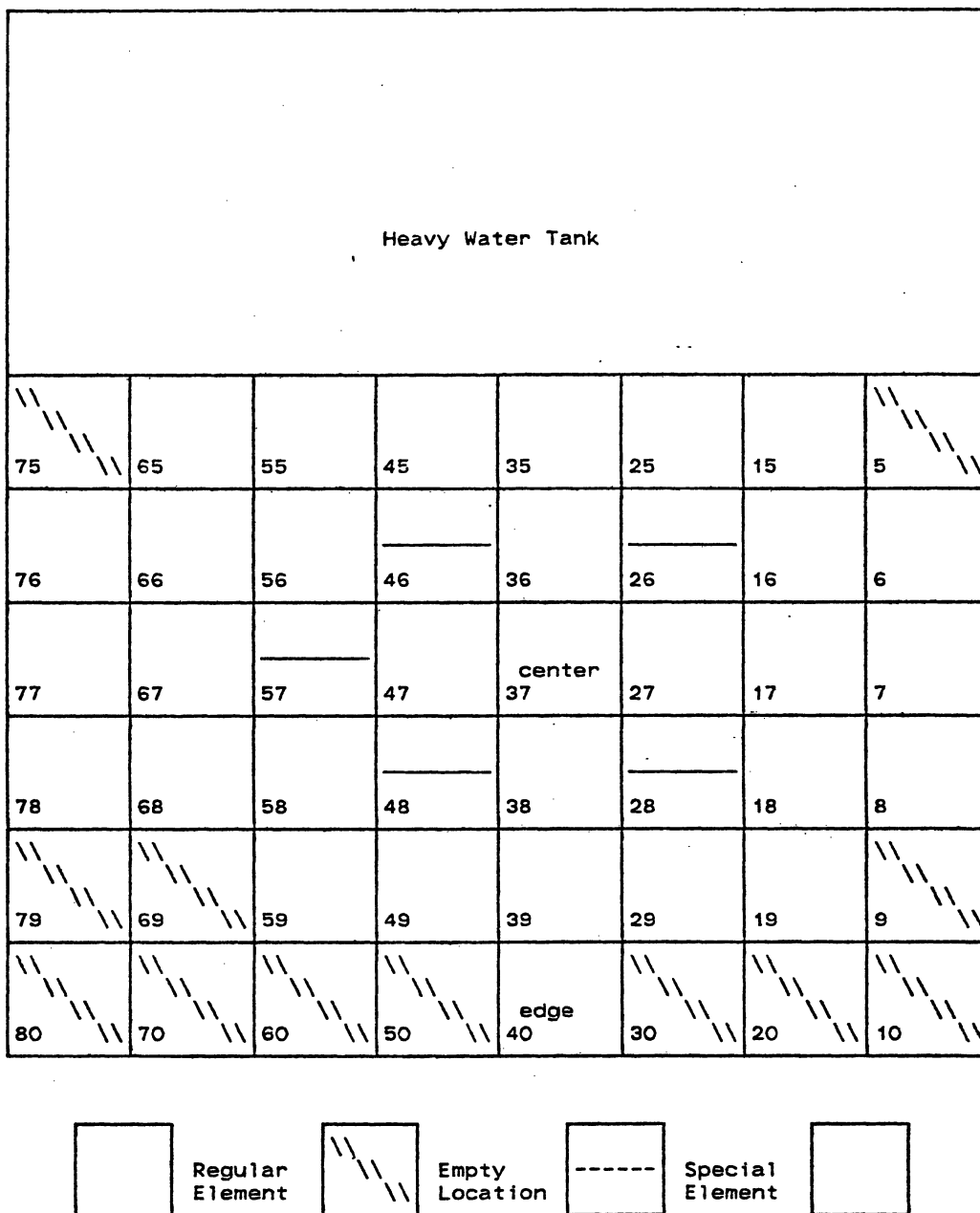


Figure 1. Core Configuration for Single-Element Exchange Experiments

( $k_{\text{eff}}(\text{LEU}) > k_{\text{eff}}(\text{HEU})$ ), as predicted by the 2DB-UM code. This is also seen by comparing the migration area,  $M^2$ , for the two fuels from the LEOPARD code, in that  $M^2(\text{LEU}) < M^2(\text{HEU})$ , indicating the LEU fuel is less "leaky". Therefore, inserting the LEU fuel in the center of the core, where the leakage is low, is similar to an infinite medium and hence results in a lower reactivity. On the other hand, inserting it on the edge of the core, where leakage dominates, the smaller  $M^2$  for the LEU fuel causes a slight reactivity increase.

### LEU Critical Loading

The December 1981 loading of the first LEU FNR core provided another opportunity to verify the ability of the computational methods to simulate an LEU experiment. The initial critical loading took two days and was completed at about noon on December 8 after the placement of the 23rd LEU element. Figure 2 shows the critical configuration, the positions of the three fission chambers, and, in the upper right corner of each element location, the order of loading. Upon withdrawal of all control rods except the regulating rod, the reactor experienced a period of 113 seconds, which corresponds to an excess reactivity of 0.067%. If the worth of the regulating rod (measured to be 0.383%) is considered, the cold, clean LEU core had an excess reactivity of 0.45%.

The critical loading sequence was simulated twice by the 2DB-UM code using a structure of 36 (6x6) mesh per fuel element. For each of the two simulations different LEOPARD generated cross sections were used: one using the old library, the other ENDF/B-IV. Table 4 presents the eigenvalues obtained from the two calculations. The nominal masses of  $^{235}\text{U}$  were those considered in the calculations. The masses labeled "actual" were calculated by summing up the mass of each loaded element as reported by the manufacturer.

The 23 element core was found to be slightly super-critical in the 2DB-UM calculation using the ENDF/B-IV cross sections but slightly sub-critical with the old library. The core simulated by the 2DB-UM code is one with all rods withdrawn. The measured critical mass was for the 23-element LEU core with the regulating rod fully inserted. The analytical and experimental results can be compared by examining (1) the multiplication constant and (2) the estimated critical mass. The LEU core with all rods withdrawn was estimated from experimental results to have a multiplication constant of 1.0045. This compares with the 2DB-UM values of 1.0025 (ENDF/B-IV) and 0.9985 (old library). From the mass of 3512.82 g for the super-critical core and the excess reactivity a critical mass of 3436 g  $^{235}\text{U}$  is estimated. The values estimated from the 2DB-UM code are 3471 g and 3545 g for the ENDF/B-IV and old libraries, respectively. The better agreement provided by the ENDF/B-IV library adds further support for the new LEOPARD library.

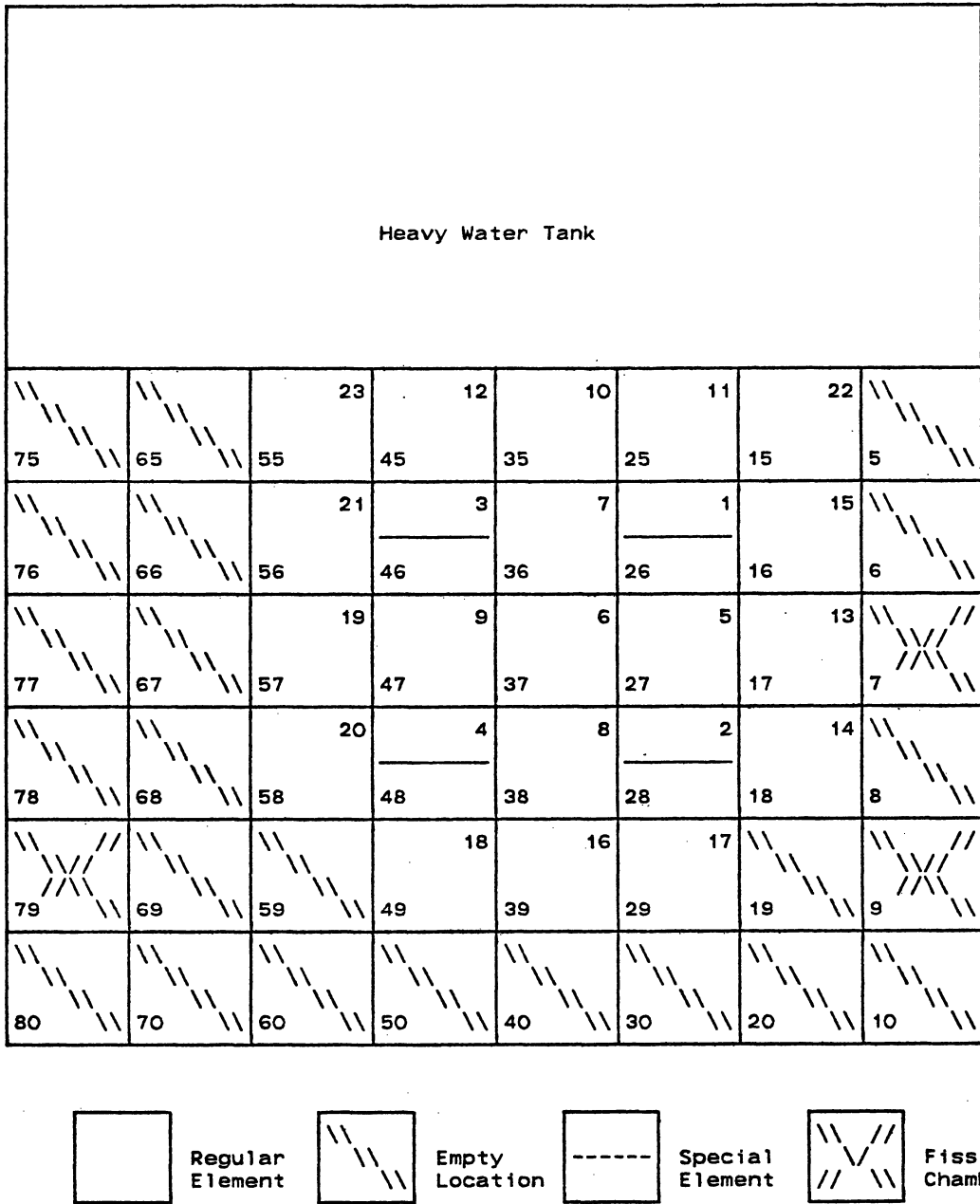


Figure 2. LEU Critical Loading Configuration at the FNR, December 8, 1981

Table 4. LEU Critical Loading

Number of LEU Elements	$^{235}\text{U}$ Mass (g)		2DB-UM calculated k	
	actual	nominal*	old library	ENDF/B-IV library
21	3117.20	3178.7	0.9792	0.9835
22	3344.85	3346.0	0.9888	0.9926
23	3512.82	3513.3	0.9985	1.0025

\* nominal elemental  $^{235}\text{U}$  masses  
regular: 167.3 g  
special: 83.65 g

#### Control Rod Worth Calculations

Among the many reactivity-related parameters measured for the LEU configurations at the FNR during the past year, our simulation effort to date has been limited to the shim rod worth data. The rod worth calculations used a combination of transport and diffusion theory codes as outlined above. In Table 5, the calculated reactivity worths of shim rods are compared with the full-rod worth measurements taken for the December 1981 LEU core. In a similar comparison for the February 1982 LEU core presented in Table 6, full-rod worths are estimated from the measured half-rod worths. Based on the full- and half-rod worths data obtained for the December 1981 LEU configurations, a multiplication factor of 1.93 is chosen to convert the half-rod worths to full-rod worths.

Table 5. Shim Rod Worth Comparison  
December, 1981 LEU Core with 27 Fuel Elements

Rod	Reactivity worth ( $\% \Delta k/k$ )		Relative error (%)
	Measured	Calculated	
A	2.22	2.28	2.7
B	2.32	2.65	14.1
C	2.28	2.25	-1.6

Table 6. Shim Rod Worth Comparison  
February, 1982 LEU Core with 30 Fuel Elements

Rod	Reactivity worth ( $\% \Delta k/k$ )			Relative error (%)
	Measured		Calculated	
	Half-rod	Full-rod*		
A	1.37	2.64	2.76	4.5
B	1.16	2.24	2.47	10.3
C	1.08	2.08	2.11	1.4

\* Estimated as 1.93 times measured half-rod worth

The comparisons given in Tables 5 and 6 indicate that the reactivity worths for shim rod B are significantly overpredicted by our calculations, while those for rods A and C are in reasonable agreement with the measured worths. This discrepancy for rod B may be associated with inaccurate flux distributions calculated for the LEU configurations, and is under further study in conjunction with the flux distribution calculations discussed below.

#### Thermal Flux Maps

Since the thermal neutron flux both in the core and reflector regions plays an important role in the use of the FNR as a research reactor, emphasis has been placed on determination of the thermal flux distribution both for LEU and HEU core configurations. Based on the favorable comparisons noted in early simulations<sup>5</sup> of the rhodium self-powered neutron detector (SPND) and iron wire activation data, all of the thermal flux mappings for the LEU configurations were performed with the SPND. Subsequent analysis and simulation of the SPND data, however, indicated considerable discrepancy between the calculated flux distributions and the SPND data. This is in part due to resetting of the reference vertical position for the SPND. To resolve this discrepancy between the calculated results and SPND maps, both iron and rhodium wire activations were performed for an HEU core configuration in October, 1982. We performed simulation of the recent HEU data as well as that of an LEU configuration of April 16, 1982 and of the HEU configuration of September 27, 1979 analyzed in Ref. 5.

For the purpose of our comparison here, the thermal flux calculated through the 2DB-UM code, with a thermal cutoff of 0.625 eV, is assumed to correspond to the integrated neutron flux below the cadmium cutoff. The 2DB-UM calculations were performed

through the steps outlined above, with 6x6 meshes per fuel element. Comparisons between the calculated thermal flux distributions and the SPND data are shown for the September 1979 HEU and April 1982 LEU cores in Figure 3 and 4, respectively. Data are given for all of the core locations where measurements were made, and also for four locations in the D<sub>2</sub>O tank on the north side of the core and four locations in the H<sub>2</sub>O reflector on the south side of the core. The fluxes are normalized so that the sum of the measured and calculated fluxes within the core are the same. The agreement between calculation and measurement is generally good in the core, with some underprediction of the thermal flux peaking in the water hole in the special fuel elements. A large underprediction is noted, however, in the 2DB-UM simulation of the SPND data in the heavy water region.

Figure 5 compares the thermal flux distributions on a north-south traverse through the center of the 1979 HEU core. In addition to the rhodium SPND data, iron wire activation data are also included in Figure 5, with the fluxes normalized at L-37. Similarly, Figure 6 compares the SPND data and 2DB-UM results for an east-west traverse through the center of the 1979 HEU core. Figure 5 indicates a good agreement between the iron wire data and the 2DB-UM results, both of which are substantially lower than the SPND measurements in the heavy water. Flux traverses for the April 1982 LEU core are compared in Figures 7 and 8, with a similar discrepancy between the 2DB-UM results and SPND data in the heavy water region. To understand this discrepancy, we compare in Figure 9 the 2DB-UM results with the iron and rhodium wire activation data and the rhodium SPND data obtained for the October 1982 HEU core. Figure 9 indicates that the 2DB-UM calculations are in reasonable agreement with the wire activation data, while a substantially higher thermal flux is obtained from the SPND data.

The large discrepancy between the thermal flux distributions obtained with the SPND, and the corresponding wire activation data and 2DB-UM calculations is currently under investigation. It appears that several factors may have to be accounted for before this discrepancy can be resolved. One factor that has not been considered explicitly in the 2DB-UM calculation is the effect of the aluminum and H<sub>2</sub>O that surround the detector when measurements are made in the D<sub>2</sub>O tank. The measurements are made in aluminum tubes that are filled with H<sub>2</sub>O that penetrate the D<sub>2</sub>O tank. The water in the tubes tends to increase the thermal flux that the detector would see. Another factor that needs to be taken into account is the difference between the thermal neutron spectrum in the core and that in the D<sub>2</sub>O tank. The spectrum is softer in the D<sub>2</sub>O tank, which increases the effective absorption cross section of the detector, yielding a larger detector current there.

The thermal flux depression is expected to be large in the rhodium SPND because of the large resonance in rhodium at 1.2 eV and also because of the Inconel paddle that the detector is

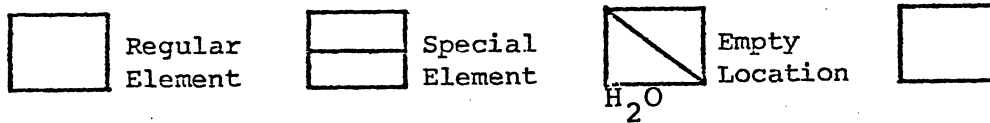
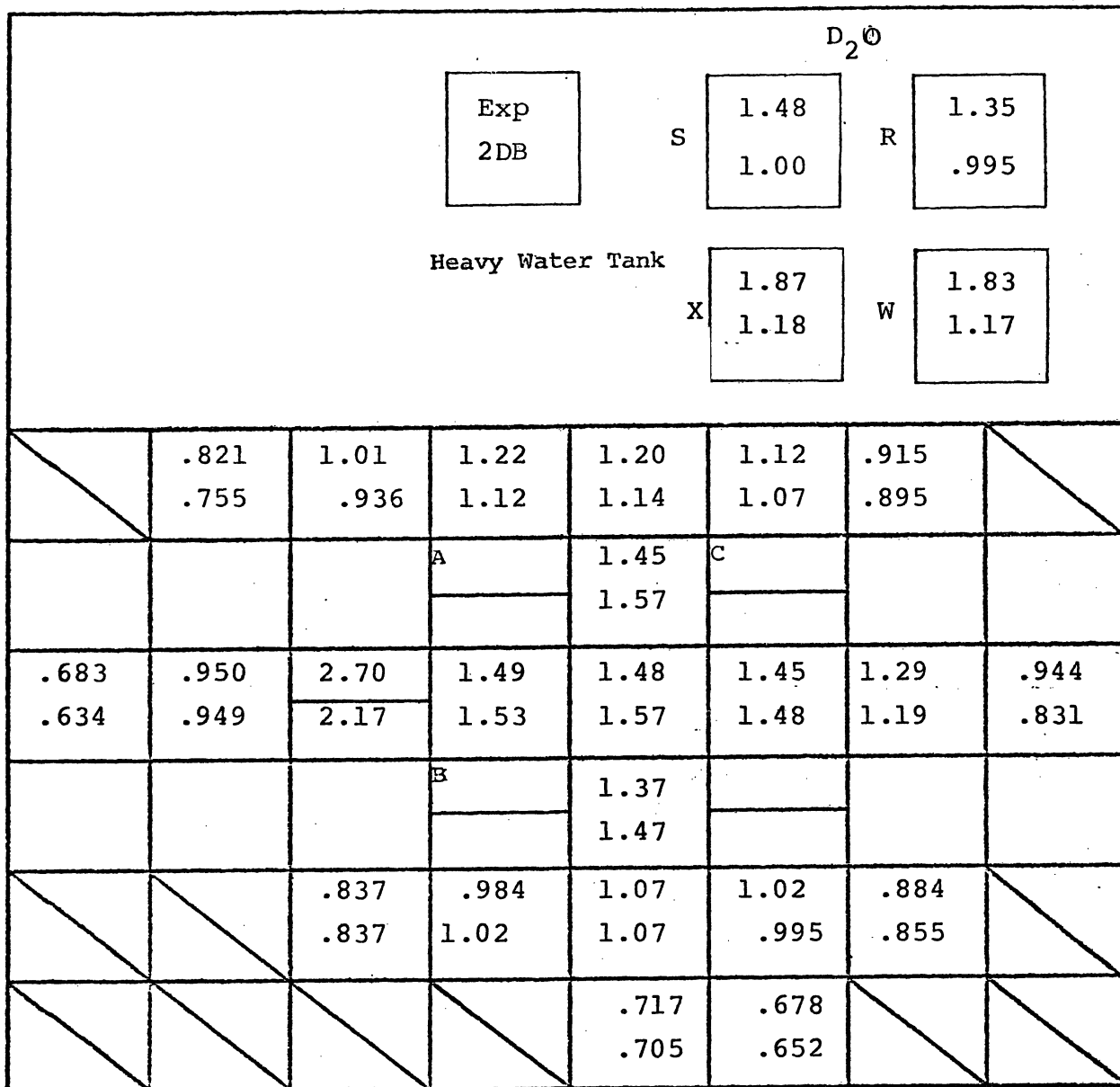
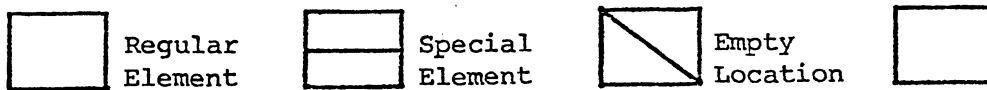
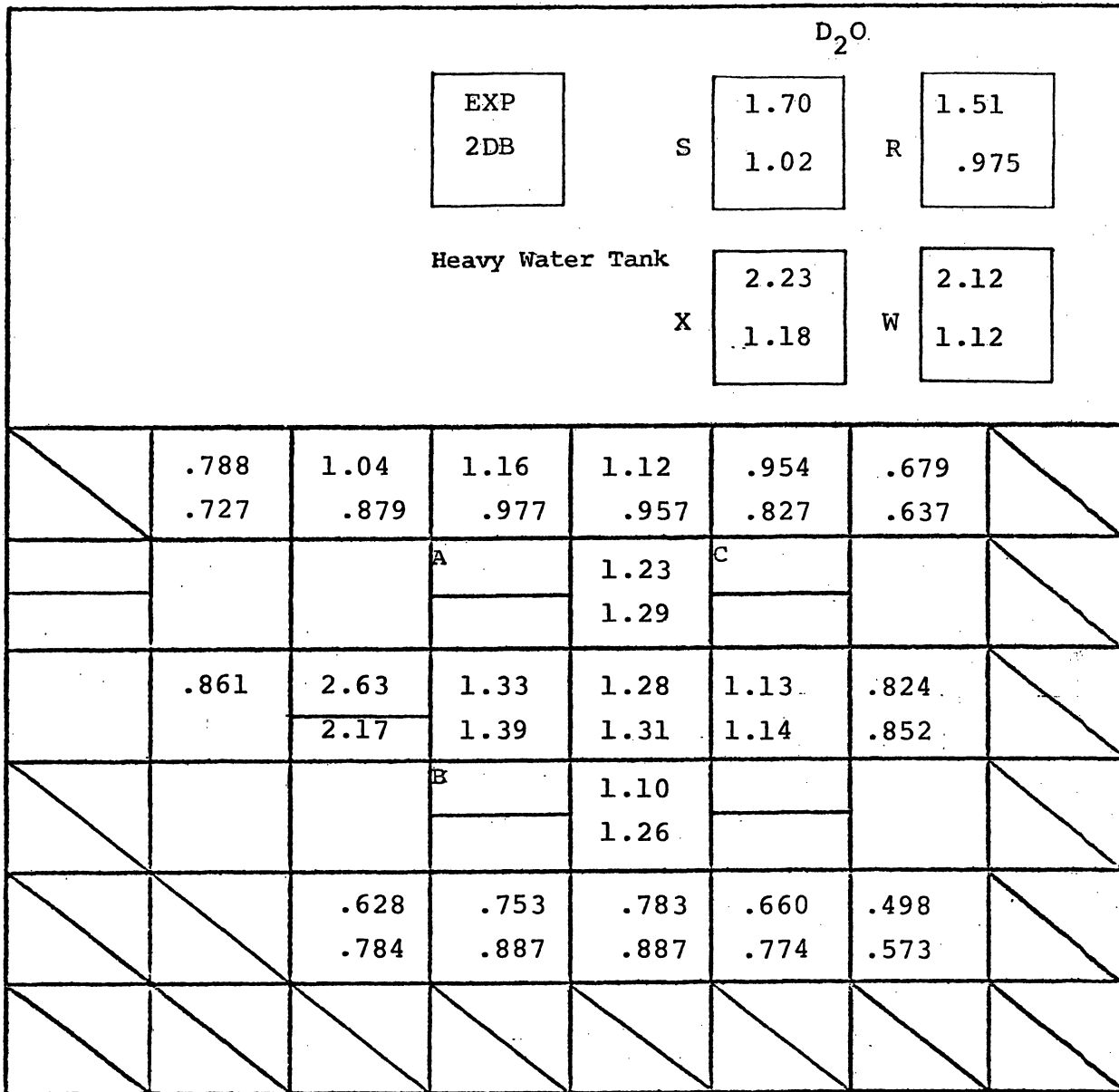


Figure 3. Thermal Flux Maps for the September 27, 1979 HEU Core

1	.859 .810
2	.843 .838
3	.727 .751
4	.612 .598





		$H_2O$
1	1.32 1.33	
2	1.32 1.50	
3	1.16 1.40	
4	1.01 1.17	

Figure 4. Thermal Flux Maps for the April 16, 1982 LEU Core.

# 9/27/79 HEU CORE NORTH-SOUTH TRAVERSE

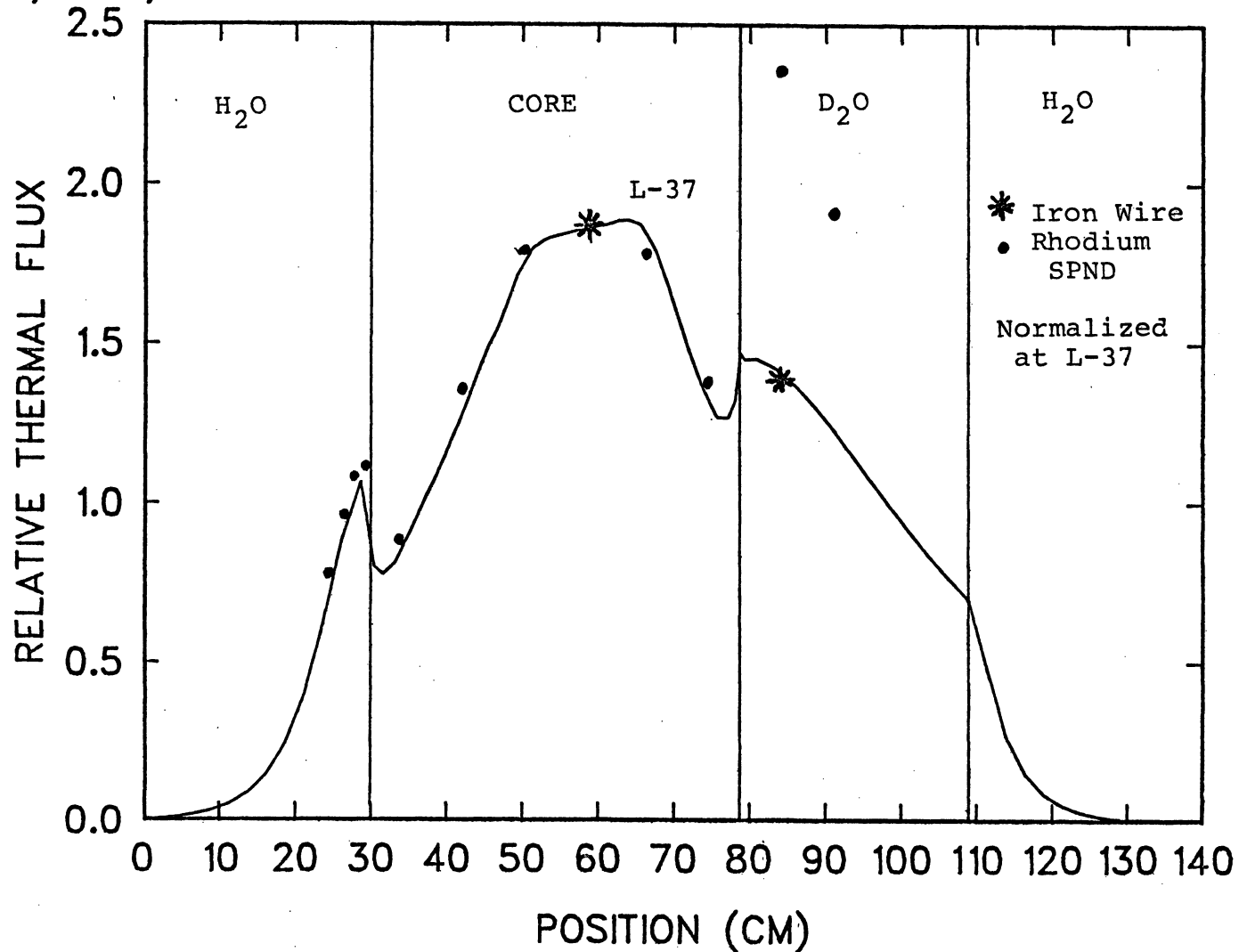


Figure 5. Thermal Flux Profiles along the North-South Traverse, September 27, 1979 HEU Core.

# 9/27/79 HEU CORE EAST-WEST TRAVERSE

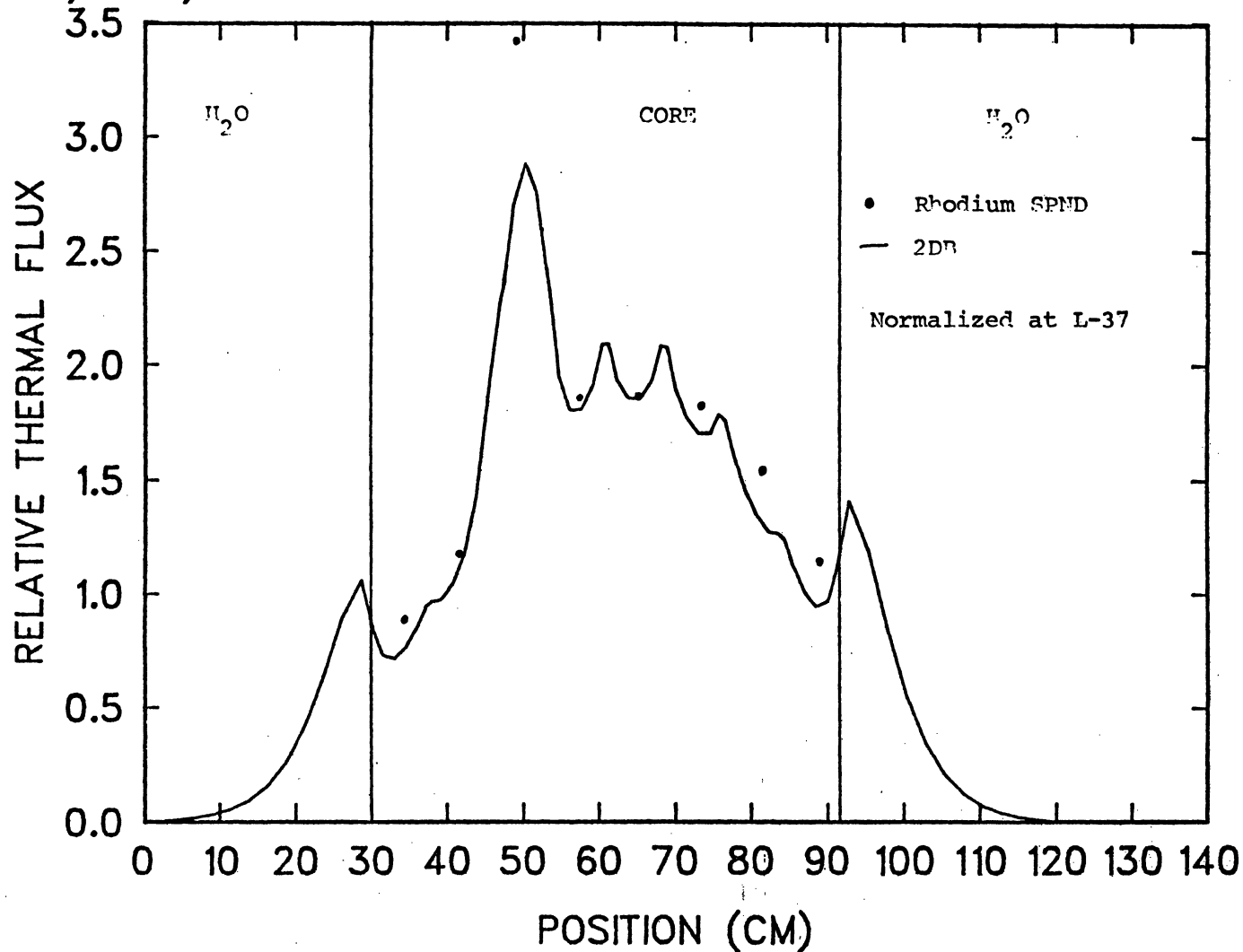


Figure 6. Thermal Flux Profiles along the East-West Traverse, September 27, 1979 HEU Core

# 4/16/82 LEU CORE NORTH-SOUTH TRAVERSE

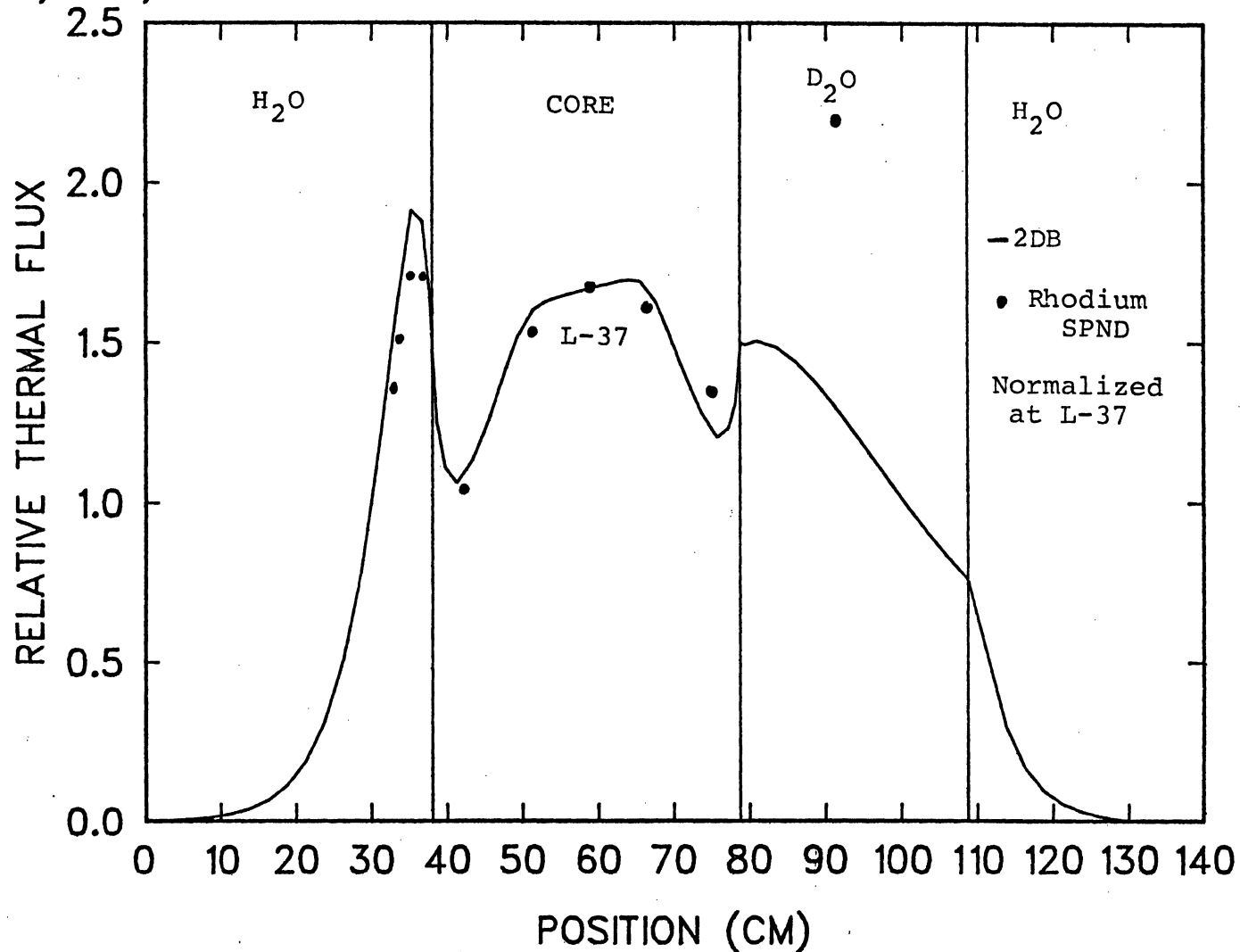


Figure 7. Thermal Flux Profiles along the North-South Traverse, April 16, 1982 LEU Core

# 4/16/82 LEU CORE EAST-WEST TRAVERSE

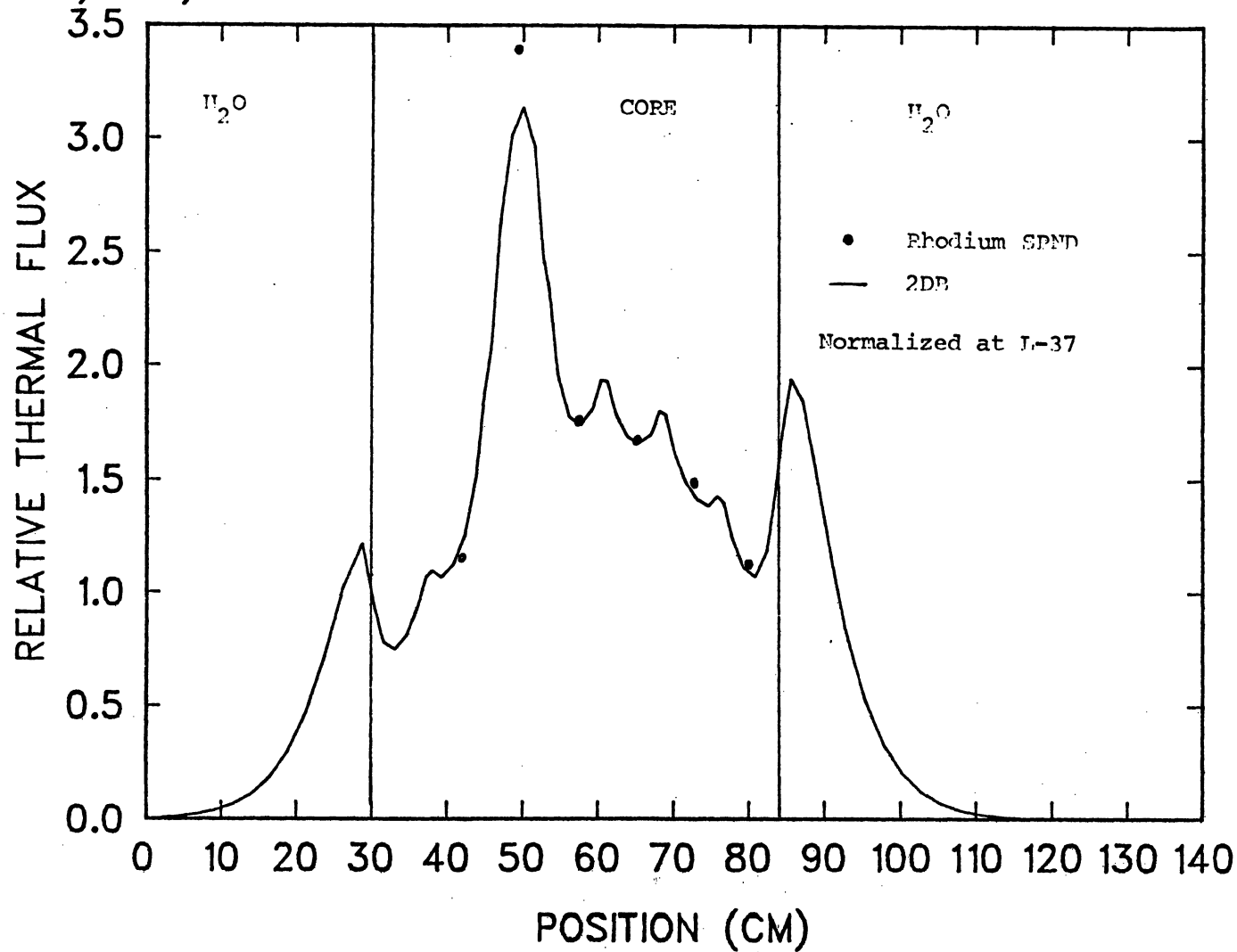


Figure 8. Thermal Flux Profiles along the East-West Traverse, April 16, 1982 Core

# 10/6/82 HEU CORE NORTH-SOUTH TRAVERSE

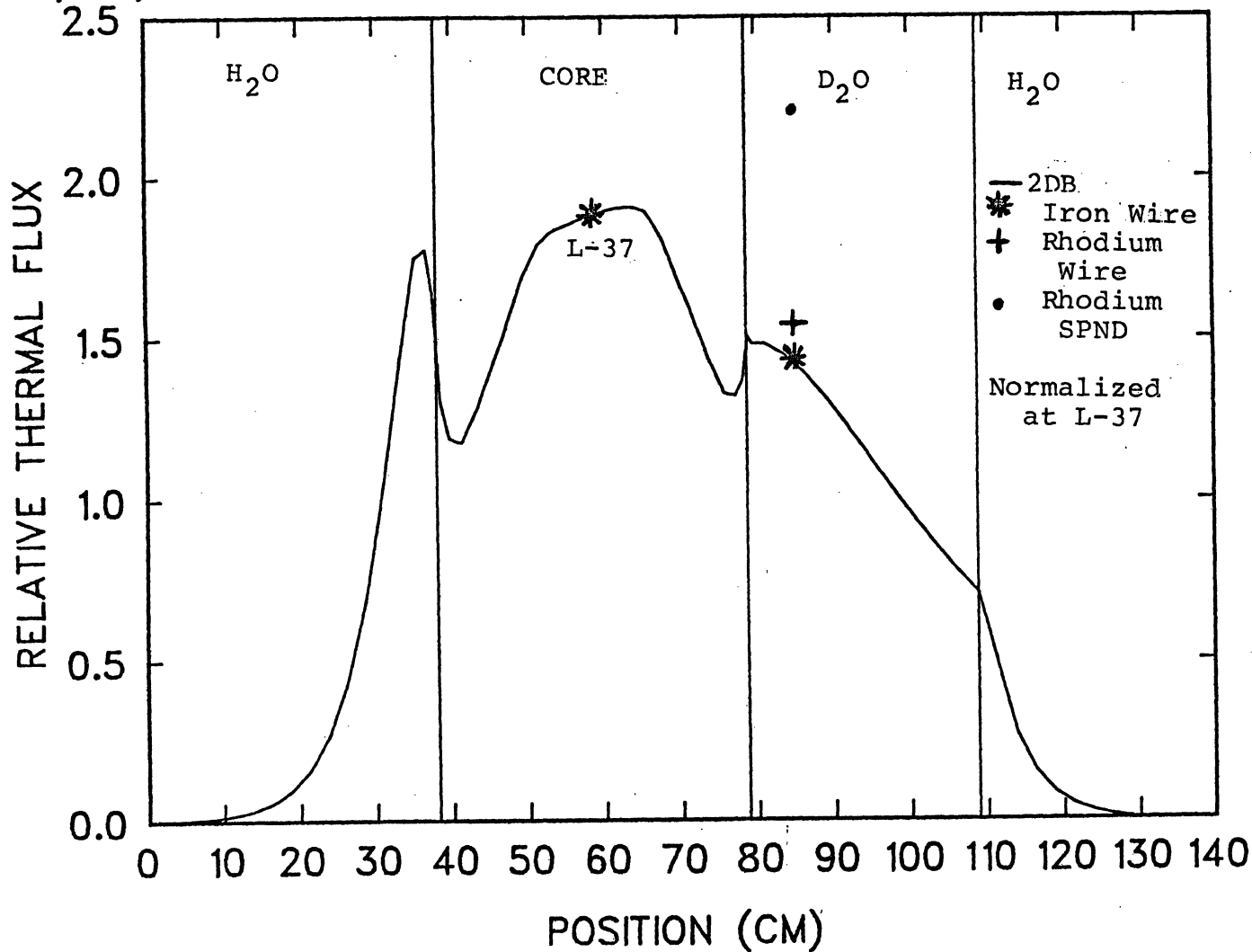


Figure 9. Thermal Flux Profiles along the North-South Traverse, October 6, 1982 HEU Core

mounted on. As indicated by Jaschik and Seifritz<sup>17</sup>, the flux depression for an SPND in D<sub>2</sub>O is expected to be smaller than in the core and in the light water reflector, which would yield, on a relative basis, a larger signal in the heavy water tank. Under investigation also is the possible effect of the difference between the actual detector configuration, characteristic of an SPND, and the simple wire geometry.

In addition, as part of our investigation to understand the uncertainties associated with the calculated flux distributions, efforts are also underway to study the sensitivity of the 2DB-UM results to different methods in generating few-group cross sections, especially the slowing down cross sections, in the D<sub>2</sub>O region and the water hole in the special fuel elements.

Finally, to gain some understanding of the difference in thermal flux distribution between the LEU and HEU configurations, we compare in Figure 10 the calculated flux distribution for the April 1982 LEU core with that for the October 1982 HEU core. The two core configurations considered here are by no means identical but rather similar along the north-south traverse compared in Figure 10. We note from Figure 10 that the thermal flux distribution is lower in the LEU configuration with the increased fuel loading and the corresponding increase in the thermal absorption cross section. The decrease in the thermal flux in the LEU configuration is much smaller in the reflector regions than in the core region. This is because the decrease in the fast flux is relatively small and the thermal flux distributions in the reflector regions is primarily influenced by fast neutrons leaking from the core into the reflectors. These observations are in agreement with the predictions presented both for the batch and equilibrium core configurations in Reference 5.

### Summary and Conclusions

This paper has summarized the current status of the effort to analyze the FNR HEU/LEU cores and to compare the calculated results with measurements. In general, calculated predictions of experimental results are quite good, especially for global parameters such as reactivity, as seen in the single HEU/LEU element substitution experiment and the LEU full core critical loading. Shim rod worths are predicted well for two of the rods but too high for a third rod possibly due to inaccurate thermal flux distribution calculation. The calculated thermal flux maps show excellent agreement with experiment throughout the FNR core. In the heavy water tank, however, experimental values for the thermal flux obtained by different methods are inconsistent among themselves as well as with the calculated finding. Work is underway to use our computational tools to correct the discrepancies between the various measurement techniques and to improve the computational results for flux distribution and the rod worth experiment.

Although uncertainties exist in our analysis, as evidenced

# 1982 LEU AND HEU NORTH-SOUTH TRAVERSE

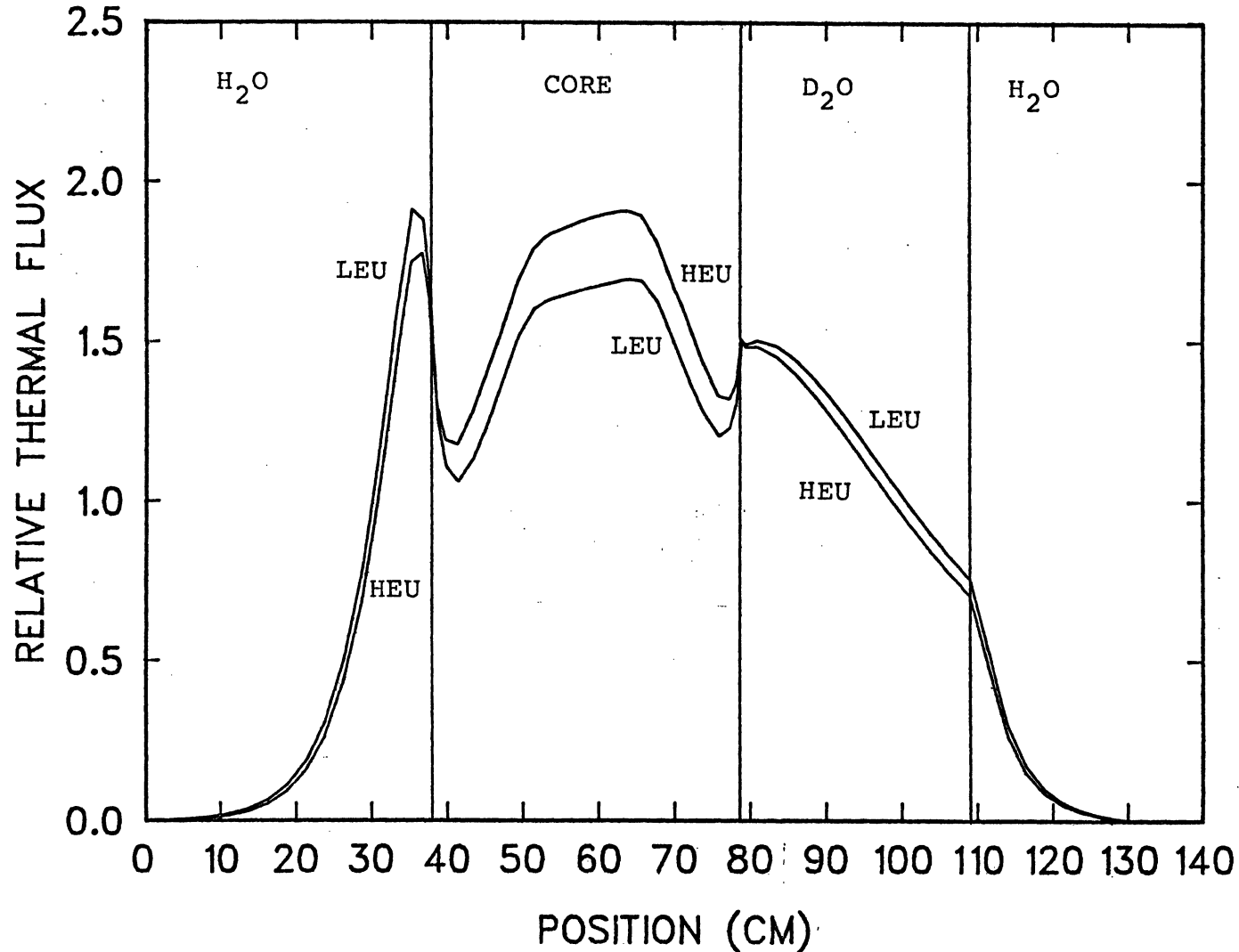


Figure 10. Comparison of Thermal Flux Profiles between the LEU and HEU Cores



by the discrepancies mentioned above, we consider our present calculational package to be a useful, reasonably accurate, and efficient system for performing analyses of MTR LEU/HEU core configurations.

#### References

1. D. K. Wehe and J. S. King, "Ford Nuclear Reactor High Enrichment/Low Enrichment Demonstration Experiments--Part I", presented at the International Meeting on Research and Test Reactor Core Conversion from HEU to LEU Fuels, Argonne National Laboratory (November 8-10, 1982).
2. D. K. Wehe and J. S. King, "Ford Nuclear Reactor High Enrichment/Low Enrichment Demonstration Experiments--Part II", presented at the International Meeting on Research and Test Reactor Core Conversion from HEU to LEU Fuels, Argonne National Laboratory (November 8-10, 1982).
3. D. K. Wehe and J. S. King, "The RERTR Demonstration Experiments Program at the Ford Nuclear Reactor", presented at the International Meeting on Research and Test Reactor Core Conversion from HEU to LEU Fuels, Argonne National Laboratory (November 12-14, 1980).
4. D. C. Losey et al., "Core Physics Analysis in Support of the FNR HEU-LEU Demonstration Experiment", presented at the International Meeting on Research and Test Reactor Core Conversion from HEU to LEU Fuels, Argonne National Laboratory (November 12-14, 1980).
5. W. Kerr et al., "Low Enrichment Fuel Evaluation and Analysis Program", Department of Nuclear Engineering and the Michigan-Memorial Phoenix Project, The University of Michigan, Ann Arbor, Michigan (January 1980).
6. R. F. Barry, "LEOPARD--A Spectrum Dependent Non-Spatial Depletion Code", WCAP-3269-26, Westinghouse Electric Corporation (September 1963).
7. H. Bohl, E. M. Gelbard, and G. H. Ryan, "MUFT-4--Fast Neutron Spectrum Code for the IBM-704", WAPD-TM-72, Westinghouse Bettis Atomic Power Laboratory (July 1957).
8. H. Amster and R. Suarez, "The Calculation of Thermal Constants Averaged over a Wigner-Wilkins Flux Spectrum; Description of the SOFOCATE Code", WAPD-TM-39, Westinghouse Bettis Atomic Power Laboratory (January 1957).
9. J. Barhen, W. Rothenstein, and E. Taviv, "The HAMMER Code System", NP-565, Electric Power Research Institute (October 1978).
10. W. W. Little, Jr. and R. W. Hardie, "2DB User's Manual--

Revision 1", BNWL-831 REV1, Battelle Pacific Northwest Laboratory (February 1969).

11. D. R. Vondy et al., "VENTURE: A Code Block for Solving the Finite-Difference Diffusion Approximation to Neutron Transport", ORNL-5062, Oak Ridge National Laboratory (1975).
12. R. W. Hardie and W. W. Little, Jr., "PERTV--A Two-Dimensional Code for Fast Reactor Analysis", BNWL-1162, Battelle Pacific Northwest Laboratory (September 1969).
13. K. D. Lathrop and F. W. Brinkley, "TWOTRAN-II--An Interfaced Exportable Version of the TWOTRAN Code for Two-Dimensional Transport", LA-4848-MS, Los Alamos Scientific Laboratory (1973).
14. W. W. Engle, Jr., "A User's Manual for ANISN, a One-Dimensional Discrete Ordinates Transport Code with Anisotropic Scattering", K-1693, Oak Ridge Gaseous Diffusion Plant (March 1967).
15. D. R. Harris, "ANDYMG3, The Basic Program of a Series of Monte Carlo Programs for Time-Dependent Transport of Particles and Photons", LA-4339, Los Alamos Scientific Laboratory (1970).
16. Private Communication, W. D. Henderson, Westinghouse Electric Corporation, to J. C. Lee, University of Michigan (August 1, 1980).
17. W. Jaschik and W. Seifritz, "Model for Calculating Prompt-Response Self-Powered Neutron Detectors", Nucl. Sci. Eng., 53, 61 (1974).